On The Dynamical Evolution Of Hierarchical Triple Systems

Nikolaos Georgakarakos

Doctor of Philosophy
University of Edinburgh
2001

To my parents,

Ilias and Christina

Abstract

A hierarchical triple system consists of two bodies forming a binary system and a third body on a wider orbit.

The evolution of the eccentricity of an initially circular inner binary of a hierarchical triple system with well separated components is examined. Systems with different mass ratios and orbital characteristics (e.g. inclination) are investigated and theoretical formulae are derived for each case. The derivation of these formulae is based on the expansion of the rate of change of the eccentric vector in terms of the orbital period ratio of the two binaries using first order perturbation theory. Some elements from secular theory are used wherever necessary. Special cases are also discussed (e.g. secular resonances). The validity of the results is tested by integrating the full equations of motion numerically and the agreement is satisfactory.

The stability of hierarchical triple systems with initially circular and coplanar orbits and small initial period ratio is also examined. Mean motion resonances are found to play an important role in the dynamics of the system. Special reference to the $3:1$ and $4:1$ resonances is made and a theoretical criterion for the $3:1$ resonance is developed. A more general stability criterion (applicable in principle to other resonances besides $3:1$) is obtained through a canonical transformation of an averaged Hamiltonian, and comparison is made with other results on the subject.

Acknowledgements

I wish to thank Professor Douglas Heggie for his valuable advice and inspiring discussions we had on every aspect of my doctoral studies. I also want to thank Dr Seppo Mikkola who kindly provided the code for integrating hierarchical triple systems. Many thanks to my officemates Steve Purchase and Alan Roy for the useful discussions we had on various aspects of my work. Finally, I want to thank my parents for all their support, which made the completion of my doctoral studies possible.

Declaration

I declare that this thesis was composed by myself and that the work contained therein is my own, except where explicitly stated otherwise in the text.

(*Nikolaos Georgakarakos*)

Contents

Chapter 1

Introduction

1.1 The three-body problem

The three-body problem is one of the most fascinating topics in mathematics and celestial mechanics. The basic definition of the problem is as follows: three point masses (or bodies of spherical symmetry) move in space, under their mutual gravitational attraction; given their initial conditions, we want to determine their subsequent motion.

Like many mathematical problems, it is not as simple as it sounds. Although the two-body problem can be solved in closed form by means of elementary functions and hence we can predict the quantitative and qualitative behaviour of the system, the three-body problem is a complicated nonlinear problem and no similar type of solution exists. More precisely, the former is integrable but the latter is not. The reason for this is that the known integrals of energy, angular momentum and centre-of-mass motion are not sufficient for the solution of the three-body problem (Szebehely and Mark 1998), because there are too many variables that have to be considered to solve the problem. Nonetheless, some particular solutions have been found (central configurations) and progress

has been made in special cases, like for example in the restricted three-body problem. Finally, it must be mentioned that, at the beginning of this century, a Finnish mathematical astronomer, Karl Sundman, gave a solution to the problem, by providing a convergent power series solution valid for all values of time. However, since the solution gives no qualitative information about the behaviour of the system and the rate of convergence is considered to be too slow for any real practical use, it leaves plenty of issues surrounding the problem to be resolved (Barrow-Green 1997).

The three-body problem has been studied by many mathematicians and astronomers in the past 300 years. Newton, Euler, Lagrange, Laplace, Jacobi, Leverrier, Newcomb, Hamilton, Delaunay, Hill, Poincaré, Sundman, Birkhoff and many others, were intrigued by the three-body problem and spent a great deal of time working on it. The effort of those people to tackle the difficulties emerging in the three-body problem is responsible for the development of methods and theories that have since found applications in many branches of science.

The three-body problem continues to be an exciting puzzle for every mathematician, even today, at a time in which our 'arsenal' has been reinforced with very fast computers, which can perform numerical integrations in a relatively short period of time. The simultaneous simplicity and complexity of the three-body problem is what made it, makes it and will be making it one of the most fascinating subjects in mathematics ever.

1.2 The hierarchical three-body problem

A special case of the three-body problem is the hierarchical three-body problem, where two of the bodies form a binary system and a distant companion perturbs

the motion of the binary.

We are going to deal with the gravitational aspect of the problem, i.e. we shall consider that there is only gravitational interaction among the bodies. Generally speaking, there could be other factors playing an important role in the dynamical evolution of the system, such as tidal friction, mass transfer in the form of Roche lobe overflowing or in the form of a stellar wind between the binary components and general relativistic effects in the case of compact objects (Valtonen, Mikkola and Pietilä 1995, Ford, Kozinsky and Rasio 2000). However, in the context of this investigation, we will concentrate on triple systems with well separated components, in which the gravitational perturbation timescales are short compared to those of the factors mentioned previously. Finally, it should be mentioned here, that a particular subject in the context of hierarchical triple systems which has attracted the research interest of many people is the stability of such systems (Harrington 1972, Szebehely and Zare 1977, Roy et al. 1984, Donnison and Mikulskis 1992, 1994 and 1995, Kiseleva, Eggleton and Anosova 1994, Kiseleva, Eggleton and Orlov 1994, Eggleton and Kiseleva 1995), which will be the main discussion topic in chapter three.

Next, we present some definitions and ideas from the two and three-body problems, along with some other mathematical techniques which will be used in the following chapters.

1.3 Some elements from the two-body problem

Consider the motion of a mass m_2 orbiting a mass m_1 in three dimensional space. In a situation like this, the following parameters can be defined (fig. 1.1): the orbital plane is generally inclined to some reference plane at angle I, called the inclination of the orbit. The line of intersection between the orbital

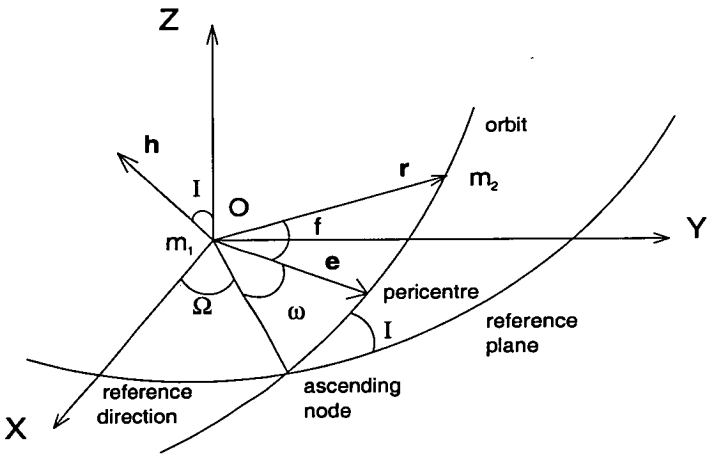

Figure 1.1: The two-body problem

and reference planes is called the line of nodes. The point in both planes where the orbit crosses the reference plane moving from below (above) to above (below) the plane is called the ascending (descending) node, while the angle Ω between a reference line and the radius vector to the ascending node is called the longitude of the ascending node. The angle ω between this same radius vector and the pericentre of the orbit is called the argument of pericentre and the angle $\varpi = \Omega + \omega$ is called the longitude of pericentre. In the case where the orbital and reference planes coincide ($I = 0°$ or $I = 180°$), ϖ is defined as the angle between the reference direction and the pericentre.

The angle f between the pericentre and the relative position vector $\vec{r}$ of mass m_2 with respect to mass m_1 , is called the true anomaly. The vector $\vec{e}$, which has the same direction as the radius vector to the pericentre and whose magnitude is equal to the eccentricity e of the orbit, is called the eccentric vector, and the angular momentum vector is the vector $\vec{h}$ in fig. 1.1. Finally, if T is the period of the orbit, we define the mean motion n as

$$n = \frac{2\pi}{T}.$$

Using this definition, we can define the mean anomaly ℓ as $\ell = n(t - \tau)$, where τ is the time of pericentre passage. To complete our set of definitions, we define the mean longitude λ as $\lambda = \ell + \varpi$.

1.4 Some elements from the three-body problem

1.4.1 The Jacobi formulation

A hierarchical triple system can be pictured as a superposition of two subsystems, a close binary and a wider binary. A very good way of studying the motion of such a system is the Jacobi decomposition of the three-body problem (fig. 1.2). It uses two vectors: the relative position vector of the inner binary $\vec{r}$ and the vector $\vec{R}$ from the centre of mass of m_1 and m_2 to the third mass m_3 (and consequently $\vec{R}$ passes through the centre of mass of the three-body system). Then the equations of motion in the Jacobi formulation are:

$$\ddot{\vec{r}} = -\frac{G(m_1 + m_2)}{r^3}\vec{r} + Gm_3\left(\frac{\vec{r}_{23}}{r_{23}^3} - \frac{\vec{r}_{13}}{r_{13}^3}\right) \tag{1.1}$$

$$\ddot{\vec{R}} = -G(m_1 + m_2 + m_3)\left(\frac{m_1}{m_1 + m_2}\frac{\vec{r}_{13}}{r_{13}^3} + \frac{m_2}{m_1 + m_2}\frac{\vec{r}_{23}}{r_{23}^3}\right), \tag{1.2}$$

where $\vec{r}_{13}$ is the vector from m_1 to m_3 and $\vec{r}_{23}$ is the vector from m_2 to m_3. The Jacobi decomposition of the three-body problem becomes really interesting in the case when $\frac{r}{R}$ is small or when one of the masses of the inner binary is significantly larger than the other two masses (e.g. the Sun and two planets) and the two binaries can be considered to be on two slowly perturbed Keplerian orbits.

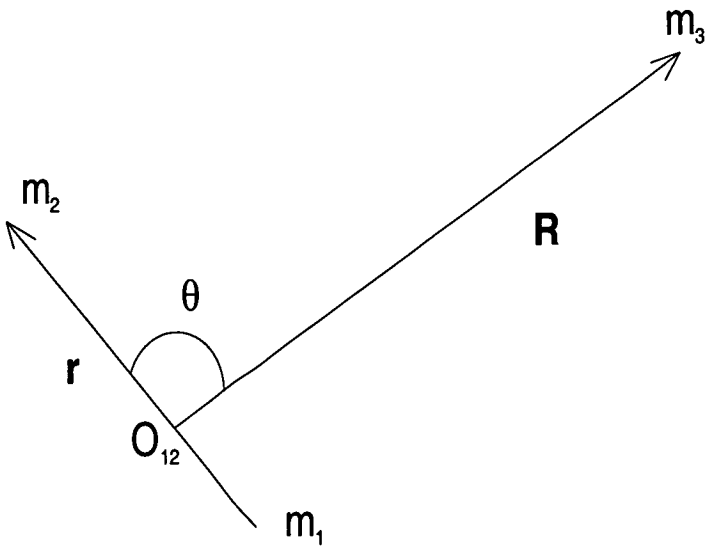

Figure 1.2: The Jacobi formulation

1.4.2 The Delaunay variables

Delaunay, in order to study the lunar problem, introduced a set of variables in which the equations of motion of the three-body problem have the Hamiltonian form. The Delaunay variables for a hierarchical three-body problem in its barycentric frame are as follows:

$$\begin{aligned} L_1 &= mn_1a_1^2 && , \quad \ell_1 \\ G_1 &= mn_1a_1^2\sqrt{1-e_1^2} && , \quad g_1 = \omega_1 \\ \mathcal{H}_1 &= mn_1a_1^2\sqrt{1-e_1^2}\cos I_1 && , \quad h_1 = \Omega_1 \end{aligned} \tag{1.3}$$

$$\begin{aligned} L_2 &= \mathcal{M}n_2a_2^2 && , \quad \ell_2 \\ G_2 &= \mathcal{M}n_2a_2^2\sqrt{1-e_2^2} && , \quad g_2 = \omega_2 \\ \mathcal{H}_2 &= \mathcal{M}n_2a_2^2\sqrt{1-e_2^2}\cos I_2 && , \quad h_2 = \Omega_2. \end{aligned} \tag{1.4}$$

The indices 1 and 2 denote the internal and external orbit respectively. The quantities m and $\mathcal{M}$ are called the reduced masses and they are defined as:

$$m = \frac{m_1m_2}{m_1+m_2} \quad , \quad \mathcal{M} = \frac{m_3(m_1+m_2)}{M},$$

where $M = m_1 + m_2 + m_3$. The variable G is the angular momentum of the orbit and $\mathcal{H}$ is the component of the angular momentum vector orthogonal to the reference plane. Finally, a is the semi-major axis of the orbit, while the rest of the quantities appearing in the two previous sets of equations have been defined in the section for the two-body problem.

1.4.3 The Hamiltonian formulation

Using the Delaunay variables, we may write the Hamiltonian of the problem in the form (Marchal 1990):

$$H = -\frac{G^2 m^3 (m_1+m_2)^2}{2L_1^2} - \frac{G^2 \mathcal{M}^3 M^2}{2L_2^2} + G m_3 \left(\frac{m_1+m_2}{R} - \frac{m_1}{r_{13}} - \frac{m_2}{r_{23}}\right) \quad (1.5)$$

and then the equations of motion of the system are:

$$\begin{aligned}
\frac{dL_1}{dt} &= -\frac{\partial H}{\partial \ell_1} \quad , \quad \frac{d\ell_1}{dt} = \frac{\partial H}{\partial L_1} \\
\frac{dG_1}{dt} &= -\frac{\partial H}{\partial g_1} \quad , \quad \frac{dg_1}{dt} = \frac{\partial H}{\partial G_1} \\
\frac{d\mathcal{H}_1}{dt} &= -\frac{\partial H}{\partial h_1} \quad , \quad \frac{dh_1}{dt} = \frac{\partial H}{\partial \mathcal{H}_1}
\end{aligned} \quad (1.6)$$

$$\begin{aligned}
\frac{dL_2}{dt} &= -\frac{\partial H}{\partial \ell_2} \quad , \quad \frac{d\ell_2}{dt} = \frac{\partial H}{\partial L_2} \\
\frac{dG_2}{dt} &= -\frac{\partial H}{\partial g_2} \quad , \quad \frac{dg_2}{dt} = \frac{\partial H}{\partial G_2} \\
\frac{d\mathcal{H}_2}{dt} &= -\frac{\partial H}{\partial h_2} \quad , \quad \frac{dh_2}{dt} = \frac{\partial H}{\partial \mathcal{H}_2}.
\end{aligned} \quad (1.7)$$

As can be easily seen, this Hamiltonian problem has six degrees of freedom. However, the degrees of freedom can be reduced by eliminating the nodes, in a rather simple way (Marchal 1990): we just choose our reference plane to be the invariable plane perpendicular to $\vec{c}$, where $\vec{c}$ is the angular momentum vector of the system (fig. 1.3).

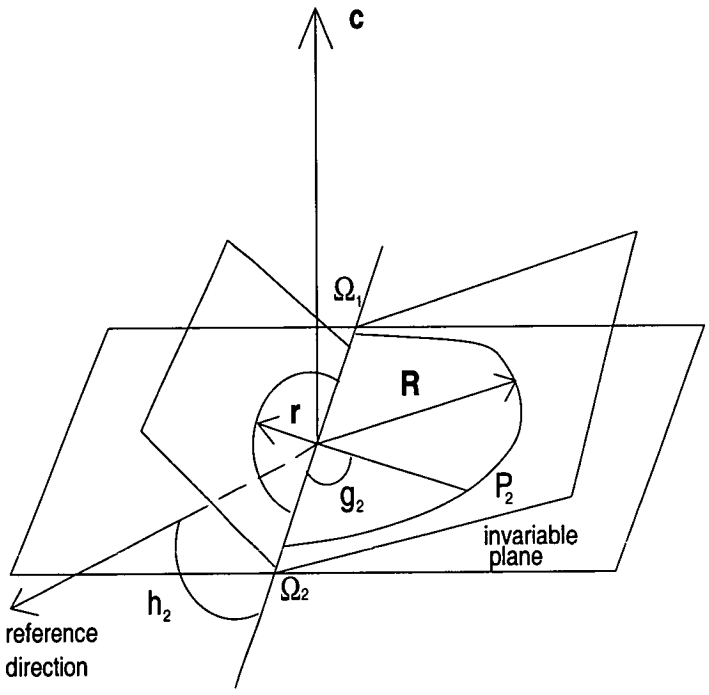

Figure 1.3: The two orbits and the elimination of the nodes

In terms of the Delaunay variables, the angular momentum is

$$\vec{c} = (\mathcal{K}_1 \sin h_1 + \mathcal{K}_2 \sin h_2, -\mathcal{K}_1 \cos h_1 - \mathcal{K}_2 \cos h_2, \mathcal{H}_1 + \mathcal{H}_2)$$

where

$$\mathcal{K}_1 = \sqrt{G_1^2 - \mathcal{H}_1^2} \quad , \quad \mathcal{K}_2 = \sqrt{G_2^2 - \mathcal{H}_2^2}.$$

With that special choice of reference frame the angular momentum vector becomes $\vec{c} = (0, 0, c)$, and we get:

$$G_1^2 - \mathcal{H}_1^2 = G_2^2 - \mathcal{H}_2^2$$

$$h_1 + \pi = h_2$$

$$\mathcal{H}_1 + \mathcal{H}_2 = c.$$

Now, for the three masses m_1, m_2 and m_3 , the Hamiltonian of the problem will be a function of the eight Delaunay variables $L_1, G_1, L_2, G_2, \ell_1, g_1, \ell_2, g_2$ and c since (fig. 1.4)

$$c^2 = G_1^2 + G_2^2 + 2G_1G_2 \cos(I_1 + I_2)$$

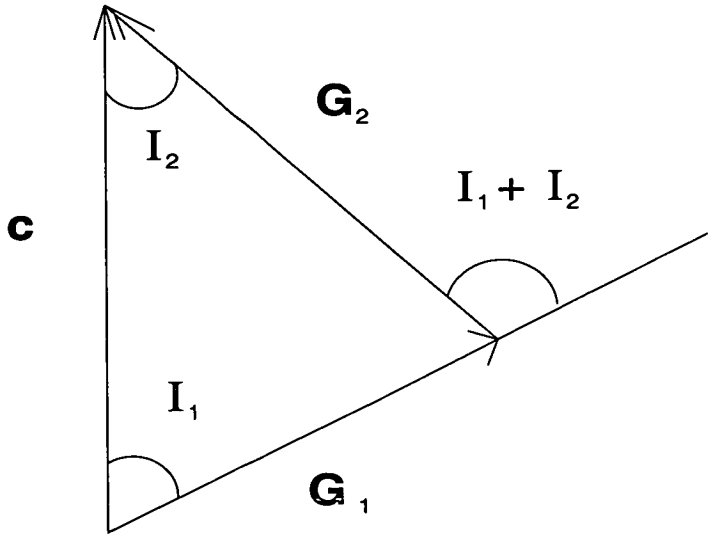

Figure 1.4: The relation between the angular momenta and the inclinations

Thus, we obtain a Hamiltonian system with only four degrees of freedom:

$$\frac{dL_1}{dt} = -\frac{\partial H}{\partial \ell_1} \quad , \quad \frac{d\ell_1}{dt} = \frac{\partial H}{\partial L_1}$$
$$\frac{dG_1}{dt} = -\frac{\partial H}{\partial g_1} \quad , \quad \frac{dg_1}{dt} = \frac{\partial H}{\partial G_1} \tag{1.8}$$

$$\frac{dL_2}{dt} = -\frac{\partial H}{\partial \ell_2} \quad , \quad \frac{d\ell_2}{dt} = \frac{\partial H}{\partial L_2}$$
$$\frac{dG_2}{dt} = -\frac{\partial H}{\partial g_2} \quad , \quad \frac{dg_2}{dt} = \frac{\partial H}{\partial G_2}. \tag{1.9}$$

The parameters eliminated earlier are given by the following relations:

$$\mathcal{H}_1 = \frac{(c^2 + G_1^2 - G_2^2)}{2c}$$
$$\mathcal{H}_2 = \frac{(c^2 - G_1^2 + G_2^2)}{2c}$$
$$h_1 + \pi = h_2 \tag{1.10}$$
$$\frac{dh_1}{dt} = \frac{\partial H}{\partial c}$$
$$\frac{dh_2}{dt} = \frac{\partial H}{\partial c}.$$

It is worth mentioning here that the rate of change of e_1 can be derived by differentiating the relation

$$G_1 = L_1\sqrt{1-e_1^2}.$$

By doing so, we get

$$\dot{e}_1 = \frac{\sqrt{1-e_1^2}}{L_1 e_1}\left(\frac{\partial H}{\partial g_1} - \sqrt{1-e_1^2}\frac{\partial H}{\partial \ell_1}\right). \tag{1.11}$$

The above equation will be used in the following chapters for obtaining expressions for $\dot{e}_1$.

1.4.4 The Von Zeipel method

The Von Zeipel method provides us with a way of studying the behaviour of a system over a long period of time (secular behaviour). It uses a generating function which leads to a Hamiltonian with only long period terms, since the short period effects have been removed with the application of the corresponding canonical transformation (Marchal 1990).

The generating function is given in terms of the old momenta and the new positions, i.e.

$$S = S(L_1, G_1, L_2, G_2, \ell_S, g_S, \ell_T, g_T, c),$$

where the indices S and T denote the inner and outer long period orbits respectively and the transition from the old canonical variables to the new ones is defined by the following equations:

$$\begin{aligned} L_S &= \frac{\partial S}{\partial \ell_S} \quad , \quad G_S = \frac{\partial S}{\partial g_S} \\ \ell_1 &= \frac{\partial S}{\partial L_1} \quad , \quad g_1 = \frac{\partial S}{\partial G_1} \\ L_T &= \frac{\partial S}{\partial \ell_T} \quad , \quad G_T = \frac{\partial S}{\partial g_T} \end{aligned} \tag{1.12}$$

$$\ell_2 = \frac{\partial S}{\partial L_2} \quad , \quad g_2 = \frac{\partial S}{\partial G_2}. \tag{1.13}$$

A common way of writing a near-identity generating function is:

$$S = L_1\ell_S + G_1 g_S + L_2\ell_T + G_2 g_T + S_1. \tag{1.14}$$

Generally, S_1 is a function of the orbital elements of the two orbits (for more details see Marchal 1990). A suitable choice of S_1 will give a Hamiltonian independent of ℓ_S and ℓ_T [1], which implies that there is no secular change in the semi-major axes of the two orbits (Harrington 1968).

1.5 Legendre polynomials

Legendre polynomials were introduced by Legendre in the theory of potential. They are related to the expansion of the reciprocal of some distance, in the Newtonian theory of potential or Coulomb potential. In section 1.6 and in later chapters, it will become quite clear how the Legendre polynomials can be used in the context of celestial mechanics, e.g. in hierarchical triples when $r/R << 1$.

From the cosine rule for the triangle OAB (fig. 1.5) :

$$r = |\vec{r}_1 - \vec{r}_2| = (r_1^2 + r_2^2 - 2r_1 r_2 \cos\theta)^{\frac{1}{2}}.$$

Then,

$$\frac{1}{r} = \frac{1}{r_2}(1 - 2\frac{r_1}{r_2}\cos\theta + \frac{r_1^2}{r_2^2})^{-\frac{1}{2}} =$$
$$= \frac{1}{r_2}\sum_{n=0}^{\infty} P_n(\cos\theta)(\frac{r_1}{r_2})^n,$$

with

$$|\frac{r_1}{r_2}| < 1.$$

[1] It is even possible to obtain a Hamiltonian independent of g_T to first order.

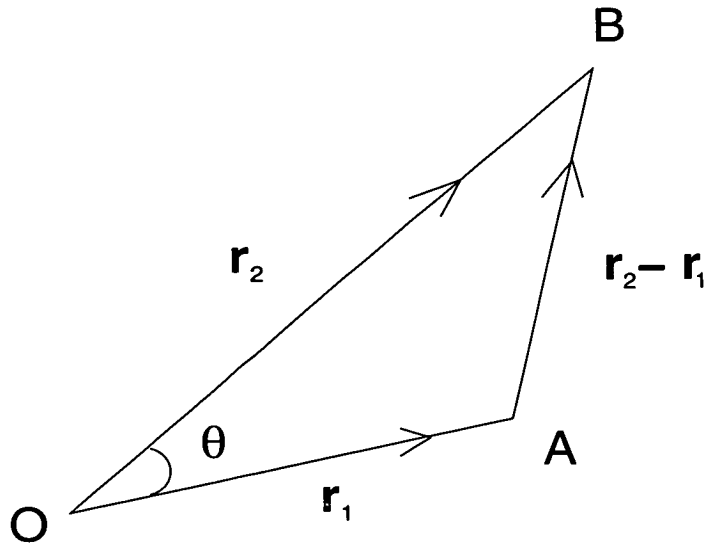

Figure 1.5: The position vectors $\vec{r}_1$ and $\vec{r}_2$ of two points A and B with respect to the origin of the coordinate system O. The angle between the position vectors is θ.

The quantities P_n are the Legendre polynomials and they can be generated from the following equation:

$$P_n(x) = \frac{(-1)^n}{2^n n!} \frac{d^n}{dx^n}(1-x^2)^n. \tag{1.15}$$

The first six Legendre polynomials are:

$$P_0(x) = 1 \quad , \quad P_1(x) = x$$

$$P_2(x) = \frac{1}{2}(3x^2 - 1) \quad , \quad P_3(x) = \frac{1}{2}(5x^3 - 3x)$$

$$P_4(x) = \frac{1}{8}(35x^4 - 30x^2 + 3) \quad , \quad P_5(x) = \frac{1}{8}(63x^5 - 70x^3 + 15x).$$

1.6 Expanding the perturbing Hamiltonian

The term

$$Gm_3\left(\frac{m_1 + m_2}{R} - \frac{m_1}{r_{13}} - \frac{m_2}{r_{23}}\right)$$

in equation (1.5) is the perturbing Hamiltonian. This can be expanded in terms of the orbital elements of the two binaries in many ways, one being the following: using the Jacobi notation, the perturbing Hamiltonian can be rewritten as

$$
\begin{aligned}
& Gm_3\left(\frac{m_1+m_2}{R}-\frac{m_1}{|\vec{R}+\mu_2\vec{r}|}-\frac{m_2}{|\vec{R}-\mu_1\vec{r}|}\right) \\
& = Gm_3\left(\frac{m_1+m_2}{R}-\frac{m_1}{R}\sum_{n=0}^{\infty}\left(-\frac{\mu_2 r}{R}\right)^n P_n(\cos\theta)-\right. \\
& \left.-\frac{m_2}{R}\sum_{n=0}^{\infty}\left(\frac{\mu_1 r}{R}\right)^n P_n(\cos\theta)\right) \\
& = Gm_3\left[-\frac{m_1}{R}\sum_{n=2}^{\infty}\left(-\frac{\mu_2 r}{R}\right)^n P_n(\cos\theta)-\frac{m_2}{R}\sum_{n=2}^{\infty}\left(\frac{\mu_1 r}{R}\right)^n P_n(\cos\theta)\right] \\
& = -\frac{Gm_3}{R}\sum_{n=2}^{\infty}\left[m_1\left(-\frac{\mu_2 r}{R}\right)^n+m_2\left(\frac{\mu_1 r}{R}\right)^n\right]P_n(\cos\theta), \qquad (1.16)
\end{aligned}
$$

where P_n are the Legendre polynomials and

$$\mu_i=\frac{m_i}{m_1+m_2}, \quad i=1,2.$$

What is needed now is to expand the above expression in terms of the orbital elements of the two subsystems using series expansions for r/R and $\cos\theta$. It is known that (Brouwer and Clemence 1961, Murray and Dermott 1999)

$$
\begin{aligned}
\frac{r}{a_1} &= 1+\frac{1}{2}e_1^2-2e_1\sum_{s=1}^{\infty}\frac{1}{s^2}\frac{d}{de_1}J_s(se_1)\cos s\ell_1 = \\
&= 1-e_1\cos\ell_1+\frac{e_1^2}{2}(1-\cos 2\ell_1)+O(e_1^3). \qquad (1.17)
\end{aligned}
$$

The quantity J_s in equation (1.17) is the Bessel function and for positive values of s it can be written as

$$J_s(x)=\frac{1}{s!}\left(\frac{x}{2}\right)^s\sum_{i=0}^{\infty}(-1)^i\frac{(x/2)^{2i}}{i!(s+1)(s+2)...(s+i)}.$$

This series is absolutely convergent for all values of x but the series expansion for r/a_1 is divergent for $e_1>0.6627434$. By replacing r by R and the index 1 by 2, a similar expresssion can be obtained for the outer orbit. Moreover, using the expansion for r/a_1, we can find expressions for $(r/a_1)^n$ for any n.

Something similar can be applied to $\cos\theta$. In the coplanar case, the angle θ can be expressed as

$$\theta = (f_2 + \varpi_2) - (f_1 + \varpi_1),$$

where f_i are the true anomalies of the two orbits. Then, using elementary trigonometry,

$$\cos\theta = (\cos f_2 \cos\varpi_2 - \sin f_2 \sin\varpi_2)(\cos f_1 \cos\varpi_1 - \sin f_1 \sin\varpi_1) +$$

$$+(\sin f_2 \cos\varpi_2 + \cos f_2 \sin\varpi_2)(\sin f_1 \cos\varpi_1 + \cos f_1 \sin\varpi_1).$$

But $\sin f_i$ and $\cos f_i$ can be expressed as series in the following way (Brouwer and Clemence 1961):

$$\begin{aligned}
\sin f_i &= 2\sqrt{1-e_i^2}\sum_{s=1}^{\infty}\frac{1}{s}\frac{d}{de_i}J_s(se_i)\sin s\ell_i = \\
&= \sin\ell_i + e_i\sin 2\ell_i + e_i^2(\frac{9}{8}\sin 3\ell_i - \frac{7}{8}\sin\ell_i) + O(e_i^3) \qquad (1.18)\\
\cos f_i &= -e_i + \frac{2(1-e_i^2)}{e_i}\sum_{s=1}^{\infty}J_s(se_i)\cos s\ell_i = \\
&= \cos\ell_i + e_i(\cos 2\ell_i - 1) + \frac{9}{8}e_i^2(\cos 3\ell_i - \cos\ell_i) + O(e_i^3). \qquad (1.19)
\end{aligned}$$

Finally, the mean anomalies can be replaced by the mean longitudes

$$\lambda_i = \ell_i + \varpi_i.$$

Hence, it is possible to derive an expansion of the perturbing Hamiltonian in terms of longitudes and eccentricities up to any order. A second order expansion of the P_2 and P_3 terms with respect to the eccentricities can be found in Appendix B.

1.7 A symplectic integrator with time transformation for the three-body problem

1.7.1 Introduction

Symplectic integrators are efficient algorithms for treating few-body systems numerically. Numerical methods which use symplectic transformations are expected to reflect the qualitative properties of a Hamiltonian system better than traditional integrators. Moreover, these methods do not show secular errors in energy and angular momentum. Studies on symplectic integrators of relevance in celestial mechanics include the works by Kinoshita, Yoshida and Nakai (1991), Wisdom and Holman (1991), Saha and Tremaine (1992), Yoshida (1990, 1993), Sanz-Serna (1992) and Gladman, Duncan and Candy (1991). However, symplectic methods have the serious disadvantage that one can not use different time-steps in different parts of the orbit without losing their good long-term behaviour (Gladman, Duncan and Candy 1991). Although the so called reversible time-step strategies (Hut, Makino and McMillan 1995, Funato et al. 1996) may work well in some occasions, the problem is still considered unsolved. Another way of dealing with this problem is to employ a time transformation and use the extended phase space (Mikkola 1997). A code based on this idea has been used for many of the numerical integrations described in chapters 2 and 3 and is now described in outline. The code itself was kindly provided by S. Mikkola.

1.7.2 Generalised leap-frog with time transformation

Consider a system with a Hamiltonian of the form

$$H = H_0 + H_1, \tag{1.20}$$

where the two parts H_0 and H_1 are integrable if each of them is considered as Hamiltonian of the system. An approximation to the motion of the system defined by equation (1.20) is to move the system first over a half time-step $\frac{h}{2}$ using H_0 as the Hamiltonian, then move the system over a full time-step h using H_1 and then use H_0 again to move the system over another half time-step. This technique can be applied to any splitting of a Hamiltonian into two integrable parts. In practice, the two parts must be not only integrable, but the advancement of the system must be easy to compute. This method is called the generalised leap-frog. An example of such a method is the Wisdom-Holman method, which is based on the splitting of the Hamiltonian of the Solar System into a sum of two-body Hamiltonians and a perturbing function which depends only on the coordinates (Wisdom and Holman 1991).

As was stated earlier, a constant time-step is necessary in symplectic integration, otherwise the good long-time behaviour of the method is lost. However, if the nearly Keplerian orbits of the system are quite eccentric, the choice of a constant time-step can lead to inaccuracy, because the motion of the system is much faster near pericentre. A choice of a smaller constant time-step should be adequate to deal with the problem, but is inefficient. Another possibility is the introduction of a time transformation from the physical time t to a fictitious time s in the form

$$dt = g(\vec{q}, t)ds \tag{1.21}$$

and a new Hamiltonian Γ:

$$\Gamma = g(\vec{q}, q_0)(H(\vec{p}, \vec{q}, q_0) + p_0), \tag{1.22}$$

where $\vec{q}$ is the coordinate vector, $\vec{p}$ is the momentum vector, p_0 has the numerical value $p_0 = -H(t)$ and $q_0 = t$. Consequently, the time t is now a coordinate and p_0 is the corresponding momentum. Dividing now the new Hamiltonian into

two integrable parts

$$\Gamma = \Gamma_0 + \Gamma_1, \tag{1.23}$$

we can apply the generalised leap-frog method to this Hamiltonian. The constant time-step is now the step in s, while the step in the physical time t varies according to equation (1.21).

1.7.3 Perturbed two-body problem

Let the Hamiltonian of the problem be

$$H = \frac{1}{2}\vec{p}^2 - \frac{M}{r} + R(\vec{r}, t), \tag{1.24}$$

where M is the total mass of the system and R is the perturbing function. The new Hamiltonian Γ is

$$\Gamma = g(\frac{1}{2}\vec{p}^2 - \frac{M}{r} + R(\vec{r}, q_0) + p_0) \tag{1.25}$$

and it can be split into two parts Γ_0 and Γ_1 as follows:

$$\Gamma_0 = g(\frac{1}{2}\vec{p}^2 - \frac{M}{r} + p_0), \quad \Gamma_1 = gR(\vec{r}, q_0).$$

Since Γ_1 is independent of the momenta, it is easily integrable for any choice of g (see equations 1.27 and 1.28). However, the choice of g should be such that Γ_0 is also easy to integrate. We also need to find an expression for the physical time t. Bearing in mind that

$$ds = \frac{1}{g}dt,$$

we obtain:

$$h = \int_t^{t+\delta t} \frac{1}{g}dt, \tag{1.26}$$

where h is the stepsize in s. In principal, by solving this equation, we obtain an expression for the corresponding physical timestep δt. Finally, the momentum

jumps between the Keplerian steps are calculated by

$$\delta\vec{p} = -h\frac{\partial(gR)}{\partial\vec{r}} \tag{1.27}$$

$$\delta p_0 = -h\frac{\partial(gR)}{\partial q_0} \tag{1.28}$$

which are to be added to the momenta before moving to the next Keplerian orbit step.

1.7.4 Hierarchical three-body problem

The same kind of treatment can also be applied to the hierarchical three-body problem. The Hamiltonian of the problem is of the form

$$H = K_1 + K_2 + R, \tag{1.29}$$

where K_1, K_2 are the Keplerian Hamiltonians of the inner and outer binary respectively, while R is the perturbing Hamiltonian (cf. equation [1.5], though R has a different meaning there). The new Hamiltonian is defined as

$$\Gamma = g(H + p_0), \tag{1.30}$$

and it can be split into

$$\Gamma_0 = g(K_1 + K_2 + p_0) \tag{1.31}$$

$$\Gamma_1 = gR. \tag{1.32}$$

1.8 Multiple stellar systems

Generally, stars have a tendency to form groups of different multiplicity, from the smallest possible (binary systems) up to large groups, like globular clusters with a population of the order of 10^7 stars. Modern observations give values for the frequency of multiple stars in the galactic field of up to 70%, and between

5% – 15% of these systems are at least triple (Gliese and Jahreiss 1988, Batten, Fletcher and McCarthy 1989, Duquennoy and Mayor 1991).

Many studies have been carried out in order to investigate the multiplicity of stars. Among the 50 nearest systems (mainly G/K/M dwarfs), there are believed to be 33 single, 13 binary and 4 triple stars (Van de Kamp 1971, Henry and McCarthy 1990) and among the 164 nearest solar type dwarfs it is claimed that there are 93 singles, 62 binaries, 7 triples and 2 quadruples (Duquennoy and Mayor 1991), with the number of triples and quadruples possibly being larger. Finally, among the 50 brightest systems there appear to be 27 singles, 15 binaries, 3 triples, 4 quadruples and 1 sextuple (Hoffleit and Jaschek 1983, Batten, Fletcher and McCarthy 1989). A significant percentage of binary systems (20% – 30%) are believed to be members of larger multiple systems (Batten, Fletcher and McCarthy 1989) and most of these are hierarchical triples (Tokovinin 1997b).

A rather large fraction of triple and quadruple systems can be found among pre-main sequence stars in star forming regions (Ghez, Neugebauer and Matthews 1993). Triple or even higher multiplicity systems, which usually have a hierarchical structure, are also found in open clusters, although it appears that they are not as numerous as in the field. Such systems have been observed in the Pleiades (Mermilliod et al. 1992), the Hyades (Griffin and Gunn 1981, Griffin et al. 1985, Mason et al. 1993), Praesepe (Mermilliod, Duquennoy and Mayor 1994), M67 (Mathieu, Latham and Griffin 1990) and in NGC 1502 (Mayer et al. 1994). So far, there is only one hierarchical triple system that has been detected in globular clusters, but it is almost certain that there are many others. This is the millisecond pulsar system PSR B1620-26 in the core of the M4 globular cluster (Backer, Foster and Sallmen 1993, Thorsett, Arzoumanian and Taylor 1993, Rasio, McMillan and Hut 1995, Thorsett et al. 1999, Ford et al. 2000).

From all the above, it becomes quite clear that it is necessary to study, numerically and analytically, the formation and dynamical evolution of hierarchical systems in the galactic field and in star clusters. Moreover, the study of the hierarchical three-body problem can find application not only in stellar systems but also in other areas, for example the solar system. (The Earth-Moon-Sun system is a hierarchical triple system.)

Chapter 2

Evolution of the inner orbital eccentricity in hierarchical triple systems

2.1 Introduction

The study of the evolution of hierarchical triple systems is very interesting, not only from the purely theoretical point of view, but also because they can play an important role in nature. For instance, the energy of a few close binaries in a globular star cluster can dominate the energy of the entire system. In fact, globular clusters are known to contain substancial fractions of binaries which were present initially (so-called "primordial" binaries). Therefore, the cores of the clusters are thought to contain a small but dynamically significant population of *triple* systems formed through dynamical interactions between primordial binaries (McMillan, Hut and Makino 1991). In simulations, these triple systems should be handled numerically with caution because they require long integrations of the orbital dynamics in order to resolve the outcome of the

interaction. Moreover, theories developed for understanding the orbital dynamics of hierarchical triple systems could be used in the context of observational astronomy, in connection with extrasolar planet detection or the identification of multiple stellar systems.

An important characteristic of an orbit is the eccentricity. The eccentricity can govern the possibility of close encounters between the components of a binary system or between the two subsystems of a hierarchical triple system, even when the semi-major axes are rather large. But close encounters mean strong interactions among the bodies and strong interactions could lead to a configuration very different from the initial one. For example, the third star can 'pump in' some eccentricity to the inner binary (as will become quite clear in the present and subsequent chapters) and, as a result of this, the inner binary and the third star, which were previously well separated, can now approach each other so closely, that the configuration of the system changes, i.e. disruption of the triple system or change of hierarchy occurs. In addition, if the orbital period of the inner binary is rather short, then an increase in the inner eccentricity would lead to the appearance of tidal friction, tidal deformation of the spherical stars, possible mass transfer etc. and hence, although we started with a purely gravitational problem which involved interaction between point masses, we have reached a point where the present description of the problem has significantly deviated from the original one and new factors need to be taken into consideration.

Thus, it becomes quite clear that understanding (rather than just determining) the processes that govern the evolution of the eccentricity of the inner binary is essential for trying to give answers to questions that have concerned astronomers for some time, such as, for example, whether the system breaks up or not.

2.2 Variation of the inner eccentricity

As was stated earlier (section 1.4.1), the motion of the members of a hierarchical triple system can be pictured as two, slowly evolving, Keplerian orbits. The main topic of discussion in this chapter will be the variation of the inner eccentricity when it is initially zero and the period ratio

$$X = \frac{T_2}{T_1} = \frac{n_1}{n_2}$$

(where T_1, T_2, n_1 and n_2 are the periods and the mean motions of the inner and outer orbit respectively) is rather large, or equivalently (for comparable masses) when $\frac{a_1}{a_2} \ll 1$. (Here a_i are the semi-major axes.) For most hierarchical triple stars, X is of the order of 100 and these systems are probably very stable dynamically. However, there are systems with much smaller period ratios, like the HD 109648 system with $X = 22$ (Jha et al. 2000), the λ Tau system, with $X = 8.3$ (Fekel and Tomkin 1982) and the CH Cyg system with $X = 7.0$ (Hinkle et al. 1993). Such systems will be the main topic of our next chapter.

The present section will be split into subsections dealing with the following cases:

$$i)\ m_1 = m_2 = m_3 \quad I = 0 \quad e_2 = 0$$

$$ii)\ m_1 \neq m_2 \quad I = 0 \quad e_2 = 0$$

$$iii)\ m_1 \neq m_2 \quad I = 0 \quad e_2 \neq 0$$

$$iv)\ m_1 \neq m_2 \quad I \neq 0 \quad e_2 \neq 0$$

$$v)\ m_1 \neq m_2 \quad I \neq 0 \quad e_2 = 0$$

$$vi)\ m_1 = m_2 = m_3 \quad I \neq 0 \quad e_2 \neq 0.$$

and for each case, a formula for the averaged eccentricity (or the averaged square eccentricity) will be derived with an aimed reliability to about 10% (20%).

2.2.1 Equal masses, coplanar orbits, circular binaries case

It has been suggested that the averaged inner eccentricity can be calculated from the formula (Eggleton and Kiseleva 1996, Kiseleva, Eggleton and Mikkola 1998):

$$\bar{e}_{in} = \frac{A}{X^{1.5}\sqrt{X-B}}, \tag{2.1}$$

where A and B depend on the mass ratios. This is an empirical formula based on results from numerical integrations of coplanar, prograde and initially circular orbits for some mass ratios. Initial conditions were such that the inner binary was 90° ahead of the outer, i.e.

$$f_1 + \varpi_1 = \frac{\pi}{2} + f_2 + \varpi_2$$

in the notation of sections 1.3 and 1.4. The motion of the system can be studied analytically by using the Jacobi decomposition of the three-body problem, which was described earlier (section 1.4.1). The equation of motion of the inner binary is

$$\ddot{\vec{r}} = -G(m_1+m_2)\frac{\vec{r}}{r^3} + \vec{F}, \tag{2.2}$$

where G is the gravitational constant and $\vec{F}$, the perturbation to the inner binary motion, is

$$\vec{F} = Gm_3\left(\frac{\vec{R}-\mu_1\vec{r}}{|\vec{R}-\mu_1\vec{r}|^3} - \frac{\vec{R}+\mu_2\vec{r}}{|\vec{R}+\mu_2\vec{r}|^3}\right) =$$

$$= Gm_3\frac{\partial}{\partial\vec{r}}\left(\frac{1}{\mu_1|\vec{R}-\mu_1\vec{r}|} + \frac{1}{\mu_2|\vec{R}+\mu_2\vec{r}|}\right) \tag{2.3}$$

with

$$\mu_i = \frac{m_i}{m_1+m_2}, \quad i = 1,2.$$

The equation of motion (2.2) is effectively the same as equation (1.1), with everything expressed in terms of $\vec{r}$ and $\vec{R}$ in the former. Now, since the third

star is at considerable distance from the inner binary, implying that r/R is small, the inverse distances in equation (2.3) can be expressed as:

$$\frac{1}{|\vec{R}-\mu_1\vec{r}|}=\frac{1}{R}\sum_{n=o}^{\infty}\left(\frac{\mu_1 r}{R}\right)^n P_n(\cos\theta)$$

and

$$\frac{1}{|\vec{R}+\mu_2\vec{r}|}=\frac{1}{R}\sum_{n=o}^{\infty}\left(-\frac{\mu_2 r}{R}\right)^n P_n(\cos\theta),$$

where P_n are the Legendre polynomials and θ is the angle between the vectors $\vec{r}$ and $\vec{R}$ (cf. section 1.5). Expanding to third order, the perturbation becomes

$$\vec{F}=Gm_3\frac{\partial}{\partial\vec{r}}\left(\frac{3}{2}\frac{(\vec{r}\cdot\vec{R})^2}{R^5}-\frac{1}{2}\frac{r^2}{R^3}-\frac{5(\mu_2^2-\mu_1^2)}{2}\frac{(\vec{r}\cdot\vec{R})^3}{R^7}+\right.$$
$$\left.+\frac{3(\mu_2^2-\mu_1^2)}{2}\frac{r^2(\vec{r}\cdot\vec{R})}{R^5}\right). \tag{2.4}$$

The first two terms in the above equation come from the quadrupole term (P_2), while the other two come from the octupole term (P_3). However, since at the moment we are dealing with the case of equal masses, $\mu_1=\mu_2$ and equation (2.4) reduces to

$$\vec{F}=Gm_3\frac{\partial}{\partial\vec{r}}\left(\frac{3}{2}\frac{(\vec{r}\cdot\vec{R})^2}{R^5}-\frac{1}{2}\frac{r^2}{R^3}\right). \tag{2.5}$$

The eccentric vector can be used now, in order to obtain an expression for the inner eccentricity. Of course, this could also be done by applying canonical methods, but using the definition of the eccentric vector is a quite straightforward procedure which does not require any knowledge of canonical perturbation theory. The eccentric vector $\vec{e}$ is given by

$$\vec{e}=-\frac{\vec{r}}{r}+\frac{1}{\mu}(\dot{\vec{r}}\times\vec{h}), \tag{2.6}$$

where $\vec{h}=\vec{r}\times\dot{\vec{r}}$ and $\mu=G(m_1+m_2)$. If we differentiate equation (2.6) we get

$$\dot{\vec{e}}=\frac{1}{\mu}[2(\dot{\vec{r}}\cdot\vec{F})\vec{r}-(\vec{r}\cdot\vec{F})\dot{\vec{r}}] \tag{2.7}$$

(assuming that $\vec{r}\cdot\dot{\vec{r}}=0$, i.e. the inner binary remains nearly circular) and substituting for $\vec{F}$, we finally obtain:

$$\ddot{\vec{e}}=\frac{Gm_3}{\mu R^3}[6\frac{(\vec{r}\cdot\vec{R})(\dot{\vec{r}}\cdot\vec{R})}{R^2}\vec{r}-3\frac{(\vec{r}\cdot\vec{R})^2}{R^2}\ddot{\vec{r}}+r^2\ddot{\vec{r}}]. \tag{2.8}$$

Then, considering the inner binary to be 90° degrees ahead of the outer binary initially (although more generally, the calculation can be done for any initial phase), the Jacobi vectors can be represented in polar form as $\vec{r}=a_1(\cos n_1t,\sin n_1t)$ and $\vec{R}=a_2(\sin n_2t,-\cos n_2t)$. After integrating, the components x_1 and y_1 of the eccentric vector become (expanding in powers of $\frac{1}{X}$ and retaining terms up to first order):

$$x_1=\frac{Gm_3a_1^3}{\mu a_2^3}(b_1(t)+\frac{1}{X}b_2(t))+O(X^{-\frac{10}{3}}) \tag{2.9}$$

$$y_1=\frac{Gm_3a_1^3}{\mu a_2^3}(c_1(t)+\frac{1}{X}c_2(t))+O(X^{-\frac{10}{3}}) \tag{2.10}$$

where

$$b_1(t) = -\frac{9}{4}\cos(n_1-2n_2)t-\frac{1}{4}\cos(3n_1-2n_2)t-\frac{1}{2}\cos n_1t+3 \tag{2.11}$$

$$b_2(t) = -\frac{9}{2}\cos(n_1-2n_2)t-\frac{1}{6}\cos(3n_1-2n_2)t+\frac{14}{3} \tag{2.12}$$

$$c_1(t) = -\frac{1}{4}\sin(3n_1-2n_2)t+\frac{9}{4}\sin(n_1-2n_2)t-\frac{1}{2}\sin n_1t \tag{2.13}$$

$$c_2(t) = -\frac{1}{6}\sin(3n_1-2n_2)t+\frac{9}{2}\sin(n_1-2n_2)t \tag{2.14}$$

Hence,

$$e_1=(x_1^2+y_1^2)^{\frac{1}{2}}=\frac{Gm_3a_1^3}{\mu a_2^3}((b_1(t)+\frac{1}{X}b_2(t))^2+(c_1(t)+\frac{1}{X}c_2(t))^2)^{\frac{1}{2}}\approx$$

$$\approx\frac{Gm_3a_1^3}{\mu a_2^3}[(b_1(t)^2+c_1(t)^2)^{\frac{1}{2}}+\frac{1}{X}\frac{b_1(t)b_2(t)+c_1(t)c_2(t)}{(b_1(t)^2+c_1(t)^2)^{\frac{1}{2}}}]+O(X^{-\frac{10}{3}}). \tag{2.15}$$

Thus, we are now able to estimate the average inner eccentricity, which is given by

$$\bar{e}_1=\frac{1}{T}\int_0^T e_1dt,\qquad T\to\infty. \tag{2.16}$$

(Note that T here does not denote the period.) If $x = n_1 t, y = n_2 t$, then averaging the eccentricity over t is equivalent to averaging over x and y provided that n_1 and n_2 are not commensurable (Arnold 1980). Consequently (using Mathematica for the integration),

$$\begin{aligned}\bar{e}_{in} &= \frac{Gm_3 a_1^3}{\mu a_2^3}\left(\int_0^{2\pi}\int_0^{2\pi}\frac{1}{4\pi^2}\sqrt{b_1^2+c_1^2}\,dxdy + \right. \\ &\left. + \frac{1}{X}\int_0^{2\pi}\int_0^{2\pi}\frac{1}{4\pi^2}\frac{b_1 b_2 + c_1 c_2}{\sqrt{b_1^2+c_1^2}}\,dxdy\right) = \\ &= \frac{m_3}{m_1+m_2+m_3}\frac{1}{X^2}\left(3.47266 + \frac{5.68493}{X}\right) + O(X^{-\frac{10}{3}}), \qquad (2.17)\end{aligned}$$

where the distance ratio $(\frac{a_1}{a_2})^3$ has been replaced by

$$\frac{m_1+m_2}{m_1+m_2+m_3}\frac{1}{X^2}$$

using Kepler's third law. For equal masses $m_1 = m_2 = m_3$, the previous formula becomes:

$$\bar{e}_{in} = \frac{1}{3}\frac{1}{X^2}\left(3.47266 + \frac{5.72533}{X}\right) + O(X^{-\frac{10}{3}}). \qquad (2.18)$$

Now, equation (2.1) can be expanded to first order in terms of $\frac{1}{X}$, yielding

$$\bar{e}_{in} = \frac{A}{X^2}\left(1 + \frac{1}{2}\frac{B}{X}\right). \qquad (2.19)$$

Eggleton and Kiseleva found that for equal masses $A = 1.167$ and $B = 3.814$, numbers that are in satisfactory agreement with our result, since equation (2.18) yields $A = 1.15755$ and $B = 3.8168867$.

As was mentioned earlier, Eggleton and Kiseleva's result was based on numerical integrations. The fact that there is good agreement between the theory developed above and their empirical formula is an indication of how good formula (2.18) is. But in order to quantify this, we carried out numerical integrations of the full three-body equations of motion on our own. For that purpose,

Table 2.1: Error in the mean eccentricity for systems with $m_1 = m_2 = 0.5$. The behaviour of the error is consistent with the truncation of terms of order $X^{-\frac{10}{3}}$ in equation (2.18).

a_2	$m_3 = 0.5$	$m_3 = 5$
10	3%	15%
20	0.8%	4%
50	0.2%	-

we have used a symplectic integrator with a time transformation (cf. section 1.7). The units have been chosen such that $G = 1$ and $m_1 + m_2 = 1$.

Several numerical integrations were performed for various values of the outer semi-major axis ($a_1 = 1$ in our simulations). The integrations were performed over a 10 outer orbit period span and some of these results are presented in table 2.1. Generally, the results were very good, as expected. However, there was a small discrepancy when the third mass became rather large. For $m_3 = 5$, which is 10 times each of the inner masses (among stellar triples, mass ratios are rare outside a range of 10:1, as stated in Eggleton and Kiseleva 1995) and $a_2 = 10$, the error was 15%, because of terms of order $X^{-\frac{10}{3}}$ which are not included in our formula. However, the error dropped to just 4% when the outer semi-major axis was increased to 20. It should be pointed out here that the initial aim was to investigate the behaviour of the inner eccentricity in systems with large period ratio X. Getting an error of 15% in a situation where $X = 12.9$, which is close to the lower extreme in real systems, like λ Tau and CH Cyg, is not worrying.

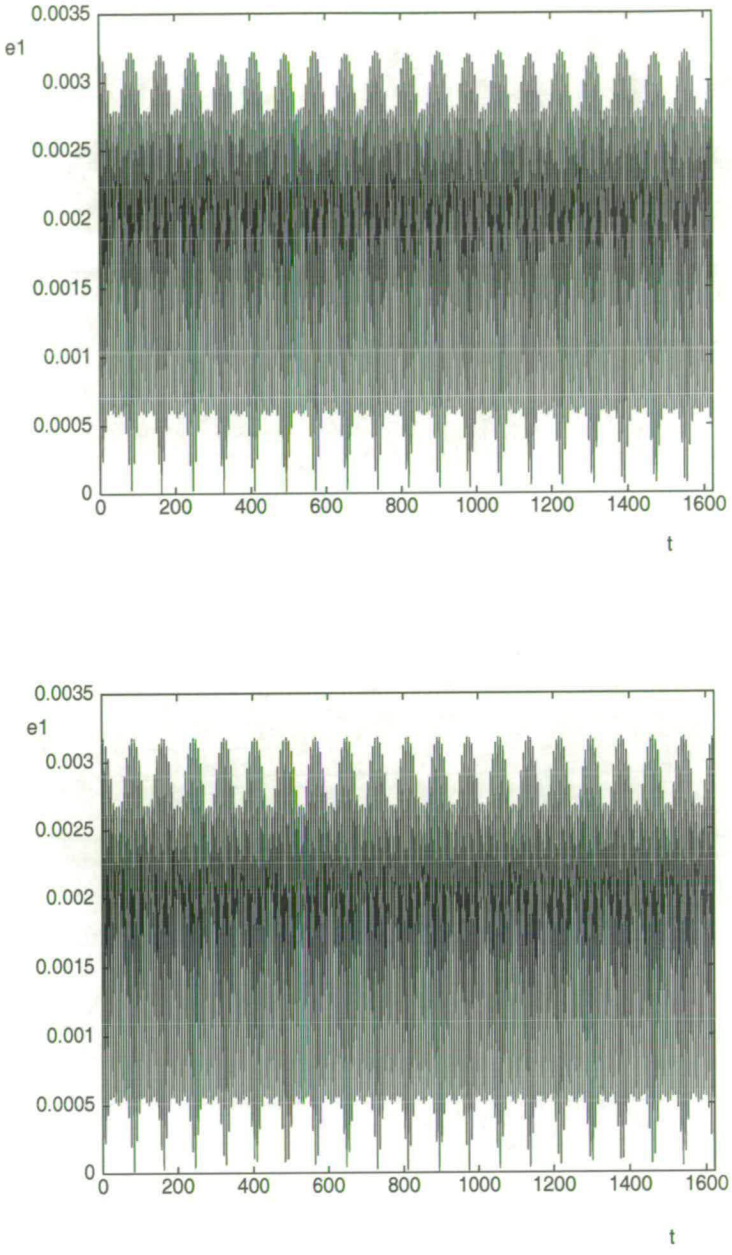

Figure 2.1: Eccentricity against time for equal masses and $a_2 = 10$. The upper graph is from the numerical integration of the full equations of motion, while the lower one is based on our theoretical model. The agreement is more than satisfactory.

2.2.2 Unequal masses, coplanar orbits, circular binaries case

The calculation of the previous section can be extended for the case of unequal masses (all three and not just the third one). This means that the perturbation will be given by equation (2.4) approximately, and following the same steps as previously (the outer binary was started 90° ahead of the inner binary and this initial configuration will hold for the rest of this chapter), we obtain:

$$x_1 = \frac{Gm_3a_1^3}{\mu a_2^3}(b_1(t) + X^{\frac{1}{3}}b_2(t)) + O(X^{-\frac{8}{3}}) \tag{2.20}$$

$$y_1 = \frac{Gm_3a_1^3}{\mu a_2^3}(c_1(t) + X^{\frac{1}{3}}c_2(t)) + O(X^{-\frac{8}{3}}) \tag{2.21}$$

with

$$b_1(t) = -\frac{1}{4}\cos(3n_1 - 2n_2)t - \frac{9}{4}\cos(n_1 - 2n_2)t - \frac{1}{2}\cos n_1 t + 3 \tag{2.22}$$

$$b_2(t) = -\frac{15}{16}M_* \sin n_2 t \tag{2.23}$$

$$c_1(t) = -\frac{1}{4}\sin(3n_1 - 2n_2)t + \frac{9}{4}\sin(n_1 - 2n_2)t - \frac{1}{2}\sin n_1 t \tag{2.24}$$

$$c_2(t) = \frac{15}{16}M_*(\cos n_2 t - 1) \tag{2.25}$$

and

$$M_* = \frac{m_2 - m_1}{(m_1 + m_2)^{\frac{2}{3}}(m_1 + m_2 + m_3)^{\frac{1}{3}}}. \tag{2.26}$$

This time, the calculation was done for $\overline{e_{in}^2}$ instead of $\bar{e}_{in}$, since the former is easier to calculate. However, that does not affect our qualitative understanding of the eccentricity behaviour (see below).

In fact, averaging over the inner and outer period yields:

$$\begin{aligned}\overline{e_{in}^2} = &\left(\frac{Gm_3a_1^3}{\mu a_2^3}\right)^2 \Big(\int_0^{2\pi}\int_0^{2\pi} \frac{1}{4\pi^2}(b_1^2 + c_1^2)dxdy + \\ &+2X^{\frac{1}{3}}\int_0^{2\pi}\int_0^{2\pi} \frac{1}{4\pi^2}(b_1b_2 + c_1c_2)dxdy +\end{aligned}$$

$$+X^{\frac{2}{3}}\int_0^{2\pi}\int_0^{2\pi}\frac{1}{4\pi^2}(b_2^2+c_2^2)dxdy) \Rightarrow$$

$$\Rightarrow \overline{e_{in}^2} = \frac{m_3^2}{(m_1+m_2+m_3)^2}\frac{1}{X^4}(\frac{115}{8}+\frac{225}{128}M_*^2X^{\frac{2}{3}})+O(X^{-\frac{13}{3}}). \quad (2.27)$$

The interesting thing here is that the dominant contribution to the eccentricity comes from the P_3 term with a factor of $X^{\frac{2}{3}}$ and not from the P_2 term, as one might expect. This is because the P_3 term varies on a timescale of the order of the period of the outer binary, while the P_2 term varies on a timescale of the order of the period of the inner binary. This is probably the reason why Eggleton and Kiseleva found that equation (2.1) did not give a good fit for some mass ratios (though unfortunately it is not known which ratios they were talking about).

It is worth mentioning that for equal masses and to leading order

$$\sqrt{\overline{e_{in}^2}} = 1.26381\frac{1}{X^2},$$

while we have already found that

$$\bar{e}_{in} = 1.15755\frac{1}{X^2}$$

to leading order, by equation (2.18). This illustrates that the mean and root mean square are almost equal.

As before, the theory was tested by running numerical integrations of the full equations of motion. Table 2.2 presents some results from these integrations. The integrations were performed for 10 outer orbital periods and the results were in good agreement with the theory. For instance, the error in the mean square eccentricity for systems with $m_1 = 0.333, m_2 = 0.667, m_3 = 1$ and semi-major axes $a_2 = 10$ (fig. 2.2), $20, 50$ were $22\%, 8\%$ and 2% respectively. Note that an error of 22% would be about double the error in the root mean square eccentricity. The approximate formula seems to fail when the outer mass gets large compared to the inner binary bodies (e.g. for $m_3 = 7$ and $a_2 = 10$, we have

Table 2.2: Error in the mean square eccentricity for systems with $m_1 = 0.333$ and $m_2 = 0.667$. The behaviour of the error is consistent with the truncation of terms of order $X^{-\frac{13}{3}}$ in equation (2.27).

a_2	$m_3 = 1$	$m_3 = 7$
10	22%	50%
20	8%	18%
50	2%	-

an error of 50%, which drops to 18% when we increase the outer semi-major axis to 20) because the perturbation is rather strong and the neglected terms of order $X^{-\frac{13}{3}}$ in equation (2.27) become important. Finally, there were also some problems with some smaller outer masses. A simulation for the same inner pair but for outer mass $m_3 = 0.2$ and $a_2 = 10$, for 200 outer orbit periods, revealed an error of 20%. As can be seen from figure 2.3, secular terms contribute to the evolution of the inner eccentricity and that explains why there was an error of 20%, although m_3 was not very large compared to the other two bodies and hence the perturbation to the motion of the inner binary was not very strong. (Note that the eccentricity is smaller than in fig. 2.2.) Here secular terms play a noticeable but minor role. They become important in the situations considered below.

2.2.3 Unequal masses, coplanar orbits, eccentric outer binary case

The last case that remains from the coplanar regime is the eccentric outer binary case. Secular terms are expected to play an important role in this case because of the non-zero outer eccentricity, as we shall see, and for investigating this case,

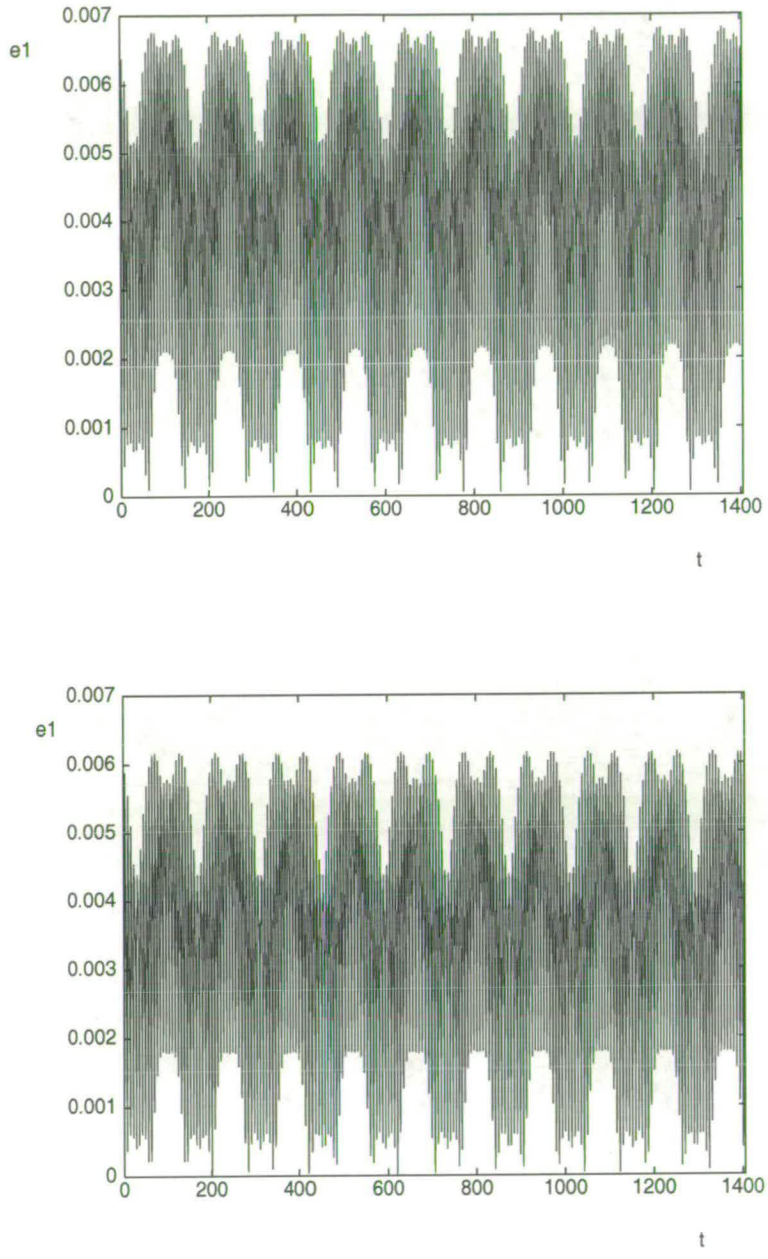

Figure 2.2: Eccentricity against time for unequal masses and $a_2 = 10$. The upper graph is from the numerical integration of the full equations of motion, while the lower one is based on our theoretical model.

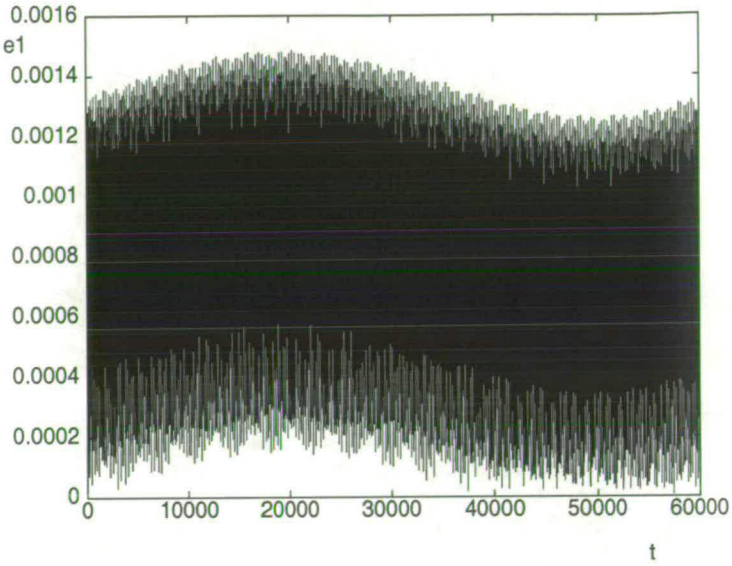

Figure 2.3: Eccentricity against time for a system with $m_1 = 0.333$, $m_2 = 0.667$, $m_3 = 0.2$ and $a_2 = 10$. The secular contribution to the inner eccentricity evolution can be clearly seen.

some elements from secular theory, which were presented in the introductory chapter (section 1.4.4), will be used.

The Hamiltonian of the averaged system is (Marchal 1990):

$$H = -\frac{G^2 m^3 (m_1 + m_2)^2}{2L_S^2} - \frac{G^2 \mathcal{M}^3 M^2}{2L_T^2} + Q + Q_1 + Q_2, \quad (2.28)$$

where

$$Q = \frac{G m m_3 a_S^2}{8 b_T^3}(-2 - 3e_S^2), \quad (2.29)$$

$$Q_1 = -\frac{75 G m m_3^2 n_T a_S^2 e_S^2 \sqrt{1 - e_S^2}}{64 M n_S a_T^3 (1 - e_T^2)^3}(3 + 2e_T^2) \quad (2.30)$$

and

$$Q_2 = \frac{15 G m m_3 (m_1 - m_2) a_S^3 e_S e_T}{64 (m_1 + m_2) b_T^4 (1 - e_T^2)^{\frac{1}{2}}} \cos(g_S - g_T)(4 + 3e_S^2), \quad (2.31)$$

with m, $\mathcal{M}$ and M were defined in section (1.4.2). The first term in the Hamiltonian is the Keplerian energy of the inner binary, the second term is the Keplerian energy of the outer binary, while the other three terms represent the interaction

between the two binaries. The Q term comes from the P_2 Legendre polynomial, the Q_2 term comes from the P_3 Legendre polynomial and the Q_1 term arises from the canonical transformation.

By using equations (1.8) and (1.9), we can now derive the averaged equations of motion of the system. However, instead of using e_S and g_S, the variables $x_S = e_S \cos g_S$ and $y_S = e_S \sin g_S$ will be used. The x_S and y_S variables, which are the components of the eccentric vector, are introduced to help us get over certain mathematical problems arising in the equations of motion, i.e. singularities resulting from the fact that e_S may be initially zero. Then, bearing in mind that $e_S = \sqrt{x_S^2 + y_S^2}$, the equations of motion of the system are:

$$\begin{aligned}
\frac{dx_S}{d\tau} &= \frac{5}{16}\alpha\frac{e_T}{(1-e_T^2)^{\frac{5}{2}}}(1-e_S^2)^{\frac{1}{2}}[(4+3e_S^2)\sin g_T + 6(x_S y_S \cos g_T + \\
&\quad + y_S^2 \sin g_T)] - [\frac{(1-e_S^2)^{\frac{1}{2}}}{(1-e_T^2)^{\frac{3}{2}}} + \frac{25}{8}\gamma\frac{3+2e_T^2}{(1-e_T^2)^3}(1-\frac{3}{2}e_S^2)]y_S \qquad (2.32)\\
\frac{dy_S}{d\tau} &= -\frac{5}{16}\alpha\frac{e_T}{(1-e_T^2)^{\frac{5}{2}}}(1-e_S^2)^{\frac{1}{2}}[(4+3e_S^2)\cos g_T + 6(x_S^2 \cos g_T + \\
&\quad + x_S y_S \sin g_T)] + [\frac{(1-e_S^2)^{\frac{1}{2}}}{(1-e_T^2)^{\frac{3}{2}}} + \frac{25}{8}\gamma\frac{3+2e_T^2}{(1-e_T^2)^3}(1-\frac{3}{2}e_S^2)]x_S \qquad (2.33)\\
\frac{dg_T}{d\tau} &= \frac{\beta(2+3e_S^2)}{2(1-e_T^2)^2} - \frac{5}{16}\frac{\alpha\beta(1+4e_T^2)}{e_T(1-e_T^2)^3}(4+3e_S^2)(x_S\cos g_T + y_S \sin g_T) + \\
&\quad + \frac{25}{8}\beta\gamma\frac{11+4e_T^2}{(1-e_T^2)^{\frac{7}{2}}}e_S^2(1-e_S^2)^{\frac{1}{2}} \qquad (2.34)\\
\frac{de_T}{d\tau} &= \frac{5}{16}\frac{\alpha\beta}{(1-e_T^2)^2}(4+3e_S^2)(y_S\cos g_T - x_S \sin g_T) \qquad (2.35)
\end{aligned}$$

where

$$\alpha = \frac{m_1 - m_2}{m_1 + m_2}\frac{a_S}{a_T}, \beta = \frac{m_1 m_2 M^{\frac{1}{2}}}{m_3(m_1+m_2)^{\frac{3}{2}}}(\frac{a_S}{a_T})^{\frac{1}{2}}, \gamma = \frac{m_3}{M^{\frac{1}{2}}(m_1+m_2)^{\frac{1}{2}}}(\frac{a_S}{a_T})^{\frac{3}{2}}$$

and

$$d\tau = \frac{3}{4}\frac{G^{\frac{1}{2}} m_3 a_S^{\frac{3}{2}}}{a_T^3 (m_1+m_2)^{\frac{1}{2}}}dt.$$

After running a few simulations for reasonable sets of parameters, using a 4th-order Runge-Kutta method with variable stepsize (Press et al. 1996), it was

noticed that e_T remained almost constant. If that approximation is taken as an assumption, terms of order e_S^2 are neglected and only the dominant terms are retained, then the system can be reduced to one that can be solved analytically:

$$\begin{aligned} \frac{dx_S}{d\tau} &= -By_S + C\sin g_T \\ \frac{dy_S}{d\tau} &= Bx_S - C\cos g_T \\ \frac{dg_T}{d\tau} &= A, \end{aligned} \tag{2.36}$$

where

$$A = \frac{\beta}{(1-e_T^2)^2}, B = \frac{1}{(1-e_T^2)^{\frac{3}{2}}} + \frac{25}{8}\gamma\frac{(3+2e_T^2)}{(1-e_T^2)^3},$$
$$C = \frac{5}{4}\alpha\frac{e_T}{(1-e_T^2)^{\frac{5}{2}}}.$$

The solution to the above system is:

$$\begin{aligned} x_S(\tau) &= (C_1 + \frac{C}{A-B}\cos g_{T0})\cos B\tau + (C_2 - \\ &\quad -\frac{C}{A-B}\frac{A}{B}\sin g_{T0})\sin B\tau - \frac{C}{A-B}\cos(A\tau + g_{T0}) \end{aligned} \tag{2.37}$$

$$\begin{aligned} y_S(\tau) &= (C_1 + \frac{C}{A-B}\cos g_{T0})\sin B\tau + (\frac{C}{A-B}\frac{A}{B}\sin g_{T0} - \\ &\quad -C_2)\cos B\tau - \frac{C}{A-B}\sin(A\tau + g_{T0}), \end{aligned} \tag{2.38}$$

where C_1, C_2 are constants of integration and g_{T0} is the initial value of the outer longitude of pericentre g_T.

Now, having calculated the secular contribution to the inner eccentricity, we can add approximate expressions for the non-secular terms by using the theory developed earlier (section 2.2.1) except that we now allow for the eccentricity of the outer orbit. In this case, the vector $\vec{R}$ is given by

$$\vec{R} = R(\cos(f_2 + \varpi_2), \sin(f_2 + \varpi_2)),$$

where f_2 is the true anomaly and ϖ_2 is the longitude of pericentre of the outer binary. To lowest order in the ratio a_1/a_2, the components of the eccentric vector now become:

$$x_1(t) = \frac{Gm_3a_1^3}{\mu a_2^3(1-e_2^2)^3}(1+e_2\cos f_2)^3[\frac{1}{4}\cos(3n_1t-2(f_2+\varpi_2))+$$
$$+\frac{9}{4}\cos(n_1t-2(f_2+\varpi_2))-\frac{1}{2}\cos n_1t]+C_x+O(X^{-\frac{5}{3}}) \quad (2.39)$$
$$y_1(t) = \frac{Gm_3a_1^3}{\mu a_2^3(1-e_2^2)^3}(1+e_2\cos f_2)^3[\frac{1}{4}\sin(3n_1t-2(f_2+\varpi_2))-$$
$$-\frac{9}{4}\sin(n_1t-2(f_2+\varpi_2))-\frac{1}{2}\sin n_1t]+C_y+O(X^{-\frac{5}{3}}) \quad (2.40)$$

in place of the leading terms in equations (2.9) and (2.10), where C_x, C_y are constants of integration. These constants can be replaced by equations (2.37) and (2.38), since $x_S(\tau)$ and $y_S(\tau)$ vary slowly compared to x_1 and y_1 of equations (2.39) and (2.40). That way, the constants C_1 and C_2 in the secular solution can be determined more accurately and an expression for the eccentricity that includes both secular and short period effects can be obtained [1].

Adding now the secular and non-secular parts, we get (after averaging):

$$\overline{e_{in}^2} = \frac{m_3^2}{(m_1+m_2+m_3)^2}\frac{1}{(1-e_2^2)^{\frac{9}{2}}}\frac{1}{X^4}(\frac{43}{8}+\frac{129}{8}e_2^2+\frac{129}{64}e_2^4)+$$
$$+(C_1+\frac{C}{A-B}\cos\varpi_{20})^2+(C_2-\frac{C}{A-B}\frac{A}{B}\sin\varpi_{20})^2+$$
$$+(\frac{C}{A-B})^2+O(X^{-\frac{7}{3}}). \quad (2.41)$$

C_1 and C_2 are determined from the initial conditions (i.e. zero initial inner eccentricity):

$$C_1 = \frac{Gm_3a_1^3}{\mu a_2^3(1-e_2^2)^3}(1+e_2\cos f_{20})^3[3-5\cos^2(f_{20}+\varpi_{20})] \quad (2.42)$$

$$C_2 = \frac{C}{B}\sin\varpi_{20}+2\frac{Gm_3a_1^3}{\mu a_2^3(1-e_2^2)^3}(1+e_2\cos f_{20})^3\sin 2(f_{20}+\varpi_{20}). \quad (2.43)$$

The validity of the above theoretical result can be checked by running several simulations for different outer masses, outer eccentricities and outer semi-major

[1] An alternative way of seeing this is to note that, in the Von Zeipel method, we effectively write $x_1 = x_S + \delta x$, where δx denotes short-period terms.

axes, using $m_1 = 0.333$ and $m_2 = 0.667$. Some of these results are shown in table 2.3. Generally, the results were in satisfactory agreement with equation (2.41). For instance, for $m_3 = 1$, $e_2 = 0.2$ and $a_2 = 10$, we had an error of 21%, which became 10% and 5% for $a_2 = 20$ (fig. 2.4) and $a_2 = 30$ respectively. For a situation where $m_3 = 1$, $e_2 = 0.7$ and $a_2 = 20$, the error was just 5%. Formula (2.41) seemed to deviate a bit from the numerical results when the outer mass was increased to $m_3 = 7$. Having an outer orbit of $e_2 = 0.2$ and with a semi major-axis of $a_2 = 10$, the error was 46%, but dropped to 29% when the outer semi-major axis was doubled. That is a reasonable result, considering that the perturbation is strong for that combination of outer mass and distance. The reason for the discrepancy is that the eccentricity evolution is dominated by short period terms, which are included in our calculations only at lowest order. Apparently, there are situations where the contribution of terms of order $X^{-\frac{5}{3}}$ in equations (2.39) and (2.40) is significant. Of course, it would always be possible to improve the theory by adding more short period terms to obtain satisfactory agreement for this problem. No matter how good the approximation is, there will always be some range of parameters where it becomes unsatisfactory.

Finally, it is clear from the solution for the secular part of the eccentricity (equations [2.37] and [2.38]) that, when $A - B = 0$, the eccentricity is expected to become infinite. But since A is the frequency of the outer pericentre and B is the frequency of the inner one, it means that we are dealing with a secular resonance, i.e. the two secular frequencies are nearly equal. Although equations (2.37) and (2.38) can not describe the eccentricity evolution in this case, they can be used to determine the location of the resonance by solving the equation $A - B = 0$. After substituting, the latter leads to

$$\frac{m_1 m_2 M^{\frac{1}{2}}}{m_3 (m_1 + m_2)^{\frac{3}{2}}} (\frac{a_S}{a_T})^{\frac{1}{2}} (1 - e_T^2) - (1 - e_T^2)^{\frac{3}{2}} - \frac{25}{8} \frac{m_3}{M^{\frac{1}{2}} (m_1 + m_2)^{\frac{1}{2}}} \times$$

Table 2.3: Error in the mean square eccentricity for systems with $m_1 = 0.333$ and $m_2 = 0.667$. The behaviour of the error is in satisfactory agreement with the truncation of terms of order $X^{-\frac{7}{3}}$ in equation (2.41).

m_3	a_2	e_2	Error
1	10	0.2	21%
1	20	0.2	10%
1	30	0.2	5%
1	20	0.7	5%
7	10	0.2	46%
7	20	0.2	29%

$$\times(\frac{a_S}{a_T})^{\frac{3}{2}}(3 + 2e_T^2) = 0. \tag{2.44}$$

Therefore, there are sets of orbital parameters which satisfy the above equation and for which the evolution of a triple system is driven by the secular resonance. Figure 2.5 is an example of such a situation.

2.2.4 Unequal masses,non-coplanar orbits, eccentric outer binary case

In this case, something similar to the coplanar case might be expected to happen. Here, however, the approach to the problem is slighty more complex due to the inclination I of the two planes of motion. The investigation of the inner eccentricity of non-coplanar orbits with an eccentric outer binary will be carried out in two parts:

$$(i) \qquad I_0 < 39.23^\circ \quad or \quad I_0 > 140.77^\circ$$

$$(ii) \qquad 39.23^\circ < I_0 < 140.77^\circ,$$

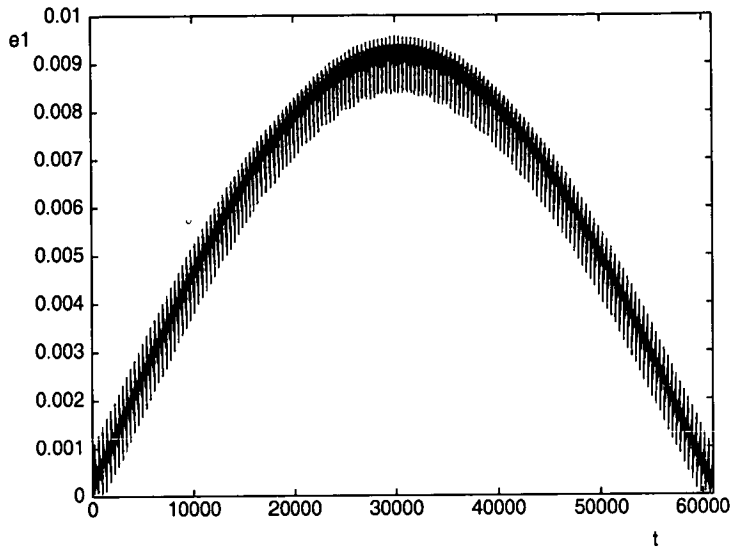

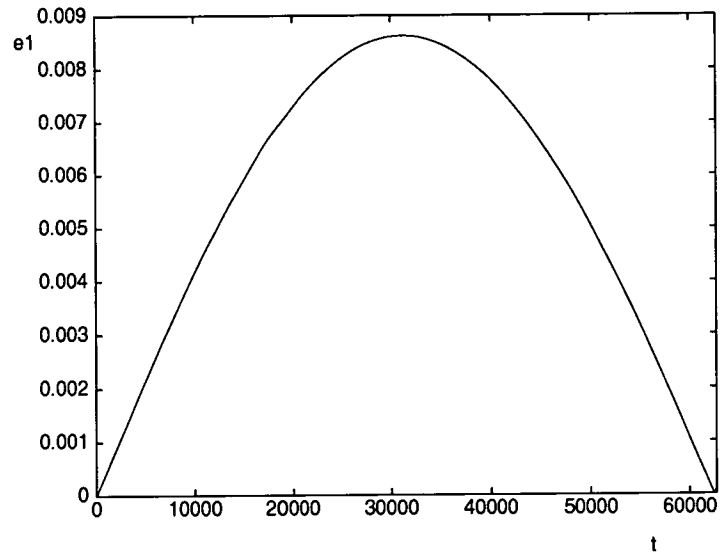

Figure 2.4: Eccentricity against time for $m_1 = 0.333, m_2 = 0.667, m_3 = 1, a_2 = 20$ and $e_2 = 0.2$. The upper graph is from the numerical integration of the full equations of motion, while the lower graph is based on equations (2.37) and (2.38). The spikes in the upper graph are the effects of the short period terms in the evolution of the inner eccentricity.

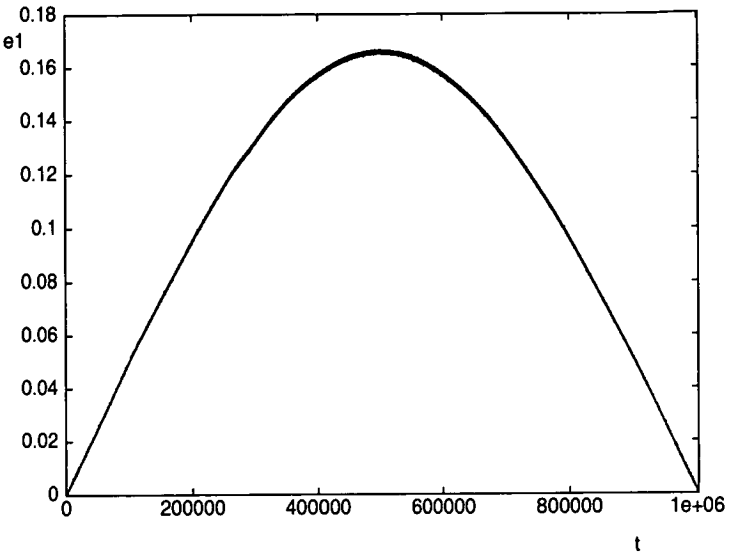

Figure 2.5: Secular resonance between the two pericentre frequencies for $m_1 = 0.333, m_2 = 0.667, m_3 = 0.07, a_2 = 10$ and $e_2 = 0.2$. Note the very long period.

where I_0 is the initial inclination of the two orbits. The reason for this split is that, as we shall see shortly, in case (i), $e_S = 0$ is a stable equilibrium point for the secular problem, while in case (ii), the equilibrium point is unstable and, though the eccentricity is initially zero, we can end up with a large eccentricity, even $e_1 = 1$.

In the quadrupole level of approximation, if we define x as $x = 1 - e_S^2$, then we can write (Marchal 1990)

$$\dot{x} = \pm C[P_1(x)P_2(x)]^{\frac{1}{2}} \tag{2.45}$$

where

$$\begin{aligned} P_1(x) &= 5e_S^2 \sin^2 I \sin^2 g_S \\ P_2(x) &= 5e_S^2(1 - e_S^2) \sin^2 I \cos^2 g_S \end{aligned}$$

and C is a constant depending on masses and constant orbital parameters. At

lowest order in the averaged problem, the quantities

$$A = \sqrt{1 - e_S^2}\cos I$$

$$Z = (1 - e_S^2)(1 + \sin^2 I) + 5e_S^2 \sin^2 I \sin^2 g_S$$

are constants. The first is proportional to the component of the inner angular momentum parallel to the total angular momentum, while the second arises from the fact the Q term in the Hamiltonian is constant (equation 2.50). (It must be noted that A is different from the constant denoted by the same symbols in previous sections). In terms of these constants we may write

$$P_1(x) = -2x + Z + A^2 \tag{2.46}$$

$$P_2(x) = -3x^2 + x(5 - Z + 4A^2) - 5A^2. \tag{2.47}$$

Equation (2.45) can be rewritten as

$$\dot{x}^2 = C^2 P_1(x) P_2(x) \tag{2.48}$$

and then, by differentiating the above equation, one can obtain:

$$\ddot{x} = \frac{1}{2} C^2 (P_1'(x) P_2(x) + P_1(x) P_2'(x)). \tag{2.49}$$

A Taylor expansion of the right hand side of equation (2.49) up to first order with respect to x and around $x = 1$, yields:

$$\ddot{x} = C^2 P_1'(1) P_2'(1)(x - 1).$$

Consequently, depending on the sign of $P_1'(1)P_2'(1)$, $x = 1$ (i.e. $e_S = 0$) can be a stable or an unstable equilibrium point. But

$$P_1'(1)P_2'(1) = -2(5\cos^2 I - 3),$$

which is negative (stable) for

$$I_0 < 39.23^\circ \quad or \quad I_0 > 140.77^\circ$$

and positive (unstable) for

$$39.23^\circ < I_0 < 140.77^\circ.$$

The Low Inclination Regime ($I_0 < 39.23°$ or $I_0 > 140.77°$)

The Hamiltonian of the system is of the same form as (2.28), but with:

$$Q = \frac{Gmm_3a_S^2}{8b_T^3}[-2-3e_S^2+3\sin^2 I(1-e_S^2+5e_S^2\sin^2 g_S)] \tag{2.50}$$

$$Q_1 = -\frac{3Gmm_3^2n_Ta_S^2\sqrt{1-e_S^2}}{64Mn_Sa_T^3(1-e_T^2)^3}(3+2e_T^2)\cos I[25e_S^2+\sin^2 I(1- \\ -e_S^2-15e_S^2\sin^2 g_S)] \tag{2.51}$$

$$Q_2 = \frac{15Gmm_3(m_1-m_2)a_S^3e_Se_T}{64(m_1+m_2)b_T^4(1-e_T^2)^{\frac{1}{2}}}[(\sin g_S\sin g_T\cos I + \\ +\cos g_S\cos g_T)(4+3e_S^2-5\sin^2 I(1-e_S^2+7e_S^2\sin^2 g_S))- \\ -10(1-e_S^2)\sin^2 I\cos I\sin g_S\sin g_T]. \tag{2.52}$$

After some exploratory numerical integrations of the five equations of motion of the system (see Appendix A), it became clear that the outer eccentricity and the inclination remained almost constant. That, along with the fact that the inner eccentricity was not expected to reach large values (which justifies neglecting powers of x_S and y_S above the first order), was used to produce a simpler system of differential equations. Thus, the system assumes the following form:

$$\begin{aligned}\frac{dg_T}{d\tau} &= A \\ \frac{dx_S}{d\tau} &= -By_S + C\sin g_T \\ \frac{dy_S}{d\tau} &= Dx_S - E\cos g_T\end{aligned} \tag{2.53}$$

where

$$A = \frac{\cos I}{(1-e_T^2)^{\frac{3}{2}}}+\frac{1}{2}\frac{\beta(4-5\sin^2 I)}{(1-e_T^2)^2}-\frac{1}{16}\frac{\gamma(3+2e_T^2)(2-3\sin^2 I)}{(1-e_T^2)^3}$$

$$B = \frac{2-5\sin^2 I}{(1-e_T^2)^{\frac{3}{2}}}+\frac{\beta\cos I}{(1-e_T^2)^2}-\frac{\gamma(3+2e_T^2)\cos I(\frac{15}{8}\sin^2 I-3)}{(1-e_T^2)^3}$$

$$
\begin{aligned}
C &= \frac{5}{16}\frac{\alpha e_T \cos I(4-15\sin^2 I)}{(1-e_T^2)^{\frac{5}{2}}} \\
D &= \frac{2}{(1-e_T^2)^{\frac{3}{2}}} + \frac{\beta\cos I}{(1-e_T^2)^2} + 3\frac{\gamma(3+2e_T^2)\cos I}{(1-e_T^2)^3} \\
E &= \frac{5}{16}\frac{\alpha e_T(4-5\sin^2 I)}{(1-e_T^2)^{\frac{5}{2}}}
\end{aligned}
$$

and $\alpha, \beta, \gamma, \tau$ have the same meaning as in section (2.2.3). The above system, which differs from system (2.36) because of the way g_T is defined in the non-coplanar regime ($g_T = \varpi_T - \Omega_T$), can be solved analytically, yielding:

$$
\begin{aligned}
x_S(\tau) &= (C_1 + \frac{AC+BE}{A^2-BD}\cos g_{T0})\cos\sqrt{BD}\tau + (C_2 - \\
&\quad -\frac{AC+BE}{A^2-BD}\frac{A}{\sqrt{BD}}\sin g_{T0})\sin\sqrt{BD}\tau - \\
&\quad -\frac{AC+BE}{A^2-BD}\cos(A\tau + g_{T0}) \qquad (2.54) \\
y_S(\tau) &= (\frac{C}{B} - \frac{AC+BE}{A^2-BD}\frac{A}{B})\sin(A\tau + g_{T0}) + \sqrt{\frac{D}{B}}(C_1 + \\
&\quad +\frac{AC+BE}{A^2-BD}\cos g_{T0})\sin\sqrt{BD}\tau + (\frac{AC+BE}{A^2-BD}\frac{A}{B}\sin g_{T0} - \\
&\quad -\sqrt{\frac{D}{B}}C_2)\cos\sqrt{BD}\tau, \qquad (2.55)
\end{aligned}
$$

with C_1, C_2 constants of integration.

Again, in order to produce a more accurate formula, some short period effects in the evolution of the eccentricity were calculated, by using the technique described earlier. If a frame of reference is chosen such that the line of nodes is initially on the x-axis, with the positive direction of the x-axis pointing at the ascending node of the outer orbit, $\vec{r} = a_1(\cos nt, \sin nt, 0)$ and

$$
\vec{R} = R(\cos(f_2 + \varpi_2), \cos I \sin(f_2 + \varpi_2), \sin I \sin(f_2 + \varpi_2)),
$$

(because of the above choice of coordinate system the argument and the longitude of pericentre coincide initially), expand in powers of $\frac{1}{X}$ and retain the leading term, we arrive at

$$
\begin{aligned}
x_1 &= \frac{Gm_3a_1^3}{\mu a_2^3(1-e_2^2)^3}(1+e_2\cos f_2)^3\{\frac{1}{16}\cos(3n_1t-2(f_2+\varpi_2))+\\
&+\frac{1}{16}\cos(3n_1t+2(f_2+\varpi_2))+\frac{3}{16}\cos(n_1t-2(f_2+\varpi_2))+\\
&+\frac{3}{16}\cos(n_1t+2(f_2+\varpi_2))+\frac{11}{8}\cos n_1t+\frac{1}{8}\cos 3n_1t+\\
&+\cos I[\frac{9}{8}\cos(n_1t-2(f_2+\varpi_2))-\\
&-\frac{9}{8}\cos(n_1t+2(f_2+\varpi_2))+\frac{1}{8}\cos(3n_1t-2(f_2+\varpi_2))-\\
&-\frac{1}{8}\cos(3n_1t+2(f_2+\varpi_2))]+\cos^2 I[-\frac{1}{8}\cos 3n_1t-\frac{15}{8}\cos n_1t+\\
&+\frac{1}{16}\cos(3n_1t-2(f_2+\varpi_2))+\frac{1}{16}\cos(3n_1t+2(f_2+\varpi_2))+\\
&+\frac{15}{16}\cos(n_1t-2(f_2+\varpi_2))+\frac{15}{16}\cos(n_1t+2(f_2+\varpi_2))]\}+\\
&+C_x+O(X^{-\frac{5}{3}}) \qquad (2.56)\\
y_1 &= \frac{Gm_3a_1^3}{\mu a_2^3(1-e_2^2)^3}(1+e_2\cos f_2)^3\{\frac{1}{16}\sin(3n_1t+2(f_2+\varpi_2))+\\
&+\frac{1}{16}\sin(3n_1t-2(f_2+\varpi_2))-\frac{15}{16}\sin(n_1t+2(f_2+\varpi_2))-\\
&-\frac{15}{16}\sin(n_1t-2(f_2+\varpi_2))-\frac{7}{8}\sin n_1t+\frac{1}{8}\sin 3n_1t+\\
&+\cos I[\frac{9}{8}\sin(n_1t+2(f_2+\varpi_2))-\\
&-\frac{9}{8}\sin(n_1t-2(f_2+\varpi_2))+\frac{1}{8}\sin(3n_1t-2(f_2+\varpi_2))-\\
&-\frac{1}{8}\sin(3n_1t+2(f_2+\varpi_2))]+\cos^2 I[-\frac{1}{8}\sin 3n_1t+\frac{3}{8}\sin n_1t+\\
&+\frac{1}{16}\sin(3n_1t-2(f_2+\varpi_2))+\frac{1}{16}\sin(3n_1t+2(f_2+\varpi_2))-\\
&-\frac{3}{16}\sin(n_1t-2(f_2+\varpi_2))-\frac{3}{16}\sin(n_1t+2(f_2+\varpi_2))]\}+\\
&+C_y+O(X^{-\frac{5}{3}}) \qquad (2.57)
\end{aligned}
$$

with C_x, C_y constants of integration. It should be mentioned here that, in the calculation for short period terms in the components of the inner eccentric vector, ϖ_2 was treated as a constant parameter. Furthermore, because the orbital binary planes are inclined to each other, the inner binary plane is expected to precess, with its normal moving on a conical surface which has for its axis the

normal of the outer binary plane approximately. Because of this additional motion, the orientation of the line of nodes will not be the same throughout the orbital evolution of the triple system. However, for the calculation of the short period terms, we can neglect that additional motion (and all secular evolution), without significant error.

Finally, combining the secular and non-secular terms as in section (2.2.3), after averaging we obtain:

$$\begin{aligned}
\overline{e_1^2} &= \frac{m_3^2}{(m_1+m_2+m_3)^2}\frac{1}{(1-e_2^2)^{\frac{9}{2}}}\frac{1}{X^4}\{\frac{145}{64}+e_2^2(\frac{435}{64}+ \\
&+\frac{105}{32}\cos 2\varpi_{20})+e_2^4(\frac{435}{512}+\frac{35}{64}\cos 2\varpi_{20}+\frac{59}{1024}\cos 4\varpi_{20})+ \\
&+\cos^2 I[\frac{11}{32}+e_2^2(\frac{33}{32}+\frac{9}{4}\cos 2\varpi_{20})+e_2^4(\frac{33}{256}+\frac{3}{8}\cos 2\varpi_{20}- \\
&-\frac{59}{512}\cos 4\varpi_{20})]+\cos^4 I[\frac{177}{64}+e_2^2(\frac{531}{64}-\frac{177}{32}\cos 2\varpi_{20})+ \\
&+e_2^4(\frac{531}{512}-\frac{59}{64}\cos 2\varpi_{20}+\frac{59}{1024}\cos 4\varpi_{20})]\}+ \\
&+\frac{1}{2}[(1+\frac{D}{B})(C_1-\frac{AC+BE}{A^2-BD}\cos\varpi_{20})^2+(1+\frac{D}{B})\times \\
&\times(C_2+\frac{AC+BE}{A^2-BD}\frac{A}{\sqrt{BD}}\sin\varpi_{20})^2+(\frac{AC+BE}{A^2-BD})^2+ \\
&+(\frac{C}{B}-\frac{AC+BE}{A^2-BD}\frac{A}{B})^2]+O(X^{-\frac{7}{3}}), \qquad (2.58)
\end{aligned}$$

with C_1 and C_2 determined by the zero initial eccentricity as follows:

$$\begin{aligned}
C_1 &= -\frac{Gm_3a_1^3}{\mu a_2^3(1-e_2^2)^3}(1+e_2\cos f_{20})^3[4\cos^2 I\sin^2(f_{20}+\varpi_{20})- \\
&-1-\cos^2(f_{20}+\varpi_{20})] \qquad (2.59) \\
C_2 &= -\sqrt{\frac{B}{D}}[2\frac{Gm_3a_1^3}{\mu a_2^3(1-e_2^2)^3}(1+e_2\cos f_{20})^3\cos I\sin 2(f_{20}+\varpi_{20})+ \\
&+\frac{C}{B}\sin\varpi_{20}]. \qquad (2.60)
\end{aligned}$$

To check these results, several simulations were performed, using various values for the orbital elements of the outer orbit (inclination, eccentricity, semi-major axis). The results were in good agreement with the theory, except again in

Table 2.4: Error in the mean square eccentricity for systems with $m_1 = 0.333$ and $m_2 = 0.667$ and $I = 15°$. The behaviour of the error is in satisfactory agreement with the truncation of terms of order $X^{-\frac{7}{3}}$ in equation (2.58).

m_3	a_2	e_2	Error
1	10	0.2	21%
1	20	0.2	10%
1	30	0.2	5%
1	20	0.7	8%
7	10	0.2	45%
7	20	0.2	28%

the case of large third mass and when the parameters of the hierarchical system led to very small values of the quantity $A - \sqrt{BD}$ in equations (2.54) and (2.55), i.e. when we were near a secular resonance between the two pericentre frequencies.

To get an idea of how well the theory works, we present some results in table 2.4 and figure 2.6 for $I = 15°$. Again, several systems with $m_1 = 0.333$, $m_2 = 0.667$ and $m_3 = 1$ were integrated. Starting the outer binary at apocentre, with $e_2 = 0.2$ and $a_2 = 10$, the error was 21%, which was reduced significantly as the third star moved outwards (10% and 5% for $a_2 = 20$ and $a_2 = 30$ respectively). The theory worked well even when the outer eccentricity was increased to $e_2 = 0.7$. For $a_2 = 20$ the error was just 8%. Finally, for $m_3 = 7$, $e_2 = 0.2$ and $a_2 = 10$ the error rose to 45%, and dropped, as expected, to 28% as the outer semi-major axis was increased to $a_2 = 20$. It is worth mentioning that comparing the results of tables 2.3 and 2.4, it appears that the error in the mean square eccentricity is roughly independent of the inclination of the orbits.

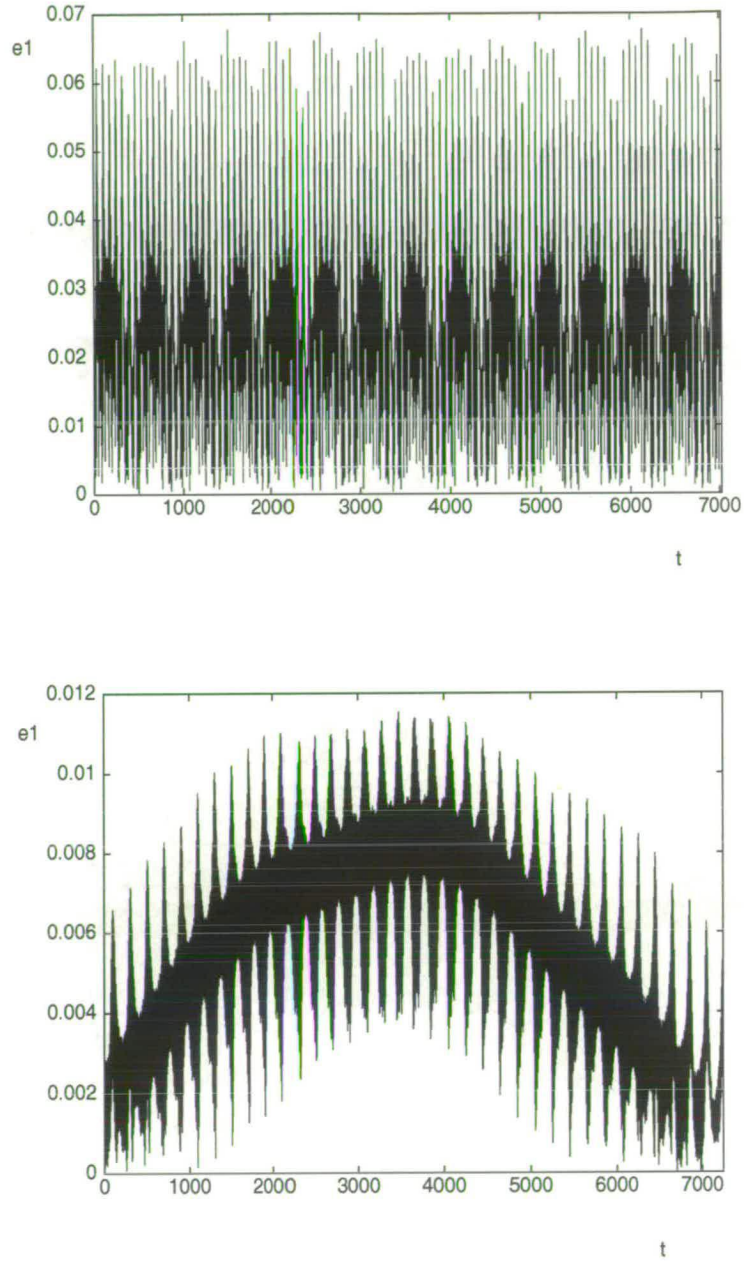

Figure 2.6: Eccentricity against time for $I = 15°$. The upper graph is from a numerical integration of a triple system with $m_3 = 7$, $e_2 = 0.2$ and $a_2 = 10$, while the lower graph is from a numerical integration of the same system, but with $a_2 = 20$. It is very clear that, in the upper graph, the eccentricity evolution is dominated by short period terms, while in the lower graph, the secular contribution can be easily noted.

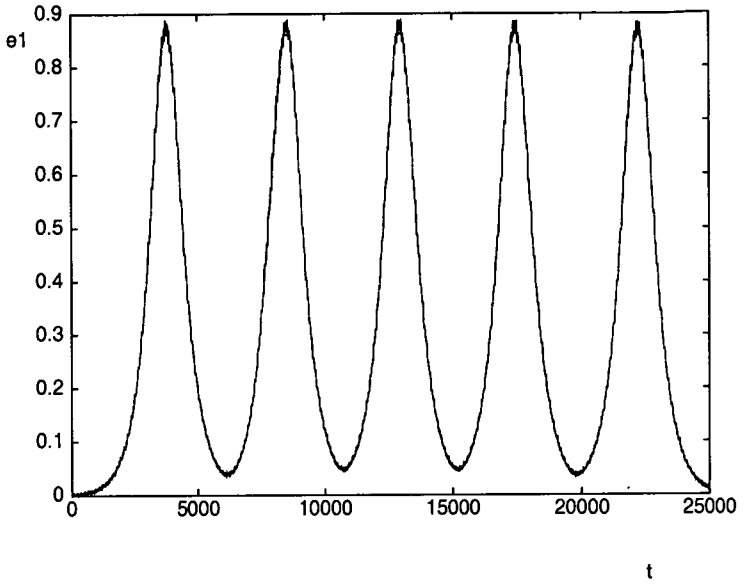

Figure 2.7: An example of inner eccentricity evolution in the high inclination regime. The integration parameters are: $m_1 = 0.333$, $m_2 = 0.667$, $m_3 = 1$, $a_2 = 10$, $e_2 = 0.2$ and $I = 70°$.

The High Inclination Regime ($39.23° < I_0 < 140.77°$)

As was mentioned earlier, the zero eccentricity is an unstable equilibrium point of the secular equations for $39.23° < I_0 < 140.77°$. In this case, short period terms and the secular P_3 term will provide us with the initial perturbation we need to create a non-zero eccentricity. (Recall that $e_S = 0$ is an equilibrium point for the secular P_2 problem.) Thus, at the early stages of the evolution of the eccentricity and while it is still small, the motion will be controlled by the P_2 and the P_3 terms. As soon as the eccentricity becomes significant, however, the motion is dominated by the P_2 term. Although the problem is integrable if one considers a perturbing Hamiltonian expansion with just the P_2 term (cf. equation [2.50]), the use of the P_3 term is necessary, if we want to obtain the right period of the oscillation in e_S (Ford, Kozinsky and Rasio 2000).

Although it is possible to obtain a solution for the secular P_2 problem in terms of elliptic functions, we will only derive an expression for the maximum

value of the eccentricity in the high inclination regime (at the quadrupole level of the approximation). As seen in the previous subsection,

$$\dot{x} = \pm C[P_1(x)P_2(x)]^{\frac{1}{2}} \tag{2.61}$$

Thus, the maximum value for e_S can be obtained by solving the equation

$$\dot{x} = 0. \tag{2.62}$$

Using the fact that e_S is initially nearly zero, which yields that $Z = 2 - A^2$, we finally find that

$$e_{max} = \sqrt{1 - \frac{5}{3}\cos^2 I_0} \tag{2.63}$$

if $|\cos I| < \sqrt{\frac{3}{5}}$. For example, $e_{\max} \approx 0.90$ when $I_0 = 70°$ (fig. 2.7). It becomes clear from the above formula that when $I_0 = 90°$, the secular eccentricity becomes one. The above result also helps to explain the distinction between high and low inclination regimes, as the boundary at $\cos^{-1}\sqrt{\frac{3}{5}} = 39.23°$ approximately coincides with the change of stability. It should be mentioned here that the high inclination regime was first investigated in the context of the asteroidal motion in the solar system by Kozai (1962).

2.2.5 Unequal masses, non-coplanar orbits, circular binaries case

In this case, as can be seen from equations (2.52), there is no secular contribution from the P_3 term, due to the fact that the outer binary is circular. (More correctly, there will be some, because of eccentricity generated in the outer binary by perturbation, but it will be tiny.)

The short period terms were obtained in the usual way, using

$$\vec{R} = R(-\sin n_2 t, \cos I \cos n_2 t, \sin I \cos n_2 t),$$

while for the secular part we used system (2.53), after setting $e_T = 0$. The components of the eccentric vector are in this case (including secular and non secular parts)

$$
\begin{aligned}
x_1 \;=\; & \frac{Gm_3a_1^3}{\mu a_2^3}\{\frac{11}{8}\cos n_1t + \frac{1}{8}\cos 3n_1t - \frac{1}{16}\cos(3n_1 - 2n_2)t - \\
& -\frac{1}{16}\cos(3n_1 + 2n_2)t - \frac{3}{16}\cos(n_1 - 2n_2)t - \\
& -\frac{3}{16}\cos(n_1 + 2n_2)t + \cos I[\frac{1}{8}\cos(3n_1t + 2n_2)t - \\
& -\frac{1}{8}\cos(3n_1t - 2n_2)t + \frac{9}{8}\cos(n_1t + 2n_2)t - \\
& -\frac{9}{8}\cos(n_1t - 2n_2)t] + \cos^2 I[-\frac{1}{16}\cos(3n_1t - 2n_2)t - \\
& -\frac{1}{16}\cos(3n_1t + 2n_2)t - \frac{15}{16}\cos(n_1t - 2n_2)t - \\
& -\frac{15}{16}\cos(n_1t + 2n_2)t - \frac{1}{8}\cos 3n_1t - \frac{15}{8}\cos n_1t] + \\
& +M_*X^{\frac{1}{3}}[\cos I(-\frac{25}{64}\sin 3n_2t - \frac{165}{64}\sin n_2t) + \\
& +\cos^3 I(\frac{225}{64}\sin n_2t + \frac{25}{64}\sin 3n_2t)] + (4\cos^2 I - \\
& -1)\cos\sqrt{BD}\tau + M_*X^{\frac{1}{3}}\sqrt{\frac{B}{D}}(\frac{5}{8} - \frac{25}{16}\cos^2 I)\sin\sqrt{BD}\tau]\} + \\
& +O(X^{-\frac{8}{3}}) \qquad (2.64)\\
y_1 \;=\; & \frac{Gm_3a_1^3}{\mu a_2^3}\{-\frac{7}{8}\sin n_1t + \frac{1}{8}\sin 3n_1t - \frac{1}{16}\sin(3n_1 - 2n_2)t - \\
& -\frac{1}{16}\sin(3n_1 + 2n_2)t + \frac{15}{16}\sin(n_1 - 2n_2)t + \\
& +\frac{15}{16}\cos(n_1 + 2n_2)t + \cos I[\frac{1}{8}\sin(3n_1t + 2n_2)t - \\
& -\frac{1}{8}\sin(3n_1t - 2n_2)t - \frac{9}{8}\sin(n_1t + 2n_2)t + \\
& +\frac{9}{8}\sin(n_1t - 2n_2)t] + \cos^2 I[-\frac{1}{16}\sin(3n_1t - 2n_2)t - \\
& -\frac{1}{16}\sin(3n_1t + 2n_2)t + \frac{3}{16}\sin(n_1t - 2n_2)t + \\
& +\frac{3}{16}\sin(n_1t + 2n_2)t - \frac{1}{8}\sin 3n_1t + \frac{3}{8}\sin n_1t] + \\
& +M_*X^{\frac{1}{3}}[\frac{25}{64}\cos 3n_2t + \frac{15}{64}\cos n_2t + \\
& +\cos^2 I(-\frac{75}{64}\cos n_2t - \frac{25}{64}\cos 3n_2t)] +
\end{aligned}
$$

$$+\sqrt{\frac{D}{B}}(4\cos^2 I - 1)\sin\sqrt{BD}\tau -$$
$$-M_* X^{\frac{1}{3}}(\frac{5}{8} - \frac{25}{16}\cos^2 I)\cos\sqrt{BD}\tau\} + O(X^{-\frac{8}{3}}), \quad (2.65)$$

where B and D are the same as in system (2.53) but with $e_T = 0$. After the usual averaging, we obtain:

$$\begin{aligned}\overline{e_{in}^2} &= \frac{m_3^2}{(m_1+m_2+m_3)^2}\frac{1}{X^4}\{\frac{145}{64} + \frac{11}{32}\cos^2 I + \frac{177}{64}\cos^4 I + \\ &+M_*^2 X^{\frac{2}{3}}(\frac{425}{4096} + \frac{12175}{4096}\cos^2 I - \frac{34625}{4096}\cos^4 I + \\ &+\frac{25625}{4096}\cos^6 I) + \frac{1}{2}(1+\frac{D}{B})[(4\cos^2 I - 1)^2 + \\ &+M_*^2 X^{\frac{2}{3}}\frac{B}{D}(\frac{5}{8} - \frac{25}{16}\cos^2 I)^2]\} + O(X^{-\frac{13}{3}}). \quad (2.66)\end{aligned}$$

The above equation is not completely obtainable from equation (2.58) by setting $e_2 = 0$, because equation (2.66) is deduced from the averaging of equations (2.64) and (2.65), which include more short period terms compared to the equations which were averaged to produce equation (2.58).

The numerical tests did not reveal any surprises. The eccentricity was driven mainly by short period terms plus some secular contribution from the P_2 term. The formula works very well except when we enter the high inclination regime ($39.23° < I < 140.77°$) and we get large eccentricity values. Considering again $m_1 = 0.333$, $m_2 = 0.667$, $m_3 = 1$, $I = 20°$ and varying the outer semi-major axis, the error was 20%, 9% and 6% for $a_2 = 10$ (fig. 2.8), $a_2 = 20$ and $a_2 = 30$ respectively. The usual problems arose when we took $m_3 = 7$, because of terms of order $X^{-\frac{13}{3}}$ neglected in equation (2.66).

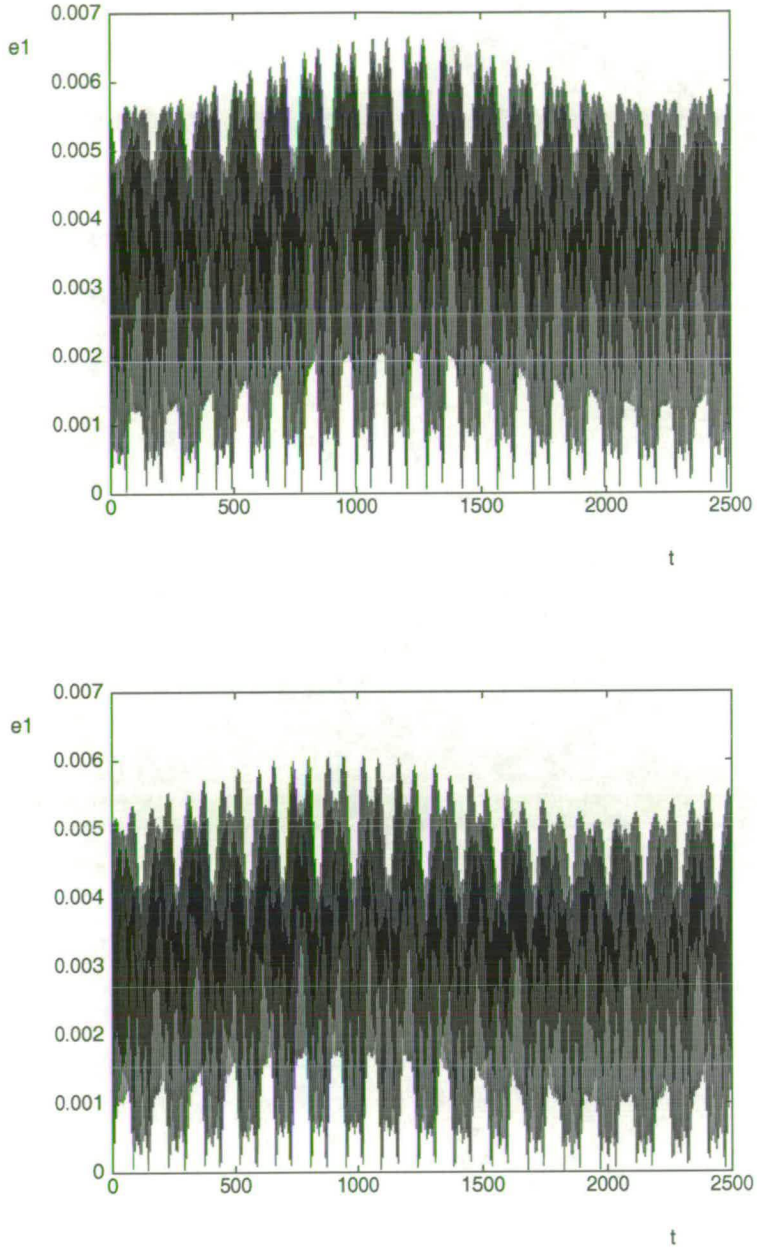

Figure 2.8: Eccentricity against time for $m_1 = 0.333, m_2 = 0.667, m_3 = 1, a_2 = 10$ and $I = 20°$. The upper graph is from the numerical integration of the full equations of motion, while the lower one is based on the theoretical model.

2.2.6 Equal masses,non-coplanar orbits, eccentric outer binary case

Finally, for the completeness of the problem, $\overline{e_{in}^2}$ is calculated for the case of equal masses, non coplanar orbits and eccentric outer binary. The equal masses have the same effect as the zero outer eccentricity, i.e. there is no secular contribution from the P_3 term and not even short period terms. The secular solution can be obtained from system (2.53) by setting $m_1 = m_2$, while the short period terms can be obtained by following the usual procedure and choosing

$$\vec{R} = R(\cos(f_2 + \varpi_2), \cos I \sin(f_2 + \varpi_2), \sin I \sin(f_2 + \varpi_2)).$$

The components of the eccentric vector are (combining secular and non-secular parts):

$$\begin{aligned}
x_1 &= \frac{Gm_3a_1^3}{\mu a_2^3(1-e_2^2)^3}[(1+e_2\cos f_2)^3[\frac{1}{16}\cos(3n_1t - 2(f_2+\varpi_2)) + \\
&+\frac{1}{16}\cos(3n_1t + 2(f_2+\varpi_2)) + \frac{3}{16}\cos(n_1t - 2(f_2+\varpi_2)) + \\
&+\frac{3}{16}\cos(n_1t + 2(f_2+\varpi_2)) + \frac{11}{8}\cos n_1t + \frac{1}{8}\cos 3n_1t + \\
&+\cos I[\frac{9}{8}\cos(n_1t - 2(f_2+\varpi_2)) - \\
&-\frac{9}{8}\cos(n_1t + 2(f_2+\varpi_2)) + \frac{1}{8}\cos(3n_1t - 2(f_2+\varpi_2)) - \\
&-\frac{1}{8}\cos(3n_1t + 2(f_2+\varpi_2))] + \cos^2 I[-\frac{1}{8}\cos 3n_1t - \frac{15}{8}\cos n_1t + \\
&+\frac{1}{16}\cos(3n_1t - 2(f_2+\varpi_2)) + \frac{1}{16}\cos(3n_1t + 2(f_2+\varpi_2)) + \\
&+\frac{15}{16}\cos(n_1t - 2(f_2+\varpi_2)) + \frac{15}{16}\cos(n_1t + 2(f_2+\varpi_2))]] - \\
&-(1+e_2\cos f_{20})^3(\cos^2(f_{20}+\varpi_{20}) + 1 - \\
&-4\sin^2(f_{20}+\varpi_{20})\cos^2 I)\cos\sqrt{BD}\tau + 2\sqrt{\frac{B}{D}}(1 + \\
&+e_2\cos f_{20})^3\sin 2(f_{20}+\varpi_{20})\cos I\sin\sqrt{BD}\tau] + O(X^{-3}) \qquad (2.67) \\
y_1 &= \frac{Gm_3a_1^3}{\mu a_2^3(1-e_2^2)^3}[(1+e_2\cos f_2)^3[\frac{1}{16}\sin(3n_1t + 2(f_2+\varpi_2)) +
\end{aligned}$$

$$+\frac{1}{16}\sin(3n_1t-2(f_2+\varpi_2))-\frac{15}{16}\sin(n_1t+2(f_2+\varpi_2))-$$
$$-\frac{15}{16}\sin(n_1t-2(f_2+\varpi_2))-\frac{7}{8}\sin n_1t+\frac{1}{8}\sin 3n_1t+$$
$$+\cos I[\frac{9}{8}\sin(n_1t+2(f_2+\varpi_2))-$$
$$-\frac{9}{8}\sin(n_1t-2(f_2+\varpi_2))+\frac{1}{8}\sin(3n_1t-2(f_2+\varpi_2))-$$
$$-\frac{1}{8}\sin(3n_1t+2(f_2+\varpi_2))]+\cos^2 I[-\frac{1}{8}\sin 3n_1t+\frac{3}{8}\sin n_1t+$$
$$+\frac{1}{16}\sin(3n_1t-2(f_2+\varpi_2))+\frac{1}{16}\sin(3n_1t+2(f_2+\varpi_2))-$$
$$-\frac{3}{16}\sin(n_1t-2(f_2+\varpi_2))-\frac{3}{16}\sin(n_1t+2(f_2+\varpi_2))]]-$$
$$-\sqrt{\frac{D}{B}}(1+e_2\cos f_{20})^3(\cos^2(f_{20}+\varpi_{20})+$$
$$+1-4\sin^2(f_{20}+\varpi_{20})\cos^2 I)\sin\sqrt{BD}\tau-$$
$$-2(1+e_2\cos f_{20})^3\sin 2(f_{20}+\varpi_{20})\cos I\cos\sqrt{BD}\tau]+O(X^{-3}) \quad (2.68)$$

and the final form of the formula for the averaged square eccentricity is:

$$\begin{aligned}
\overline{e_1^2} \;=\; & \frac{1}{9}\frac{1}{X^4}\{\frac{1}{(1-e_2^2)^{\frac{9}{2}}}[\frac{145}{64}+e_2^2(\frac{435}{64}+\frac{105}{32}\cos 2\varpi_{20})+\\
& +e_2^4(\frac{435}{512}+\frac{35}{64}\cos 2\varpi_{20}+\frac{59}{1024}\cos 4\varpi_{20})+\\
& +\cos^2 I[\frac{11}{32}+e_2^2(\frac{33}{32}+\frac{9}{4}\cos 2\varpi_{20})+e_2^4(\frac{33}{256}+\frac{3}{8}\cos 2\varpi_{20}-\\
& -\frac{59}{512}\cos 4\varpi_{20})]+\cos^4 I[\frac{177}{64}+e_2^2(\frac{531}{64}-\frac{177}{32}\cos 2\varpi_{20})+\\
& +e_2^4(\frac{531}{512}-\frac{59}{64}\cos 2\varpi_{20}+\frac{59}{1024}\cos 4\varpi_{20})]]+\\
& +\frac{1}{2}\frac{1}{(1-e_2^2)^6}(1+e_2\cos f_{20})^6(1+\\
& +\frac{D}{B})[(4\sin^2(f_{20}+\varpi_{20})\cos^2 I-1-\cos^2(f_{20}+\varpi_{20}))^2+\\
& +4\frac{B}{D}\cos^2 I\sin^2 2(f_{20}+\varpi_{20})]\}+O(X^{-5}). \qquad (2.69)
\end{aligned}$$

The results from numerical integrations for systems with equal masses, non-coplanar orbits and eccentric outer binary showed good agreement with the theoretical result given by equation (2.69) (table 2.5). For instance, for an eccentric outer binary ($e_2 = 0.2$), 90° ahead of the inner one and starting at

Table 2.5: Error in the mean square eccentricity for systems with equal masses and $I = 20°$. The behaviour of the error is consistent with the truncation of terms of order X^{-5} in equation (2.69).

a_2	e_2	Error
10	0.2	23%
20	0.2	9%
30	0.2	5%
20	0.7	43%

pericentre initially, inclined at 20° to the plane of the inner binary and with $a_2 = 10,\ 20,\ 30$ there was an error of 23%, 9% and 5% respectively. There seemed to be a rather significant discrepancy when the outer binary was higly eccentric ($e_2 = 0.7$). In this case, for $a_2 = 20$ and $I = 20°$ the error was 43%. The reason for that disagreement is the importance of terms of order X^{-3} in the expansion of the components of the eccentric vector: these will provide better initial conditions for the secular part of the eccentricity, in addition of course to the improvement of the accuracy of the short period terms themselves. This is illustrated in figures (2.9), where graphs from the solution of the full equations of motion and secular motion are compared. Note that the starting value of the secular motion is too small.

2.2.7 Conclusion

The idea of the present chapter was to investigate the evolution of the inner eccentricity in a hierarchical triple system when the period ratio X of the two binaries is rather large. The results were quite satisfactory and covered a rather wide range of parameters (masses, eccentricities etc.).

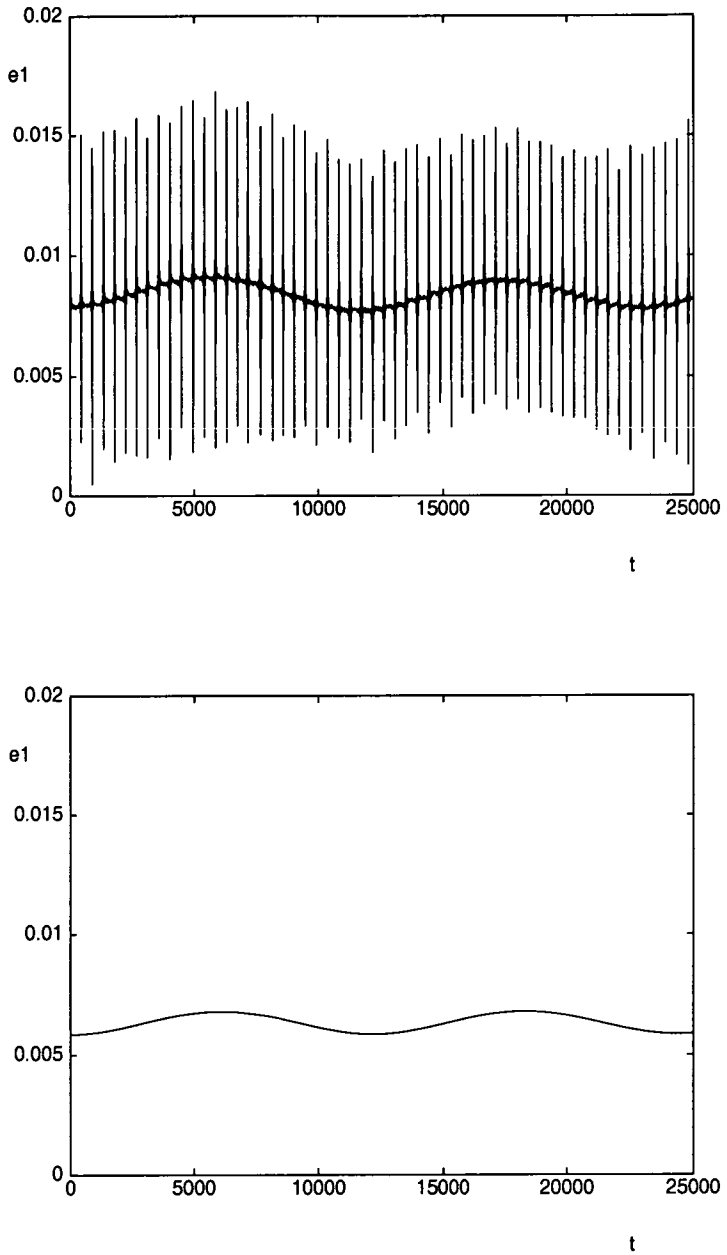

Figure 2.9: Eccentricity against time for equal masses, $a_2 = 20$, $e_2 = 0.7$ and $I = 15°$. The upper graph is from the numerical integration of the full equations of motion, while the lower graph is a plot of the secular eccentricity obtained from system (2.53) by setting $m_1 = m_2$ and by using the short period solution to determine the initial conditions for the secular problem.

Generally, the theory developed above does not apply accurately when the eccentricity gets rather large ($e_{in} > 0.1$), or when we have a mean motion commensurability, or when we are close to a secular resonance, as was seen earlier. These situations may require special treatment, although it is expected that if we are close to a mean motion resonance, the effect on the eccentricity evolution would be weak due to the fact that we are dealing with systems with large period ratio. Moreover, problems could arise in situations with extreme mass ratios, but one must bear in mind that in real stellar systems, the stars have comparable masses: $1 : 10$ is the usual limit of mass ratios.

Further improvements to the formulae can be made, but even without any improvements, we believe that they give a reasonable estimate of the inner eccentricity. However, one should always bear in mind that the most important thing is to understand the dynamics of the system and hence to have a qualitative picture of the situation.

Chapter 3

Stability of hierarchical triple systems

3.1 Introduction

The stability of a hierarchical triple system is an intriguing problem which remains unsolved up to date. It has been a subject of study by many people and the appearance of computers, with their ability of performing numerical intergrations with large speed, has proved very useful. The work that has been done on the stability of hierarchical triple systems can be divided into two categories: analytical and numerical.

The analytical work is based on the generalisation of the concept of surfaces of zero velocity of the restricted three-body problem (fig. 3.1) to the general three-body problem (Marchal 1990). The quantity c^2H, where c is the angular momentum and H is the energy of the system, is the analog to the Jacobi constant of the restricted problem. Szebehely and Zare produced an expression for c^2H, which involved the masses, the semi-major axes and the eccentricities of the system (Szebehely and Zare 1977). That expression was compared with the

value of c^2H at the collinear Langrangian points, which determine the openings and closings of the zero velocity surfaces. For instance, if the value of c^2H was smaller than the one at the inner Lagrangian point, then there could be no exchange of bodies. There is an analogous condition for escape. The criterion has been used to check if various three-body systems were stable, mainly in the context of solar system dynamics (Szebehely and McKenzie 1977, Szebehely 1980, Bozis 1981). The criterion has also been used in slightly modified forms. Roy et al. (1984) found an upper bound for the c^2H quantity, which was associated with the distance of the closest approach of m_2 to m_3, while Donnison and Williams (1983, 1985) expanded c^2H as a series in the quantity

$$x = (\frac{m_2 + m_3}{3m_1})^{\frac{1}{3}}$$

under the condition $m_1 >> m_2, m_3$ and used the modified version of the c^2H criterion to investigate the stability of satellite systems. A similar criterion has been derived by Donnison (1988), but for $m_3 >> m_1 + m_2$.

The main disadvantage of the c^2H criterion is that it is a sufficient but not a necessary condition for stability. Exchange might not occur even when the condition is violated but it certainly cannot occur when the condition is satisfied. The lobes could also be open to infinity, but the body may or may not escape to infinity. Finally, things are not clear again when the third body is started outside (inside) the lobes, since the criterion cannot give any information whether the third body will be ejected or not from the system (will keep orbiting the binary or form a binary with one of the other masses). It is worth mentioning here that, according to the c^2H criterion, prograde orbits are more stable than retrograde ones. The physical explanation is that the angular momentum contained in a counter-rotating triple system is smaller than in a direct system with all other things being equal and consequently a larger a_2/a_1 ratio is required to obtain the same angular momentum for a counter-rotating system than for a direct

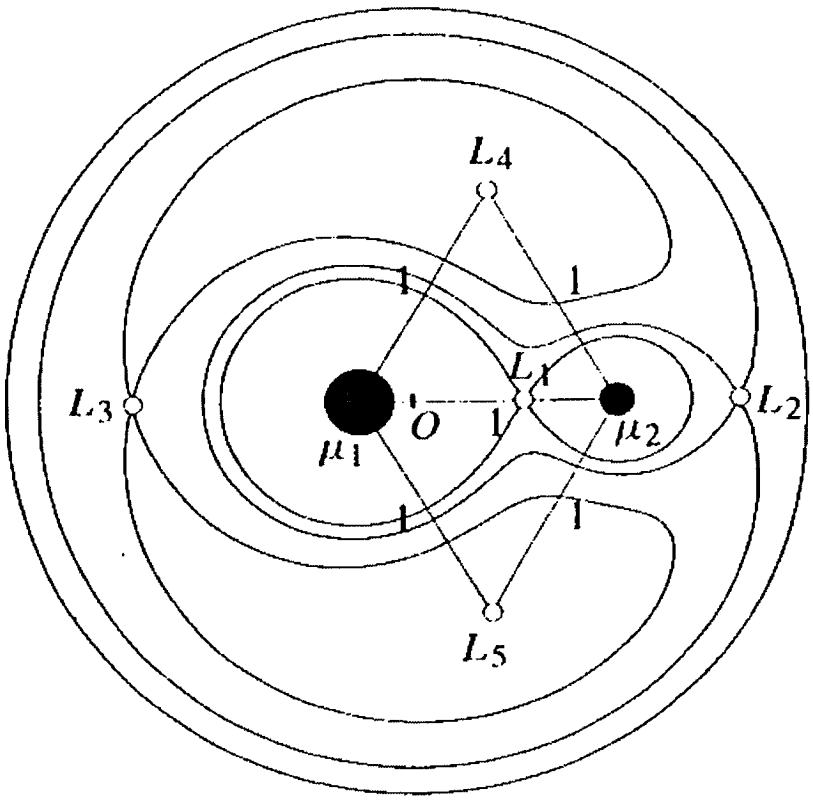

Figure 3.1: The location of the Lagrangian equilibrium points (denoted by the small open circles) and associated zero-velocity curves for $\mu_2 = m_2/(m_1 + m_2) = 0.2$. The point O denotes the centre of mass of the system. The figure is taken from Murray and Dermott (1999). Exchange is impossible if the third body lies within the curve through L_1.

system. However, the greater stability of direct systems might not be the case, and is indeed contradicted by numerical evidence, as we will see later on.

The numerical work involves a wide range of simulations of hierarchical triple systems. Harrington carried out numerical integrations of triple systems with stellar and planetary mass ratios (Harrington 1972, 1975, 1977) and he derived the following empirical condition for stability, based on his results:

$$\frac{q_2}{a_1} \geq A[1 + B \log \frac{1 + m_3/(m_1 + m_2)}{3/2}] + K, \tag{3.1}$$

where $q_2 = a_2(1 - e_2)$, A and B are determined empirically and K is 0 if this is to be a mean fit and is approximately 2 if it is to be an upper limit. For coplanar orbits, $A = 3.50$ and $B = 0.70$. An interesting thing that Harrington's integrations revealed is that the stability of the systems did not depend on the value of the inclination, except the near-perpendicular configuration, where the system was unstable for all semi-major axes. This may indicate that planar models could be sufficient for stability studies for moderate inclinations. He also found that retrograde orbits were more stable than prograde orbits, a result which is in contrast with Szebehely's results. However, the results for equal masses and direct orbits were in good agreement, although Szebehely's results allow a slightly closer outer orbit. It should of course be borne in mind that the c^2H criterion is based on the possibility of exchange of bodies. It should also be pointed out here that the definition of stability given by Harrington is a bit ambiguous. He classifies a triple system as stable if there is no "significant change" in the orbital elements during the period of integration, and in particular the semi-major axes and the eccentricities. Another point that raises some concern is that the integrations are performed for only 10 or 20 outer orbital periods. This could prove inadequate, although Harrington suggested that instabilities of this kind (exchange etc.) set in very quickly.

Graziani and Black (1981), in the context of planet formation and extrasolar

planets, used numerical integrations to model planetary systems with initially circular orbits. Based on their results, which were in agreement with the results of Nacozy (1976) and Donnison and Williams (1978), they obtained the following condition for stability [1]:

$$\mu = 0.5\frac{m_1 + m_2}{M_*} < \mu_{crit} = 0.175\Delta^3(2-\Delta)^{-\frac{3}{2}}, \quad \mu \leq 1 \tag{3.2}$$

where the planets m_1 and m_2 orbit the star M_*. The parameter Δ gives the minimum initial separation between the companions in units of their mean distance from the central star, while μ is the mean mass of the two companions in units of the mass of the star. Specifically,

$$\Delta = 2\frac{R-1}{R+1}, \quad R = \frac{R_2}{R_1}$$

with R_1 and R_2 the semi-major axes of the inner and outer orbits respectively. The above condition can be modified to apply for $\mu \geq 1$ (Black 1982). The modified stability condition is:

$$\mu \leq \mu_{crit} = 0.083\frac{\Delta^3}{(2-\Delta)^3}. \tag{3.3}$$

Both the above stability conditions were confirmed by more integrations (Pendleton and Black 1983). The results obtained by Black et al. (1981, 1982, 1983) were not always in agreement with the other results that have been presented in this section so far, especially with Harrington's results. The reason for that discrepancy is not always very clear.

A series of experiments were conducted by Donnison and Mikulskis (1992, 1994, 1995). They integrated prograde and retrograde orbits (the inner eccentricity was always initially zero) of hierarchical triple systems. They classified a system as stable if the change in semi-major axes was less than 10% and/or

[1] In their work, a system is defined as unstable if there is clear evidence for secular changes in any orbit in a triple system during an experiment.

the eccentricity of either binary altered by less than 0.1. They concluded that their results were more consistent with the results of Black and his collaborators, except in the case of equal masses when their results seemed to be closer to the results of Harrington. They also agreed with Harrington about retrograde orbits, but only qualitively. The c^2H criterion proved to be very poor for retrograde orbits, although it did well for co-rotating systems.

A more systematic approach was taken by Eggleton and his collaborators, who ran numerical integrations of hierarchical triple systems with coplanar, prograde and initially circular orbits (Kiseleva, Eggleton and Anosova 1994, Kiseleva, Eggleton and Orlov 1994). More about these results will be presented in the next section. These numerical calculations were later extended to eccentric binaries, inclined orbits (from 0° to 180°) and different initial phases, and an empirical condition for stability [2] was derived (Eggleton and Kiseleva 1995):

$$Y_0^{min} \approx 1 + \frac{3.7}{q_{out}^{1/3}} - \frac{2.2}{1+q_{out}^{1/3}} + \frac{1.4}{q_{in}^{1/3}} \frac{q_{out}^{1/3}-1}{q_{out}^{1/3}+1}, \tag{3.4}$$

where

$$q_{in} = \frac{m_1}{m_2} \geq 1, \quad q_{out} = \frac{m_1+m_2}{m_3}$$

and Y_0^{min} is the critical initial ratio of the periastron distance of the outer orbit to the apastron distance of the inner orbit. Y_0^{min} is related to the critical initial period ratio X_0^{min} by the following relation:

$$(X_0^{min})^{\frac{2}{3}} = (\frac{q_{out}}{1+q_{out}})^{\frac{1}{3}} \frac{1+e_{in}}{1-e_{out}} Y_0^{min}. \tag{3.5}$$

The criterion appears to be reliable to about 20%, which is quite good, considering the wide range of parameters and the complex nature of the critical surface. It does not work very well in situations where there is a resonance or

[2]Stability here is equivalent to no change in the hierarchical structure of the system for the integration time span.

commensurability, but these are more common in systems with extreme mass ratios (e.g. star and planets). It should be pointed out here that there is a misprint in formula (3.4) as given in Eggleton and Kiseleva: the sign of the term $\frac{2.2}{1+q_{out}^{1/3}}$ is plus, while it should be minus.

Mardling and Aarseth (1999) showed that stability against escape in the three body problem is analogous to stability against chaotic energy exchange in the binary-tides problem. They derived a criterion of instability for coplanar orbits with prograde motion. The expression is given by:

$$\frac{R_p^{out}}{a_{in}} < C[(1+q_{out})\frac{1+e_{out}}{(1-e_{out})^{\frac{1}{2}}}]^{\frac{2}{5}} \equiv \frac{R_p^{crit}}{a_{in}}, \tag{3.6}$$

where R_p^{out} is the outer periastron separation and $q_{out} = \frac{m_3}{m_1+m_2}$. C is determined empirically and it is 2.8.

Holman and Wiegert tested the stability of planetary size bodies under the gravitational influence of a stellar binary system (Holman and Wiegert 1999). They ran numerical simulations for a full range of mass ratios and binary eccentricities. The particles were started on circular, prograde orbits around the binary or around one of the stars, in the binary plane of motion and with different initial orbital longitudes. The choice of parameters was based on observational data of the α Centauri system (Wiegert and Holman 1997), in which the largest stable orbit near the stars was found to have an inclination in the plane of the binary. The integrations lasted for 10^4 binary periods. If a particle survived the whole integration time at all initial longitudes, then it was considered stable. Using a least squares fit to their data, they obtained: (i) for the inner region (particle orbiting one of the stars):

$$\begin{aligned} a_c &= [(0.464 \pm 0.006) + (-0.380 \pm 0.010)\mu + (-0.631 \pm 0.034)e + \\ &\quad +(0.586 \pm 0.061)\mu e + (0.150 \pm 0.041)e^2 + \\ &\quad +(-0.198 \pm 0.074)\mu e^2]a_b \end{aligned} \tag{3.7}$$

(ii) for the outer region (particle orbiting the binary):

$$\begin{aligned} a_c &= [(1.60 \pm 0.04) + (5.10 \pm 0.05)e + (-2.22 \pm 0.11)e^2 + \\ &\quad +(4.12 \pm 0.09)\mu + (-4.27 \pm 0.17)e\mu + (-5.09 \pm 0.11)\mu^2 + \\ &\quad +(4.61 \pm 0.36)e^2\mu^2]a_b, \end{aligned} \tag{3.8}$$

where a_c is the critical semi-major axis, a_b is the binary semi-major axis, e is the binary eccentricity and $\mu = m_2/(m_1 + m_2)$. Each coefficient is listed along with its formal uncertainty. Equation (3.7) is valid to 4% typically and to 11% in the worst case over the range of $0.1 \leq \mu \leq 0.9$ and $0.0 \leq e \leq 0.8$, while equation (3.8) is valid to 3% typically and to 6% in the worst case over the range of $0.1 \leq \mu \leq 0.9$ and $0.0 \leq e \leq 0.7$. An interesting finding was that, in the outer region, 'islands' of instability existed outside the inner unstable region; this phenomenon was attributed to mean motion resonances and indicated that there is not a sharp boundary between stable and unstable regions. It should be mentioned here that equation (3.8), as presented in the paper of Holman and Wiegert, appears not to depend on a_b at all. However, this is probably a misprint, as equation (3.7) might suggest.

Finally, in a series of papers, Dvorak and his collaborators (Dvorak 1984, 1986, Rabl and Dvorak 1988, Dvorak, Froeschle and Froeschle 1989) have investigated the stability of P-type (planet orbiting a binary star system) and S-type (planet orbiting one of the stars of a binary system) orbits in equal mass binary systems. A P-type orbit was classified as stable if its eccentricity remained smaller than 0.3 throughout the whole integration time, while an S-type orbit was considered stable if the planet remained in the vicinity of the parent star. It is worth mentioning here that, between the stable and unstable areas, there was a region of chaotic motion, chaotic in the sense of unpredictability. This chaotic region was limited by the so-called Lower and Upper Critical Orbits (LCO and

UCO hereafter). All the integrated orbits within the LCO were found to be unstable, while all the integrated orbits outside the UCO were stable.Their numerical integration results are summarised in four formulae. For P-type orbits the radii are

$$LCO = 2.09 + 2.79e - 2.07e^2 \quad (3.9)$$

$$UCO = 2.37 + 2.76e - 1.04e^2 \quad (3.10)$$

and for S-type orbits:

$$LCO = 0.262 - 0.254e - 0.060e^2 \quad (3.11)$$

$$UCO = 0.336 - 0.332e - 0.083e^2, \quad (3.12)$$

where e is the eccentricity of the stellar binary system and distance is measured in AU [3]. The separation of the binary components was taken to be 1 AU. The formulae are the outcome of a least squares parabolic fit to a discrete grid of numerical results.

3.2 Numerical integrations of circular orbits

As was mentioned in the previous section, several numerical investigations have been carried out to study the stability of hierarchical triple systems. Now we concentrate on the case of initially circular motions. Kiseleva et al. (Kiseleva, Eggleton and Anosova 1994, Kiseleva, Eggleton and Orlov 1994) considered the orbits of triple stars which were started with hierarchical, coplanar, doubly circular motion, but which have a sufficiently short ratio of orbital periods that the system is close to instability. Various systems were integrated with the triple code of Aarseth (Aarseth and Zare 1974), with the inner orbit always 90° ahead of the outer orbit initially. The integrations were normally carried out

[3]AU: astronomical unit. The mean distance between the Earth and Sun.

for 100 time units (where a time unit is the initial period of the outer binary), although there were situations where the system was integrated for 1000 or even 10000 time units. A system was classified as stable if it persisted for the length of the integration time without changing its hierarchical structure. The results from those integrations are presented in Table 3.1. Each entry in Table 3.1 is the initial period ratio X_0^{min} for the last stable configuration for a given system. Each system is uniquely defined by the three parameters α, β, X_0, where

$$\alpha = \log_{10}(\frac{m_1}{m_2}) \geq 0 \quad , \quad \beta = \log_{10}(\frac{m_1 + m_2}{m_3}).$$

Generally, if the initial period ratio X_0 is smaller than X_0^{min}, then the system is said to be unstable: either one component goes to infinity (or at least into a very long orbit), or the hierarchy of the system changes as one star moves between the other two. As can be seen from Table 3.1, there are some pairs of α and β for which two values of X_0^{min} are given. Immediately below the upper value, which is described as a disruptive resonance, the system disrupted and then, further below that value, the system became stable again, until it reached the lower value of X_0^{min}.

There are three regions in Table 3.1, each of them corresponding to a different dynamical behaviour of the triple system. The first one is shown in boldface and it corresponds roughly to systems where the outer star is the lightest and it escapes from the system by a direct ejection or a series of ejections. In the second region (which is actually two disjoint regions), shown in italics, the lightest star of the inner binary moves backwards and forwards between the other two stars. In the last region, three types of instability can occur:

(i) one or a few exchanges and then the formation of a long lived triple system with a new hierarchy. This new hierarchical system may sometimes be destroyed by the escape of the new distant body but in many cases the state may survive for at least 10000 time units. Such behaviour is rather typical for cases where

Table 3.1: Values of X_0^{min} for last stable configurations (from Eggleton and Kiseleva 1995).

α	0.0	0.2	0.4	0.6	0.8	1.0	1.2	1.4	1.6	1.8	2.0
m_1/m_{12}	*.50*	*.39*	*.28*	*.20*	*.14*	*.09*	*.06*	*.04*	*.025*	*.016*	*.01*
$\beta(m_3/m_{12})$											
-2.0(*100*)	6.09	6.14	6.28	6.31	6.37	6.40	6.45	6.46	6.45	6.47	*6.49*
-1.8(*63*)	6.09	6.19	6.30	6.38	6.42	6.45	6.48	6.50	6.53	6.53	*6.54*
-1.6(*40*)	6.09	6.22	6.30	6.41	6.50	6.54	6.53	6.59	*6.60*	*6.60*	*6.59*
-1.4(*25*)	6.07	6.20	6.36	6.46	6.51	6.58	*6.60*	*6.60*	*6.62*	*6.64*	*6.67*
-1.2(*16*)	6.11	6.20	6.37	6.42	6.52	*6.57*	*6.58*	*6.63*	*6.66*	*6.66*	*6.67*
-1.0(*10*)	5.99	6.10	6.26	6.39	*6.47*	*6.52*	*6.59*	*6.60*	*6.64*	*6.65*	*6.66*
-0.8(*6.3*)	5.86	6.00	6.15	6.29	*6.37*	*6.44*	*6.50*	*6.54*	*6.54*	*6.55*	*6.57*
-0.6(*4.0*)	5.60	5.80	5.95	*6.10*	*6.20*	*6.29*	*6.34*	*6.37*	*6.40*	*6.42*	*6.43*
-0.4(*2.5*)	5.29	5.47	5.64	*5.80*	*5.92*	*6.01*	*6.07*	*6.11*	*6.13*	*6.15*	*6.14*
-0.2(*1.6*)	4.88	5.04	5.19	*5.35*	*5.48*	*5.56*	*5.62*	*5.66*	*5.69*	*5.70*	*5.71*
0.0(*1.0*)	4.37	4.56	4.57	*4.82*	*4.90*	*4.97*	*5.03*	*5.07*	*5.09*	*5.11*	*5.12*
0.2(*0.63*	4.29	4.31	4.28	4.53	*4.15*	*4.18*	*4.26*	*4.32*	*4.36*	*4.38*	*4.39*
0.4(*.40*)	4.37	4.38	4.33	4.25	4.26	4.12	4.06	4.02	3.64	3.51	3.55
										3.41	3.46
0.6(*.25*)	4.37	4.35	4.34	4.29	4.22	4.19	4.04	4.00	*3.98*	*3.96*	*3.94*
	3.61	3.75	3.73	3.72	3.71					*3.83*	*3.84*
0.8(*.16*)	4.37	4.38	4.32	4.27	4.18	4.05	4.00	3.96	*3.92*	*3.96*	*3.88*
	3.67	3.73	3.70	3.64	3.60	3.51	3.46	3.39	*3.35*	*3.35*	*3.29*
1.0(*.10*)	4.32	4.33	4.28	4.22	3.45	3.39	3.31	3.24	3.16	*3.18*	*3.13*
	3.62	3.62	3.61	3.54							
1.2(*.063*)	4.31	4.29	4.26	3.47	3.38	3.30	3.21	3.12	3.09	3.06	*3.01*
	3.59	3.56	3.52								
1.4(*.040*)	4.27	3.54	3.48	3.40	3.31	3.20	3.15	3.08	2.93	2.88	*2.85*
	3.52										
1.6(*.025*)	3.50	3.50	3.42	3.33	3.26	3.18	3.05	2.98	2.90	2.47	2.43
									2.57		
1.8(*.016*)	3.48	3.48	3.39	3.29	3.22	3.12	3.03	2.98	2.87	2.46	2.06
								2.55	2.48		
2.0(*.010*)	3.44	3.42	3.38	3.26	3.17	3.11	3.03	2.91	2.49	2.07	2.01
								2.52			

the third star is more massive than the initial inner binary ($\beta \leq 0$);

(ii) the escape of one component after long term evolution with many exchanges;

(iii) the escape of one component (ususally the lightest one in the system) fairly soon after the first exchange, or after only a few exchanges.

3.3 Numerical results for systems with $\alpha = 2.0$

The results in Table 3.1 are ambiguous in the sense that the integration time span is not stated. From this point, a hierarchical triple system will be classified as stable if it retains the same hierarchy for 100 outer orbital periods. In the numerical integrations that follow, the Mikkola symplectic integrator, described in section 1.7, was used to integrate the full equations of motion for several triple systems with $m_1 = 0.01$ and $m_2 = 0.99$ ($\alpha = 2.0$) but different m_3. The bodies started on circular orbits, with the outer binary 90° ahead of the inner one. The integrations were extended to 1000 outer orbital periods in order to see how sensitive the stability limit was to the integration time span. As expected, the instability region was slightly enlarged and some systems that appeared to be stable within 100 outer periods, broke up when the integration time was taken up to 1000 outer orbital periods. The results from these numerical integrations are presented in Table 3.2 and figures 3.2. Each entry in Table 3.2 represents, as X decreases, the first initial period ratio for which the system disrupted. There were some systems which demonstrated a more complicated behaviour: the system broke up for some values of X_0, then it became stable and then it became unstable again. For instance, for $m_3 = 0.4$ the system broke up for $X_0 = 3.57$, then it became stable for $X_0 = 3.52$ until it disrupted again for $X_0 = 3.45$.

3.4 The 3:1 resonance

In order to understand the results of Table 3.1 better, we shall consider a particular triple system and study it in more detail. For that purpose, we chose the system with $m_1 = 0.01, m_2 = 0.99$ and $m_3 = 0.1$ ($\alpha = 2.0$ and $\beta = 1.0$), whose last stable configuration, according to Table 3.1, had $X_0^{min} = 3.13$.

Table 3.2: Extreme values of X_0 for which a system with $m_1 = 0.01$ and $m_2 = 0.99$ breaks up for the first time within 100 and 1000 outer orbital periods.

m_3	$t = 100T_{out}$	$t = 1000T_{out}$
0.01	2.01	2.05
0.016	2.01	2.07
0.02	2.11	2.15
0.025	2.41	2.46
0.04	2.74	2.79
0.063	2.92	2.93
0.08	3.02	3.07
0.10	3.07	3.11
0.12	3.09	3.18
0.14	3.17	3.23
0.16	3.18, 3.86-3.87	3.29, 3.85-3.89
0.18	3.24, 3.79-3.84	3.29, 3.79-3.91
0.20	3.25, 3.72-3.84	3.36, 3.72-3.91
0.23	3.33, 3.56-3.86	3.40, 3.55-3.86
0.25	3.82	3.82, 3.88-3.93
0.30	3.68, 3.78-3.79	3.68, 3.78-3.87
0.35	3.27, 3.60-3.72	3.27, 3.59-3.73
0.40	3.45, 3.53-3.57	3.46, 3.51-3.58

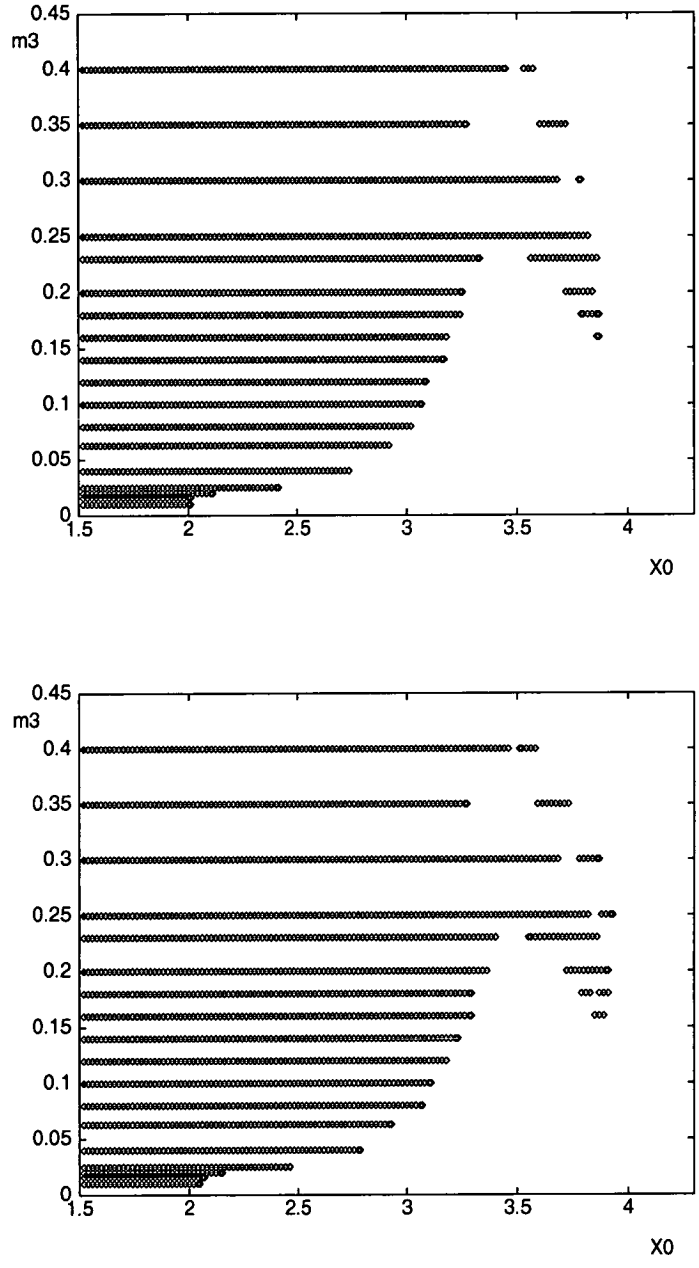

Figure 3.2: Outer mass m_3 against initial period ratio X_0, for which a system with $m_1 = 0.01$ and $m_2 = 0.99$ becomes unstable. The upper graph is for 100 outer orbital periods, while the lower one is for 1000 outer orbital periods. The dots denote instability.

3.4.1 Some numerical results

Once more, Mikkola's symplectic integrator was used for the numerical integration of the triple system. The integrations were started with the outer binary 90° ahead of the inner one. Some results from the simulations can be seen in figures 3.3 and 3.4. The outer eccentricity and longitude of pericentre did not change much, since the mass m_1 is small compared to the other two and it would not affect the motion of the outer binary significantly. However, the inner eccentricity and pericentre showed a very interesting behaviour. The eccentricity oscillated from very small values ($e_1 \approx 0$) to quite significant values ($e_1 \approx 0.35$), while the pericentre appeared to circulate for some periods and remain almost constant at others (this will become more clear in the next section). This pattern became more clearly visible as we approached the last stable configuration of the system (according to the definition of stability mentioned in the previous section, i.e. the system keeps the same hierarchy for 100 outer orbital periods), which was found to be for $X_0^{min} = 3.08$. It was also noticed that the eccentricity reached large values when the longitude of the pericentre was almost stationary. It is worth mentioning that for $X_0^{min} = 3.07$ (which is the initial period ratio of the first unstable configuration of the system), by estimation from figure 3.3, the pericentre frequency during the first four outer binary periods has roughly the same magnitude as the outer mean motion but the opposite sign, i.e. $\dot{\varpi}_1 \approx -n_2$. There is also clear evidence that the dynamical behaviour of the triple system is mainly determined by the fact that the period ratio and hence the mean motion ratio is close to three. This is confirmed by figure 3.5, where the maximum inner eccentricity e_{max} within 100 outer orbital periods, is plotted against the initial period ratio. For a slight change in the initial period ratio, from $X_0 = 3.08$ ($a_2 = 2.18$) to $X_0 = 3.3$ ($a_2 = 2.28$), i.e. a change of order 7%, there was a 50% change in the maximum eccentricity, something that might be

expected to happen if the system was close to a mean motion resonance.

3.4.2 A qualitative analysis of the 3:1 resonance

A common theoretical approach in a situation like this is to isolate those arguments in the expansion of the perturbing potential which would play an important role in the dynamical evolution of the system. It should be noticed that, even when the pericentre circulates, the inner binary orbit is still close to a circle and consequently $\dot{\lambda}_1 \approx n_1$. When the pericentre is almost stationary, again, $\dot{\lambda}_1 \approx \dot{\ell}_1 \approx n_1$. For the outer binary, $\dot{\lambda}_2 \approx n_2$, since the outer orbit remains nearly circular with almost constant semi-major axis throughout the evolution. Since the configuration of the three bodies is such that the system is close to a 3:1 orbital resonance, arguments that contain the quantity $\lambda_1 - 3\lambda_2$ are expected to be important because of its small frequency. However, because $e_2 \approx 0$, terms which are proportional to e_2 in the expression of the perturbing Hamiltonian, can be neglected. Taking that approximation into account, there is only one argument containing the combination $\lambda_1 - 3\lambda_2$:

$$\lambda_1 - 3\lambda_2 + 2\varpi_1,$$

which comes from the P_3 term, as seen in the expansion of the perturbing Hamiltonian in Appendix B. But because of the behaviour of the pericentre, the frequency of the resonant argument is not always very small and there are time intervals (i.e. those in which the pericentre circulates) when it is roughly $-2n_2$. In these time intervals, the frequency of the argument

$$\lambda_1 - 2\lambda_2 + \varpi_1,$$

becomes small and it may be expected that this argument plays an important role in the evolution of the system. The two angles are plotted against each

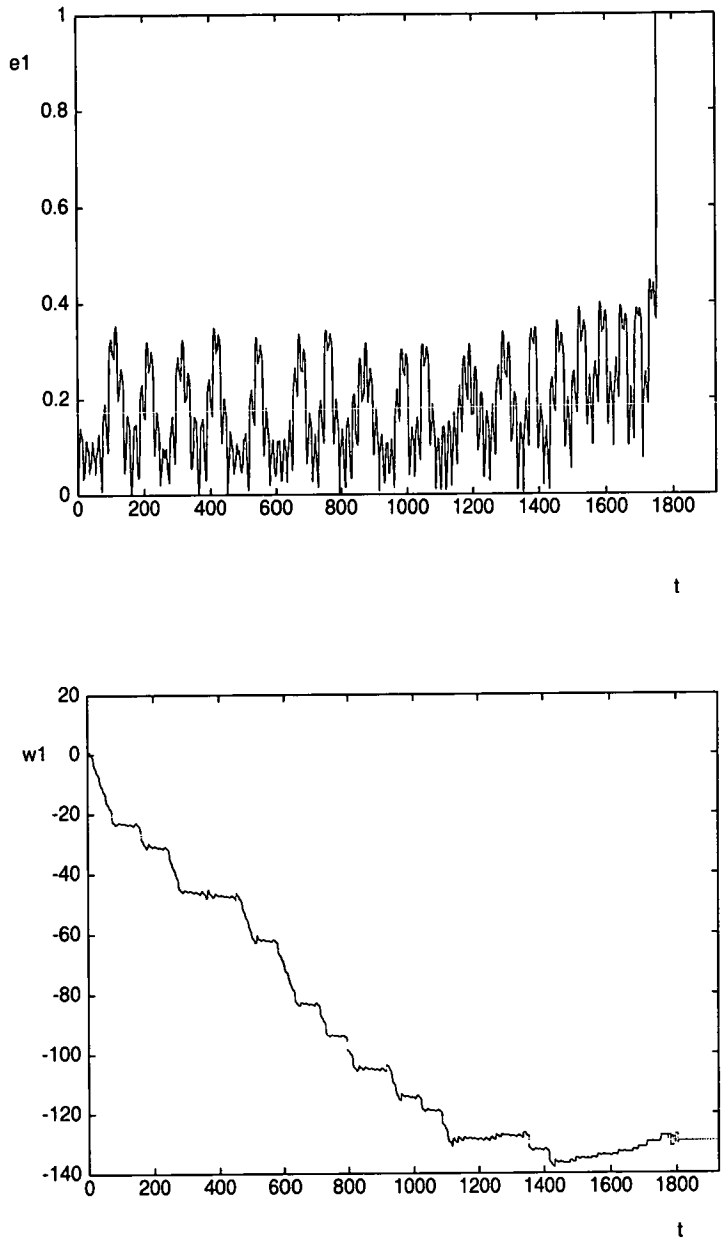

Figure 3.3: Inner binary eccentricity and longitude of pericentre against time for a triple system with $m_1 = 0.01$, $m_2 = 0.99$, $m_3 = 0.1$ and $X_0 = 3.07$. The results are from numerical integration of the full equations of motion using Mikkola's symplectic integrator. In this case, the outer orbital period is $T_2 \approx 19.30$.

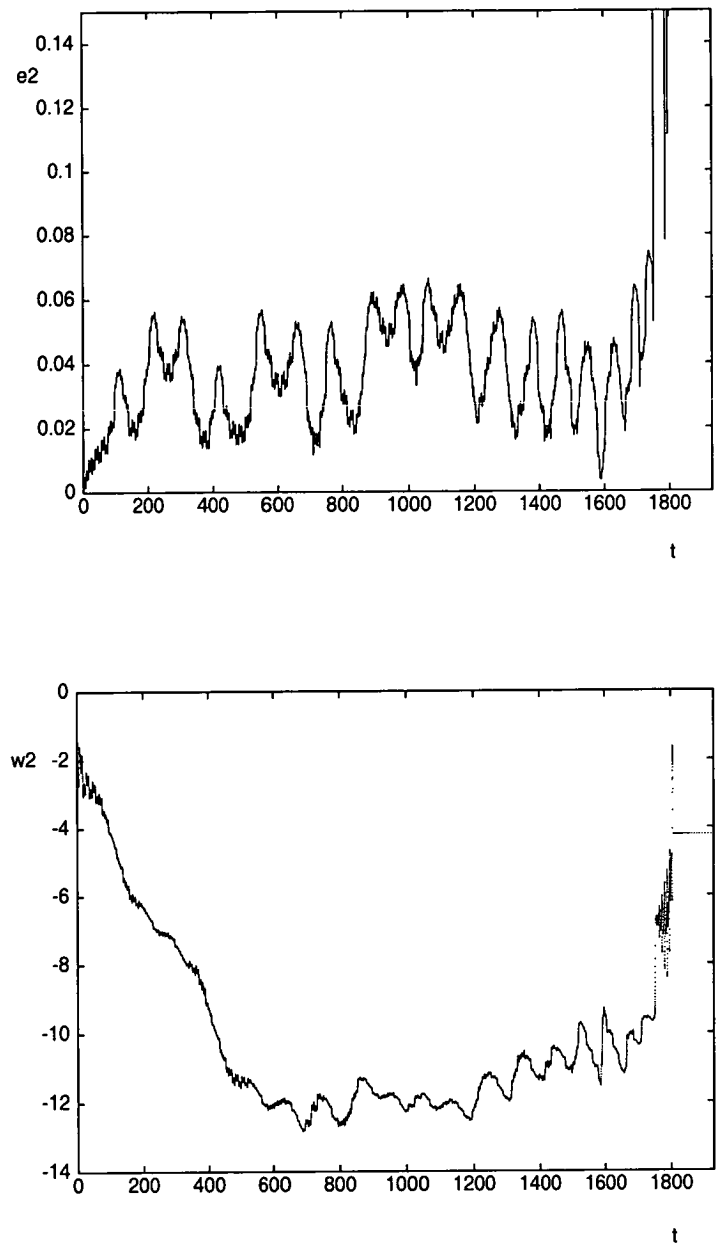

Figure 3.4: Outer binary eccentricity and longitude of pericentre against time for a triple system with $m_1 = 0.01$, $m_2 = 0.99$, $m_3 = 0.1$ and $X_0 = 3.07$. The results are from numerical integration of the full equations of motion using Mikkola's symplectic integrator.

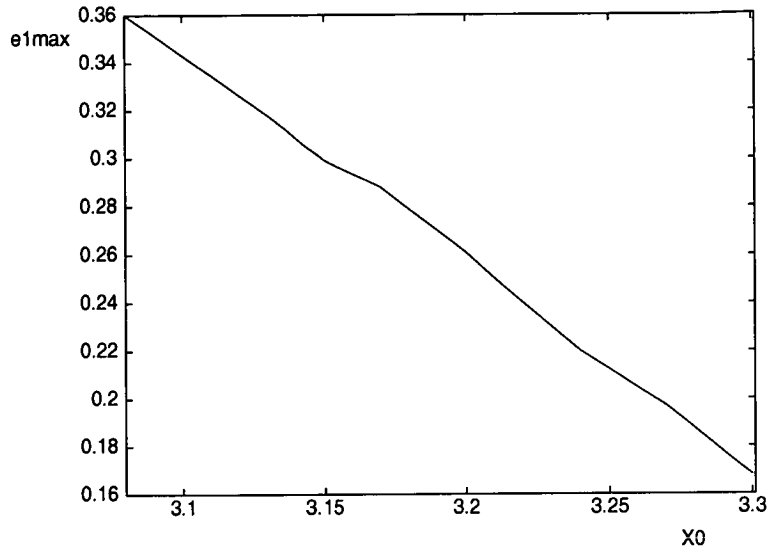

Figure 3.5: Maximum inner eccentricity against initial period ratio for a triple system with $m_1 = 0.01, m_2 = 0.99$ and $m_3 = 0.1$. The integration interval is 100 outer orbital periods.

other in figures 3.6 for a time interval of 8 outer orbital periods. It appears that when the one argument librates the other one circulates and vice versa. Of course, one should always bear in mind that, besides the frequency, the coefficient of the argument in the expression of the perturbing potential is also important in determining its significance.

If one isolates in Appendix B the terms that contain the arguments $\lambda_1 - 2\lambda_2 + \varpi_1$ and $\lambda_1 - 3\lambda_2 + 2\varpi_1$, the following perturbing Hamiltonian H_p will be obtained:

$$\begin{aligned} H_p &= \frac{1}{2}\frac{Gm_1m_2m_3}{m_1+m_2}\frac{a_1^2}{a_2^3}[\frac{9}{2}e_1\cos(\lambda_1 - 2\lambda_2 + \varpi_1) - \\ &\quad -\frac{285}{32}\frac{m_1-m_2}{m_1+m_2}\frac{a_1}{a_2}e_1^2\cos(\lambda_1 - 3\lambda_2 + 2\varpi_1)]. \end{aligned} \tag{3.13}$$

Then, the rate of change of the inner eccentricity and longitude of pericentre can be derived using Hamilton's equations for the above perturbing Hamiltonian (cf. equation [1.11]), and are given by:

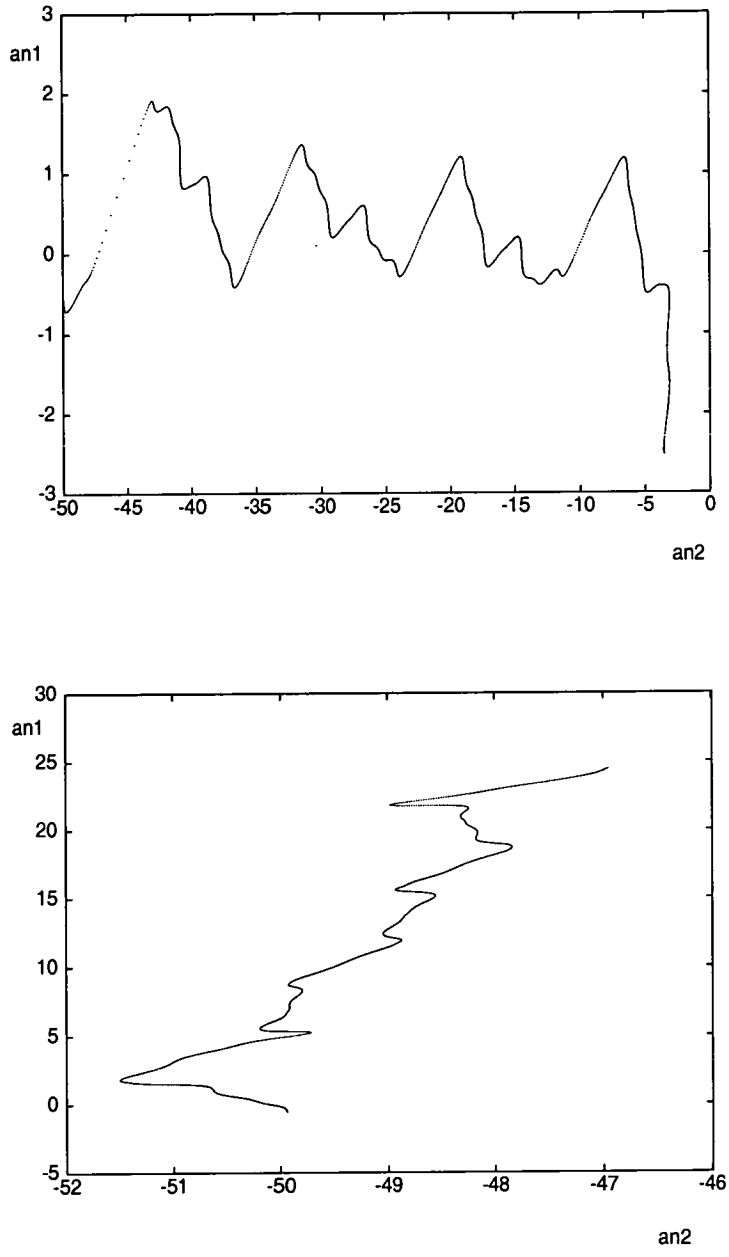

Figure 3.6: The angle $\lambda_1 - 2\lambda_2 + \varpi_1$ on the y-axis against the angle $\lambda_1 - 3\lambda_2 + 2\varpi_1$ on the x-axis. The upper graph is for $t = 0 - 4$ outer orbital periods, while the lower graph is for $t = 4 - 8$ outer orbital periods, for a triple system with $m_1 = 0.01$, $m_2 = 0.99$, $m_3 = 0.1$ and $X_0 = 3.07$. Note the very different scales of the axes on both graphs.

$$\dot{e}_1 = \frac{1}{4}\frac{Gm_3\sqrt{1-e_1^2}}{n_1 a_2^3}[9(\sqrt{1-e_1^2}-2)\sin(\lambda_1 - 2\lambda_2 + \varpi_1) + \\ + \frac{285}{16}\frac{m_1-m_2}{m_1+m_2}\frac{a_1}{a_2}e_1(3-\sqrt{1-e_1^2})\sin(\lambda_1 - 3\lambda_2 + 2\varpi_1)] \quad (3.14)$$

$$\dot{\varpi}_1 = -\frac{1}{4}\frac{Gm_3\sqrt{1-e_1^2}}{n_1 a_2^3 e_1}[9\cos(\lambda_1 - 2\lambda_2 + \varpi_1) - \\ - \frac{285}{8}\frac{m_1-m_2}{m_1+m_2}\frac{a_1}{a_2}e_1\cos(\lambda_1 - 3\lambda_2 + 2\varpi_1)]. \quad (3.15)$$

Equation (3.14) demonstrates another advantage of including the term associated with the argument $\lambda_1 - 2\lambda_2 + \varpi_1$ in the expression for the perturbing Hamiltonian. For a system with an initially zero eccentricity, the $\lambda_1 - 2\lambda_2 + \varpi_1$ term provides an initial non-zero rate of change for the eccentricity, whereas the eccentricity would remain zero without the presence of that term in our equations.

Now, if we neglect terms of order e_1^2, consider $\lambda_1 = n_1 t + \lambda_{10}$, $\lambda_2 = n_2 t + \lambda_{20}$, where $\lambda_{i0}, i = 1, 2$ are the initial values of the mean longitudes ($\lambda_{10} = 0°$ and $\lambda_{20} = 90°$) and use the variables $x_1 = e_1\cos\varpi_1$ and $y_1 = e_1\sin\varpi_1$, we obtain:

$$\dot{x}_1 = A[9\sin(n_1 - 2n_2)t + \frac{285}{8}B(x_1\cos(n_1 - 3n_2)t - y_1\sin(n_1 - 3n_2)t)] \quad (3.16)$$

$$\dot{y}_1 = A[9\cos(n_1 - 2n_2)t - \frac{285}{8}B(x_1\sin(n_1 - 3n_2)t + y_1\cos(n_1 - 3n_2)t)], \quad (3.17)$$

where

$$A = \frac{1}{4}\frac{Gm_3}{n_1 a_2^3} \quad , \quad B = \frac{m_1 - m_2}{m_1 + m_2}\frac{a_1}{a_2}.$$

Assuming that $n_1 \approx 3n_2$ and that n_1, n_2 are constant, equations (3.16) and (3.17) yield:

$$\dot{x}_1 - \frac{285}{8}ABx_1 = 9A\sin n_2 t \quad (3.18)$$

$$\dot{y}_1 + \frac{285}{8}ABy_1 = 9A\cos n_2 t \quad (3.19)$$

and the solution to the above equations is:

$$x_1 = C_x e^{\frac{285}{8}ABt} - \frac{576An_2}{64n_2^2 + 81225A^2B^2}(\cos n_2 t +$$

$$+\frac{285}{8}\frac{AB}{n_2}\sin n_2 t) \tag{3.20}$$

$$y_1 = C_y e^{-\frac{285}{8}ABt} + \frac{576An_2}{64n_2^2 + 81225A^2B^2}(\sin n_2 t + \\ +\frac{285}{8}\frac{AB}{n_2}\cos n_2 t), \tag{3.21}$$

where C_x and C_y are constants of integration. Examining the expressions for x_1 and y_1, it is quite clear that, after some time, the eccentricity will be increasing exponentially. The beginning of this exponential growth can be seen in figures 3.7, which are the graphical representations of equations (3.20) and (3.21) for appropriate choices of C_x and C_y. The lower graph from figures 3.7 demonstrates the behaviour of ϖ_1 that was mentioned previously, i.e. ϖ_1 circulates with $\dot{\varpi}_1 < 0$. According to the upper figure in figures 3.7, the eccentricity takes small values ($e_1 \lesssim 0.1$) for the first three outer orbital periods and then the effect of the exponential term becomes noticeable. At the same time, as seen from the lower graph, the pericentre starts librating. However, the quantities n_1 and n_2 do not remain quite constant, as was assumed in the derivation of equations (3.20) and (3.21); as can be seen from figure 3.9, the quantity $n_1 - 3n_2$ oscillates around zero for the initial phase of the evolution of the system, but it moves away from zero during the phase in which the eccentricity takes large values, apparently causing the eccentricity to drop.

It is worth mentioning here that the discrepancy between figure 3.8, which is from the integration of the full equations of motion, and the upper of figures 3.7, concerning the moment when the eccentricity starts to increase to large values, is because of the fact that figure 3.7 is just an approximation to the real situation. A perturbing Hamiltonian with more terms could lead to a more accurate description of the problem. However, equations (3.20) and (3.21) provide us with a semi-quantitative picture of the evolution of the inner eccentricity and longitude of pericentre during the early stages of the evolution

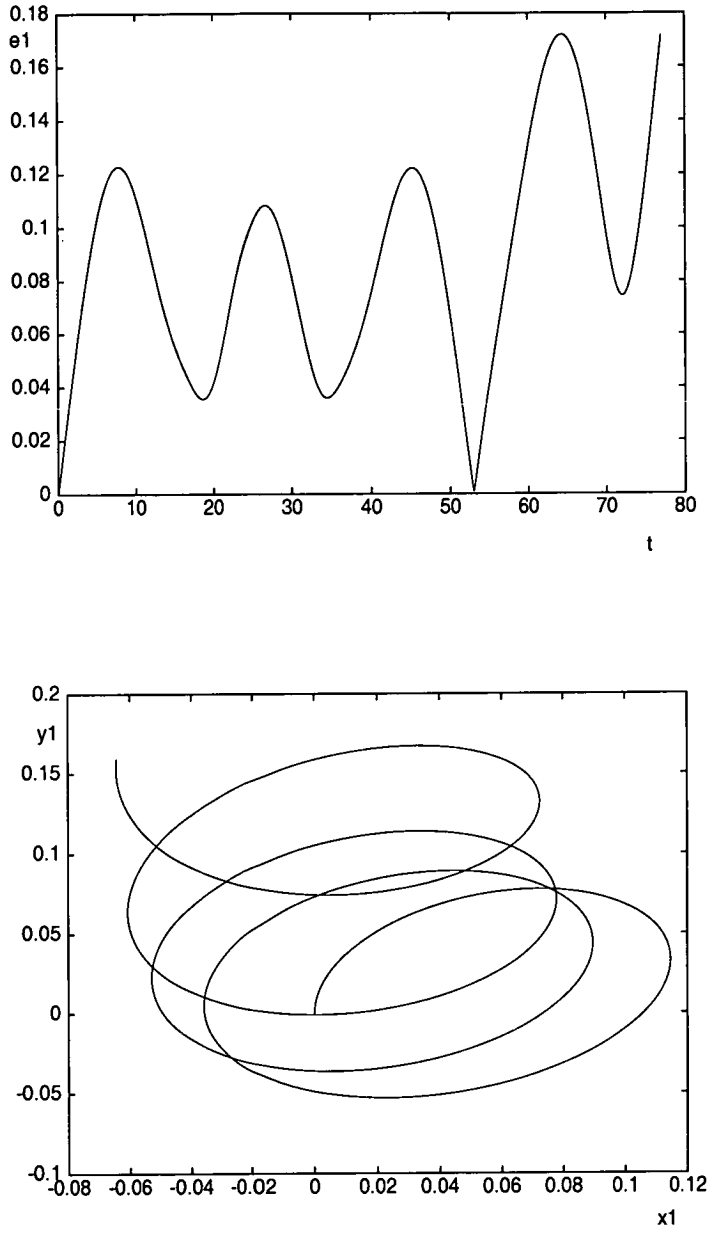

Figure 3.7: Eccentricity against time and y_1 against x_1 for $t = 0 - 4$ outer orbital periods and for a triple system with $m_1 = 0.01$, $m_2 = 0.99$, $m_3 = 0.1$ and $X_0 = 3.07$. The graphs are based on equations (3.20) and (3.21) and the initial conditions are: $x_{10} = 0, y_{10} = 0$ and $\lambda_{20} = 90°$.

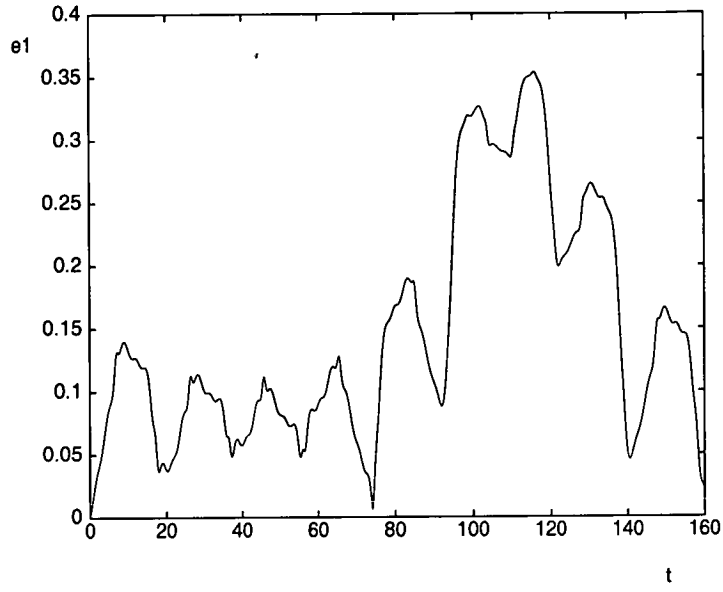

Figure 3.8: Inner eccentricity against time, for time $t = 0 - 8$ outer orbital periods, from an integration of the full equations of motion for a system with $m_1 = 0.01$, $m_2 = 0.99$, $m_3 = 0.1$ and $X_0 = 3.07$.

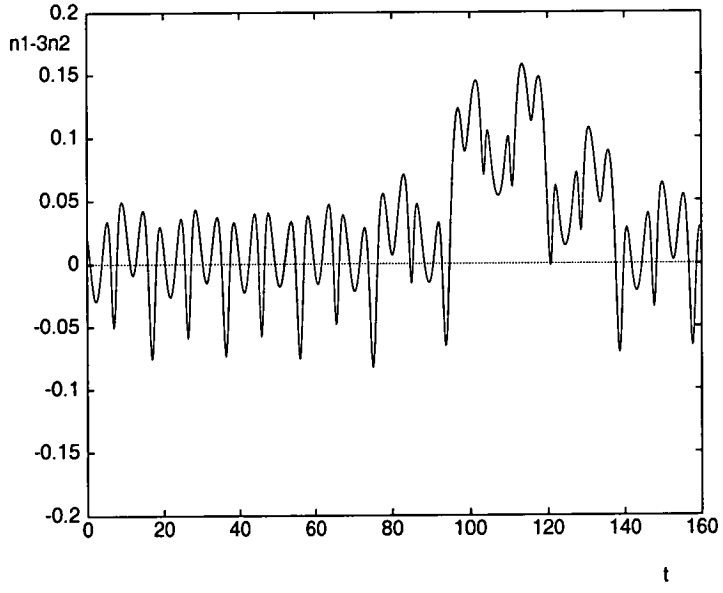

Figure 3.9: The quantity $n_1 - 3n_2$ against time, for time $t = 0 - 8$ outer orbital periods from an integration of the full equations of motion for a system with $m_1 = 0.01$, $m_2 = 0.99$, $m_3 = 0.1$ and $X_0 = 3.07$.

of the hierarchical triple system.

3.4.3 An analytical criterion for stability for the 3:1 resonance

In the previous section, equations (3.16) and (3.17) were solved analytically by the use of the approximation $n_1 \approx 3n_2$. However, these equations may be solved in a different way without using that approximation.

If a new set of complex variables z and $\bar{z}$ is introduced, defined as

$$z = x_1 + iy_1 \quad , \quad \bar{z} = x_1 - iy_1,$$

then

$$\dot{z} = \dot{x}_1 + i\dot{y}_1 \quad \text{and} \quad \dot{\bar{z}} = \dot{x}_1 - i\dot{y}_1.$$

Using equations (3.16) and (3.17) to substitute for $\dot{x}_1$ and $\dot{y}_1$, the differential equations for z and $\bar{z}$ are:

$$\dot{z} = 9Aie^{-i(n_1-2n_2)t} + \frac{285}{8}ABe^{-i(n_1-3n_2)t}\bar{z} \tag{3.22}$$

$$\dot{\bar{z}} = -9Aie^{i(n_1-2n_2)t} + \frac{285}{8}ABe^{i(n_1-3n_2)t}z. \tag{3.23}$$

Introducing a new variable

$$\omega = e^{-i(n_1-3n_2)\frac{t}{2}}\bar{z},$$

the system of differential equations takes the form

$$\begin{pmatrix} \dot{\omega} \\ \dot{\bar{\omega}} \end{pmatrix} = \begin{pmatrix} -\frac{i}{2}(n_1-3n_2) & \frac{285}{8}AB \\ \frac{285}{8}AB & \frac{i}{2}(n_1-3n_2) \end{pmatrix} \begin{pmatrix} \omega \\ \bar{\omega} \end{pmatrix} + \begin{pmatrix} -9Aie^{i(n_1-n_2)\frac{t}{2}} \\ 9Aie^{-i(n_1-n_2)\frac{t}{2}} \end{pmatrix}. \tag{3.24}$$

The characteristic equation of the matrix of coefficients leads to

$$\rho = \pm\sqrt{s} \equiv \pm\sqrt{\left(\frac{285}{8}AB\right)^2 - \frac{(n_1-3n_2)^2}{4}}, \tag{3.25}$$

where ρ denotes an eigenvalue. The dependence of s on the outer semi-major axis is shown in figure 3.10 for a typical case. A pair of real eigenvalues ($s > 0$) would lead to an exponentially growing solution in general, while a pair of purely imaginary solutions ($s < 0$) leads to a bounded solution to the problem. Hence, the equation $s = 0$ gives us a value for the period ratio X for a given triple system at which there is a qualitative change of the behaviour of the inner eccentricity. After some algebraic manipulations, the condition $s = 0$ yields:

$$X^{\frac{8}{3}} - 3X^{\frac{5}{3}} = \pm\frac{285}{16}\frac{m_3(m_1 - m_2)}{M^{\frac{4}{3}}(m_1 + m_2)^{\frac{2}{3}}}, \tag{3.26}$$

where M is the total mass of the system. Though it is easy to solve this equation numerically, we can derive an approximate solution which is more convenient and gives values very close to the solution of equation (3.26). If the equation is rearranged in the form

$$X = 3 + cX^{-\frac{5}{3}},$$

where c is the right side of equation (3.26), the equation may be solved iteratively starting at $X = 3$. The first iteration leads to

$$X = 3 \pm \frac{285}{16}\frac{m_3(m_1 - m_2)}{3^{\frac{5}{3}}M^{\frac{4}{3}}(m_1 + m_2)^{\frac{2}{3}}}, \tag{3.27}$$

which is sufficiently accurate for our purposes. Equation (3.27) is easier to use than equation (3.26) and the values it produces are very close to the roots of the exact equation. For instance, for a system with $m_1 = 0.01$, $m_2 = 0.99$ and $m_3 = 0.1$, equation (3.26) yields $X = 2.70$ and $X = 3.21$, while the corresponding values from equation (3.27) are $X = 2.75$ and $X = 3.24$. However, one should be careful when using equation (3.27), since it is not a good approximation for large m_3. This becomes clear in figure 3.11, where the solution of equation (3.26) is plotted for $m_3 = 0.1$. For large values of m_3, equation (3.26) has only one solution.

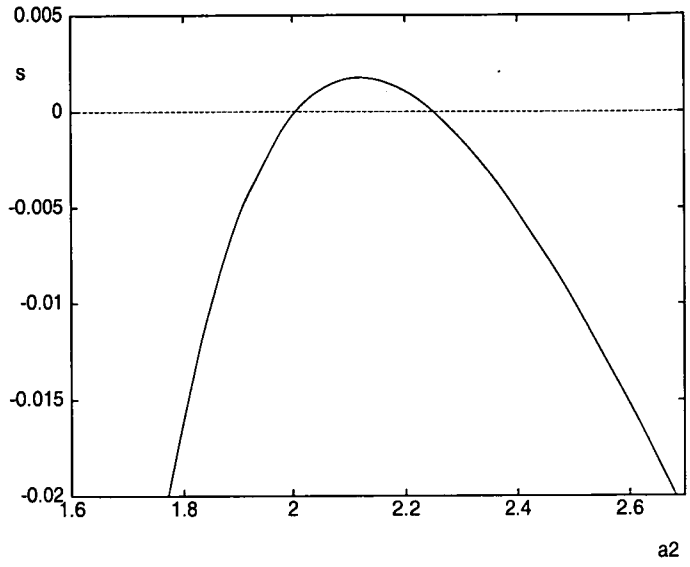

Figure 3.10: The quantity s plotted as a function of a_2 for a triple system with $m_1 = 0.01$, $m_2 = 0.99$, $m_3 = 0.1$ and $a_1 = 1$.

Table 3.3 compares values of X_0^{min} from the numerical integrations (for disruption within 100 and 1000 outer orbital periods) with values from the larger solution of equation (3.26) for a few systems in the vicinity of the system with $\alpha = 2.0$ and $\beta = 1.0$. The values which are predicted analytically are always higher than those from the numerical integrations. One reason for this may be that the simulations run for a certain time span. Systems that are stable within the integration time could be unstable for a longer integration time. Another reason is that a system could start with $s > 0$ but switch to $s < 0$ before the system breaks up. This is because the theory developed in this section assumes that the angular velocities of both binaries remain constant, which is not the case, as seen in figure 3.9. This simplification will be avoided in the improved theory presented in section 3.6. Therefore, an improvement to the analytical criterion would be to find the value of X where the system starts with positive s and when s is zero the inner eccentricity is equal to 1.

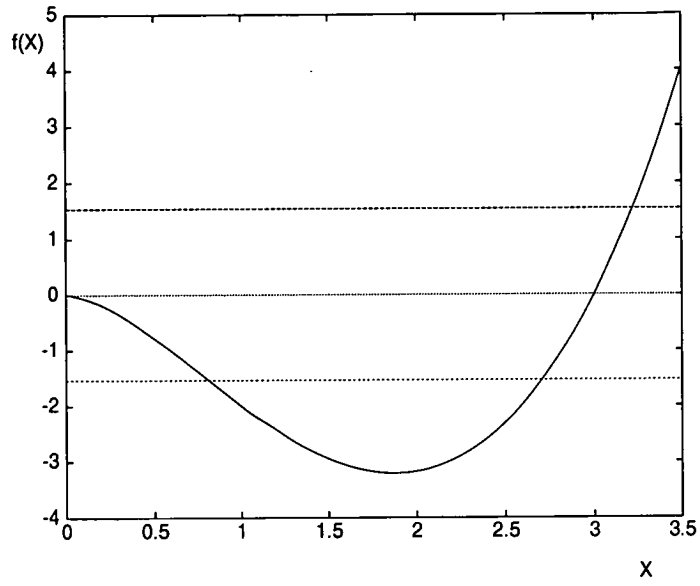

Figure 3.11: A graphical representation of equation (3.26) for a triple system with $m_1 = 0.01$, $m_2 = 0.99$, $m_3 = 0.1$. The solid curve is the graph of the left side, denoted as f(X), and the two dashed lines represent the right side. It is clear that for large m_3, equation (3.26) has only one solution.

Table 3.3: Values of X_0 for which a system with $m_1 = 0.01$ and $m_2 = 0.99$ breaks up.

m_3	$t = 100T_{out}$	$t = 1000T_{out}$	Theoretical value
0.08	3.02	3.07	3.18
0.10	3.07	3.11	3.21
0.12	3.09	3.18	3.25
0.14	3.17	3.23	3.28
0.16	3.18	3.29	3.31
0.18	3.24	3.29	3.33
0.20	3.25	3.36	3.36
0.23	3.33	3.40	3.39

3.5 The 4:1 resonance

As we move up in Table 3.1, values of X_0^{min} close to 4 appear, which indicates that the triple system disrupted in the neighbourhood of the 4:1 mean motion resonance. For example, integrations with Mikkola's symplectic integrator revealed that the systems with masses $m_1 = 0.01, m_2 = 0.99, m_3 = 0.16$ and $m_1 = 0.01, m_2 = 0.99, m_3 = 0.25$ broke up at $X_0 = 3.87$ and $X_0 = 3.82$ respectively, within the first 100 outer binary orbital periods. Figures 3.12 present a typical result (in this case $m_3 = 0.16$). The eccentricity reaches large values ($e_1 \approx 0.5$), while the pericentre progresses very slowly.

We now consider a simple model Hamiltonian analogous to equation (3.13) for the 3 : 1 resonance. In the vicinity of the 4 : 1 resonance the angle $\lambda_1 - 4\lambda_2$ is almost stationary. In the perturbation expansion equation (1.16), the first term containing this combination of angles appears in the P_4 term. It has argument $\lambda_1 - 4\lambda_2 + 3\varpi_1$ (which is nearly stationary if the inner pericentre is slowly varying, cf. figure 3.12) and has a coefficient proportional to e_1^3. This term by itself does not generate any eccentricity in a circular binary. The main term that does so is again the leading term with argument $\lambda_1 - 2\lambda_2 + \varpi_1$, because, of all terms in the expansion of the perturbing potential which depend on ϖ_1, it has the largest coefficient and the smallest frequency, though it is non-resonant.

Figures 3.13 represent the same system as figures 3.12, but show an integration of the model problem using a 4th-order Runge-Kutta integrator. Although the model on which these graphs are based is rather simple, it produces an eccentricity of significant amplitude. As already indicated, the non-resonant term provides a non-zero eccentricity for the early stages of the evolution of the system. This is confirmed by figures 3.14, where the eccentricity of a model with

a one-term perturbing Hamiltonian (the non-resonant term only) is compared to the eccentricity produced by the numerical solution of the full equations of motion during the early evolution. One should note the very good agreement between the frequency of the oscillations in the two graphs. Even when the resonant term dominates, however, and the eccentricity reaches large values, the contribution of the non-resonant term cannot be neglected: the small spikes in the eccentricity graph in figure 3.13 (and presumably also in figure 3.12) represent its contribution.

3.6 A general criterion for the k+1:1 resonance

3.6.1 General theory

As was seen in the last two sections, the dynamical evolution of the triple systems that were studied, i.e. systems with one component of the inner binary less massive than the other two bodies, was mainly determined by mean motion commensurabilities. This behaviour can be described in a more general way as follows: if the system is close to a $k+1:1$ resonance, a suitable Hamiltonian would be

$$\begin{aligned} H &= -\frac{G^2 m^3 (m_1+m_2)^2}{2L_1^2} + \frac{G m_1 m_2 m_3}{m_1+m_2}\left[\frac{a_1^2}{a_2^3}\left(-\frac{1}{4}-\frac{3}{8}e_1^2\right)+(-1)^k C_f \times\right. \\ &\left. \times \frac{m_2^k-(-m_1)^k}{(m_1+m_2)^k}\frac{a_1^{k+1}}{a_2^{k+2}} e_1^k \cos\left(\ell_1-(k+1)\lambda_2+(k+1)\varpi_1\right)\right], \end{aligned} \tag{3.28}$$

where

$$m = \frac{m_1 m_2}{m_1+m_2}$$

and C_f is the coefficient of the resonant argument in a Legendre polynomial expansion of the perturbing potential. These coefficients can be found in Murray and Dermott (1999) (for arguments with coefficients up to second order with respect to the eccentricities and for a P_2 and P_3 expansion, C_f can also be

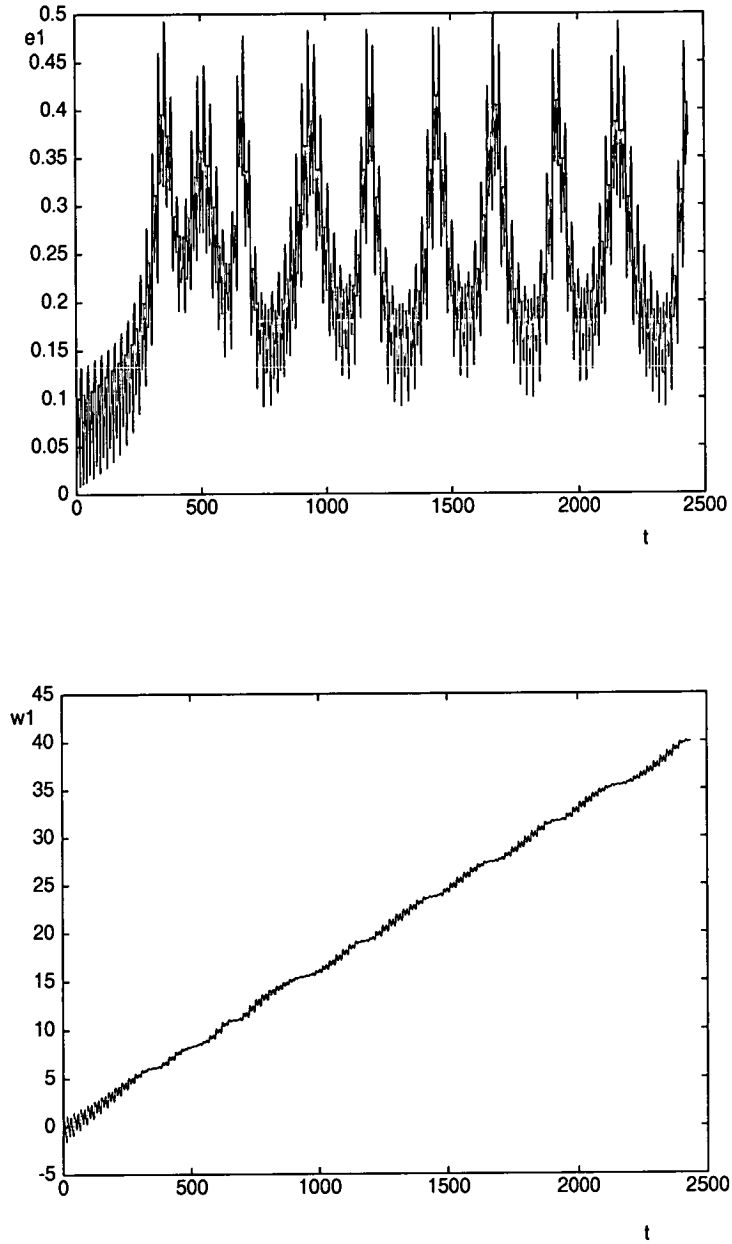

Figure 3.12: Eccentricity and longitude of pericentre against time for a system with $m_1 = 0.01$, $m_2 = 0.99$, $m_3 = 0.16$ and $X_0 = 3.88$. The graphs are from integration of the full equations of motion.

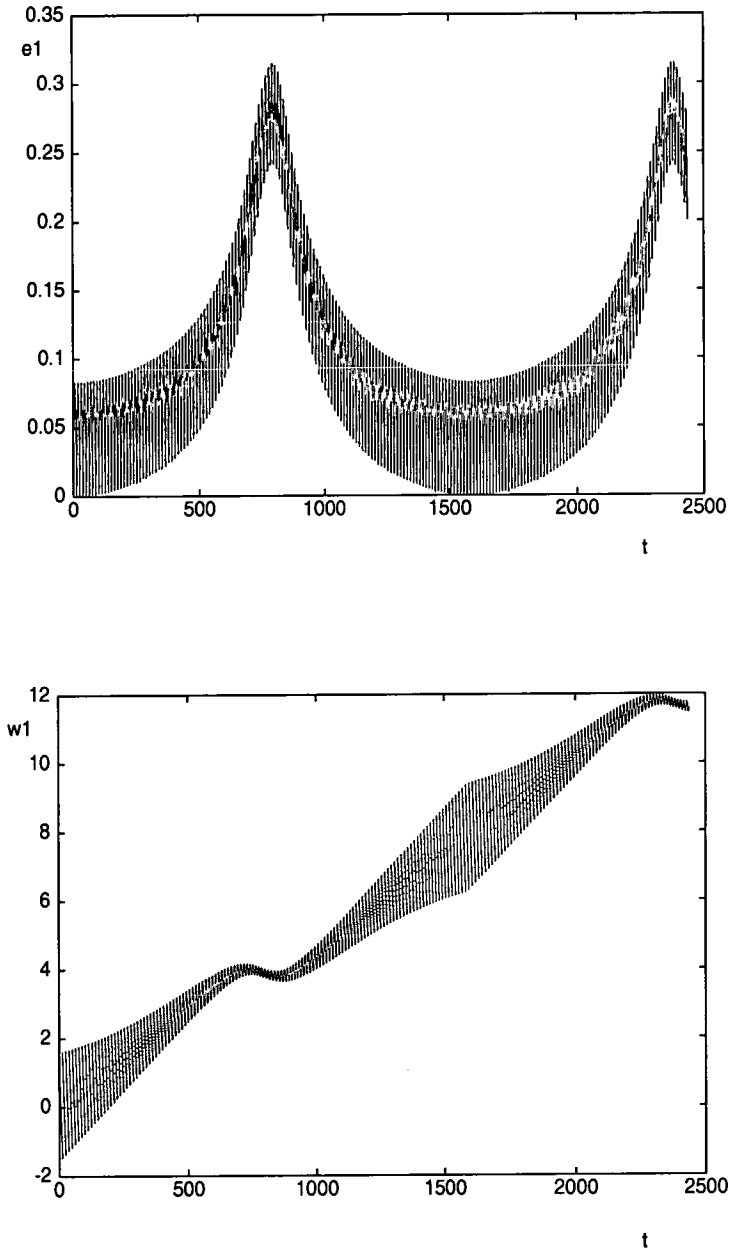

Figure 3.13: Eccentricity and longitude of pericentre against time for a system with $m_1 = 0.01$, $m_2 = 0.99$, $m_3 = 0.16$ and $X_0 = 3.88$, using an averaged Hamiltonian.

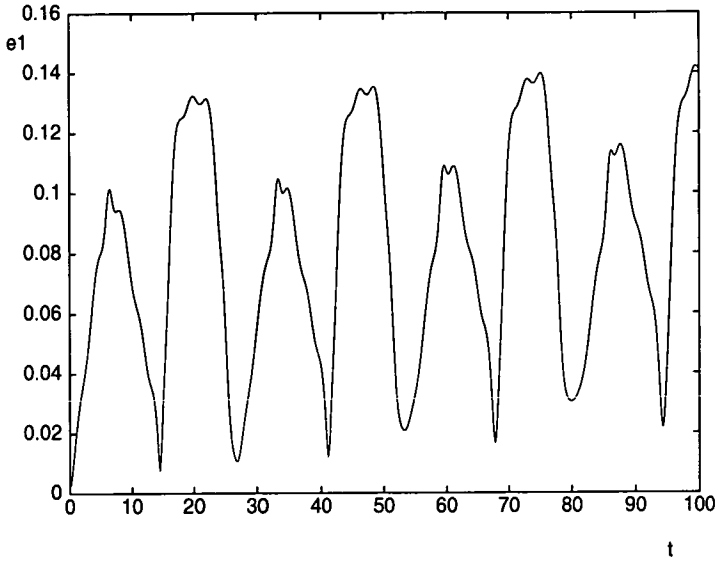

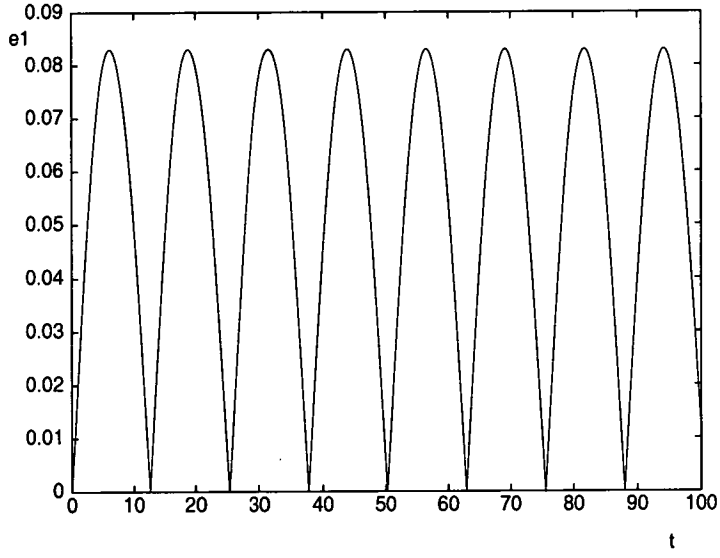

Figure 3.14: Eccentricity against time for a system with $m_1 = 0.01, m_2 = 0.99, m_3 = 0.16$ and $X_0 = 3.88$. The upper graph is from the full equations of motion while the lower one comes from the use of a single term perturbing Hamiltonian.

found in Appendix B). The first term in equation (3.28) is the unperturbed Hamiltonian for the inner binary (cf. section 1.4.3).

The perturbing Hamiltonian includes just the resonant argument, since we are interested in the phase when the inner eccentricity becomes large: ultimately, that is what leads to the disruption of the system. The resonant term appears at lowest order in P_{k+1} because of the properties that arise from expanding the perturbing potential. More details can be found in Clemence and Brouwer (1961) and in Murray and Dermott (1999). The other two terms involved in the perturbing Hamiltonian are secular terms, i.e. terms that do not involve mean longitudes and are included to provide an improvement to our approximation. These terms, which can be found in Appendix B, were not included in our approximate models of the previous sections since they do not affect the evolution of the eccentricity. They do affect the mean motions, but in our previous treatment the mean motions were assumed to be constant. In the present section, however, we make no such assumption about the mean motions (at least for the inner binary mean motion). We have neglected the term with argument

$$\lambda_1 - 2\lambda_2 + \varpi_1.$$

Its main role, however, is to generate a small initial eccentricity, and this feature of the problem will be reintroduced in due course. We now employ a canonical transformation with the generating function

$$F(q_i, J_i, t) = J_f(\ell_1 + \varpi_1) + J_s(-\ell_1 + (k+1)\lambda_2 - (k+1)\varpi_1), \qquad (3.29)$$

where q_i and J_i are the old coordinates (ℓ_1, ϖ_1) and the new momenta, respectively. The indices f and s stand for fast and slow moving variables respectively. For this type of generating function (Goldstein 1980, Szebehely 1967),

$$p_i = \frac{\partial F}{\partial q_i} \tag{3.30}$$

$$\Theta_i = \frac{\partial F}{\partial J_i} \tag{3.31}$$

$$H' = H + \frac{\partial F}{\partial t}, \tag{3.32}$$

where p_i are the old momenta (L_1, G_1), i.e. the Delaunay variables defined in section 1.4.2, Θ_i are the new coordinates and H' is the new Hamiltonian. Equation (3.30) yields

$$J_s = \frac{L_1}{2k} e_1^2 \tag{3.33}$$

$$J_f = L_1(1 + \frac{1}{2k} e_1^2) \tag{3.34}$$

to second order with respect to the eccentricities. We assume that $\lambda_2 = n_2 t + \lambda_{20}$, and so, by equation (3.32), the new Hamiltonian of the problem is

$$\begin{aligned} H' = & -\frac{G^2 m^3 (m_1+m_2)^2}{2(J_f - J_s)^2} + \frac{G m_1 m_2 m_3}{m_1+m_2}[-\frac{1}{4}\frac{(J_f-J_s)^4}{m^4\mu^2 a_2^3} - \\ & -\frac{3}{8}\frac{2k}{m^4\mu^2 a_2^3} J_s (J_f - J_s)^3 + (-1)^k \frac{m_2^k - (-m_1)^k}{(m_1+m_2)^k} \frac{(2k)^{\frac{k}{2}}}{m^{2(k+1)}\mu^{k+1}} \times \\ & \times \frac{C_f}{a_2^{k+2}} (J_f - J_s)^{2(k+1)} (\frac{J_s}{J_f - J_s})^{\frac{k}{2}} \cos\Theta_s] + (k+1) n_2 J_s, \end{aligned} \tag{3.35}$$

where $\Theta_s = -\ell_1 + (k+1)\lambda_2 - (k+1)\varpi_1$ (by equation 3.31) and $\mu = G(m_1+m_2)$.

Since $J_f >> J_s$ while the eccentricity remains small, the above Hamiltonian can be expanded with respect to J_s/J_f, and to first order we obtain

$$\begin{aligned} H' = & -\frac{G^2 m^3 (m_1+m_2)^2}{2J_f^2}(1 + 2\frac{J_s}{J_f}) + \frac{G m_1 m_2 m_3}{m_1+m_2}[\frac{1}{m^4\mu^2 a_2^3} \times \\ & \times (-\frac{1}{4} J_f^4 + (1 - \frac{3}{4}k) J_s J_f^3) + (-1)^k \frac{m_2^k - (-m_1)^k}{(m_1+m_2)^k} \times \\ & \times \frac{(2k)^{\frac{k}{2}}}{m^{2(k+1)}\mu^{k+1}} \frac{C_f}{a_2^{k+2}} J_f^{2(k+1)} (\frac{J_s}{J_f})^{\frac{k}{2}} \cos\Theta_s] + (k+1) n_2 J_s. \end{aligned} \tag{3.36}$$

(In fact the resonant term, being a perturbation, is expanded only to lowest order.) Dropping the prime, the new approximate Hamiltonian is of the form

$$H = A + B J_s + C J_s^{\frac{k}{2}} \cos\Theta_s \tag{3.37}$$

with the constants A, B and C defined as

$$A = -\frac{G^2m^3(m_1+m_2)^2}{2J_f^2} - \frac{1}{4}\frac{Gm_1m_2m_3}{m_1+m_2}\frac{J_f^4}{m^4\mu^2a_2^3} \tag{3.38}$$

$$B = -\frac{G^2m^3(m_1+m_2)^2}{J_f^3} + (1-\frac{3}{4}k)\frac{Gm_1m_2m_3}{m_1+m_2}\frac{J_f^3}{m^4\mu^2a_2^3} + \\ +(k+1)n_2 \tag{3.39}$$

$$C = (-1)^k\frac{Gm_1m_2m_3}{m_1+m_2}\frac{m_2^k-(-m_1)^k}{(m_1+m_2)^k}\frac{(2k)^{\frac{k}{2}}}{m^{2(k+1)}\mu^{k+1}}\frac{C_f}{a_2^{k+2}}J_f^{\frac{3}{2}k+2}. \tag{3.40}$$

If J_s is considered to be a function of Θ_s then, the extrema of J_s can be obtained by differentiating equation (3.37) with respect to Θ_s and they will be given by

$$\frac{dJ_s}{d\Theta_s} = \frac{CJ_s^{\frac{k}{2}}\sin\Theta_s}{B+C\frac{k}{2}J_s^{\frac{k}{2}-1}\cos\Theta_s} = 0, \tag{3.41}$$

which yields $\Theta_s = 0$ and $\Theta_s = \pi$. Hence, the curves

$$H_1 = A + BJ_s + CJ_s^{\frac{k}{2}} \tag{3.42}$$

and

$$H_2 = A + BJ_s - CJ_s^{\frac{k}{2}} \tag{3.43}$$

will be the boundaries of the motion for the system on the $H - J_s$ plane. This is demonstrated in figure 3.15. A simple analysis shows that H_1 gives the maximum value of J_s and H_2 the minimum value if $BC < 0$, whereas the roles of H_1 and H_2 are reversed if $BC > 0$.

Now we estimate the initial value of the variable J_s. This variable is used in the Hamiltonian (3.35), which omits all high-frequency terms. The omission of these terms is justified by Von Zeipel's method (section 1.4.4), i.e. a canonical form of the method of averaging. This implies, however, that J_s must be interpreted in an averaged sense, i.e. the quantity e_1^2 in equation (3.33) is the mean square eccentricity. It should be recalled that, initially, the eccentricity evolution is mainly governed by the term associated with the argument

$\lambda_1 - 2\lambda_2 + \varpi_1$. Thus, a single term perturbing Hamiltonian

$$H_p = \frac{9}{4}\frac{Gm_1m_2m_3}{m_1+m_2}\frac{a_1^2}{a_2^3}e_1\cos(\lambda_1 - 2\lambda_2 + \varpi_1) \tag{3.44}$$

leads to

$$\dot{e}_1 = -\frac{9}{4}\frac{Gm_3}{n_1a_2^3}\sin(\lambda_1 - 2\lambda_2 + \varpi_1) \tag{3.45}$$

$$\dot{\varpi}_1 = -\frac{9}{4}\frac{Gm_3}{e_1n_1a_2^3}\cos(\lambda_1 - 2\lambda_2 + \varpi_1), \tag{3.46}$$

if terms of higher order in e_1 are neglected. Switching to the variables $x_1 = e_1\cos\varpi_1$ and $y_1 = e_1\sin\varpi_1$, the above system becomes:

$$\dot{x}_1 = -\frac{9}{4}\frac{Gm_3}{n_1a_2^3}\sin(\lambda_1 - 2\lambda_2) \tag{3.47}$$

$$\dot{y}_1 = -\frac{9}{4}\frac{Gm_3}{n_1a_2^3}\cos(\lambda_1 - 2\lambda_2). \tag{3.48}$$

The corresponding solution, for initial conditions $x_{10} = y_{10} = 0, \lambda_{10} = 0°$ and $\lambda_{20} = 90°$, is:

$$x_1 = -\frac{9}{4}\frac{Gm_3}{n_1a_2^3}\frac{1}{n_1-2n_2}\cos(n_1 - 2n_2)t + \frac{9}{4}\frac{Gm_3}{n_1a_2^3}\frac{1}{n_1-2n_2} \tag{3.49}$$

$$y_1 = \frac{9}{4}\frac{Gm_3}{n_1a_2^3}\frac{1}{n_1-2n_2}\sin(n_1 - 2n_2)t, \tag{3.50}$$

with the semi-major axes and mean motions treated as constants. By using equations (3.49) and (3.50), we can obtain the following expression for the root mean square eccentricity $\sqrt{< e_1^2 >}$:

$$\sqrt{< e_1^2 >} = \frac{9}{4}\frac{m_3}{M}\frac{1}{X(X-2)} \equiv e_{10}, \tag{3.51}$$

where e_{10} stands for the initial value that will be used for e_1 in the long-period problem. Hence the initial value of the variable J_s is taken to be

$$J_{s0} = \frac{L_{10}}{2k}e_{10}^2, \tag{3.52}$$

with L_{10} being the initial value of the L_1 Delaunay variable.

3.6.2 The 3:1 resonance

For the case of the 3 : 1 resonance, $k = 2$, $C_f = \frac{285}{64}$ and the curves giving the extreme values of J_s are

$$H_2 = A + (B - C)J_s \tag{3.53}$$

and

$$H_1 = A + (B + C)J_s \tag{3.54}$$

respectively. For an indefinite increase of the variable J_s, which implies indefinite increase of the eccentricity, the slopes of the above straight lines should be of opposite sign. Hence the limits between which this behaviour is possible are given by

$$B - C = 0 \tag{3.55}$$

$$B + C = 0. \tag{3.56}$$

Using again a system of units such that $G = 1$ and $m_1 + m_2 = 1$, and taking the initial value of the inner semi-major axis to be $a_{10} = 1$, the integral of motion J_f (equation 3.34) becomes

$$J_f = m_1 m_2 \left(1 + \frac{e_{10}^2}{4}\right)$$

and equations (3.55) and (3.56) yield:

$$\frac{64}{(4+e_{10}^2)^3} X^{\frac{8}{3}} - 3X^{\frac{5}{3}} + \frac{1}{2}\frac{m_3}{M}(1+\frac{e_{10}^2}{4})^3 X^{\frac{2}{3}} = \pm\frac{285}{16}\frac{m_3(m_2-m_1)}{M^{\frac{4}{3}}}(1+\frac{e_{10}^2}{4})^5 \tag{3.57}$$

where the + and − sign correspond to equations (3.56) and (3.55) respectively. Proceeding as in the derivation of equation (3.27), the following approximate equation is obtained:

$$X = \frac{(4+e_{10}^2)^3}{64}[3 - \frac{1}{6}\frac{m_3}{M}(1+\frac{e_{10}^2}{4})^3 \pm \frac{285}{16}\frac{m_3(m_2-m_1)}{M^{\frac{4}{3}}}(1+\frac{e_{10}^2}{4})^5 \frac{1}{3^{\frac{5}{3}}}]. \tag{3.58}$$

Again, the above approximation fails for large m_3, as seen with the corresponding result in section (3.4.3). When m_3 is not too large, however, we are now

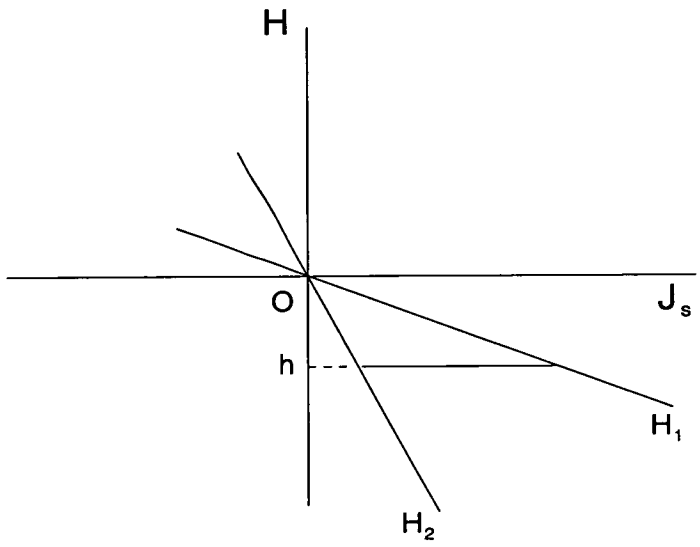

Figure 3.15: Motion boundaries on the $H - J_s$ plane for a system with its Hamiltonian value being h, in the case of the 3 : 1 resonance and for $B < 0$.

able to find an estimate for the initial period ratio for which the triple system breaks up.

3.6.3 The 4:1 resonance

The same general idea can be applied to the 4 : 1 resonance ($k = 3$). Again $C > 0$ (see below), and in this case the curve of maximum values of J_s is

$$H_1 = A + BJ_s + CJ_s^{\frac{3}{2}} \tag{3.59}$$

when $B < 0$ and

$$H_1 = A + BJ_s - CJ_s^{\frac{3}{2}} \tag{3.60}$$

when $B > 0$. Indefinite increase of $J_s$can be achieved when the value of the Hamiltonian of the system is less than (greater than) the minimum (maximum) value of the curve of maximum values for $B < 0$ ($B > 0$). This leads to the limiting conditions

$$\frac{B}{C} - \frac{4}{27}\frac{1}{J_{s0}}\frac{B^3}{C^3} = \pm J_{s0}^{\frac{1}{2}}, \tag{3.61}$$

where B and C have the form

$$B = \frac{4}{X} - \frac{216}{(6+e_{10}^2)^3} - \frac{5}{4}\frac{m_3}{M}(1+\frac{e_{10}^2}{6})^3\frac{1}{X^2} \tag{3.62}$$

$$C = \frac{6545}{768}6^{\frac{3}{2}}\frac{m_3(m_2^3+m_1^3)}{m_1^{\frac{1}{2}}m_2^{\frac{1}{2}}M^{\frac{5}{3}}}\left(1+\frac{e_{10}^2}{6}\right)^{\frac{13}{2}}\frac{1}{X^{\frac{10}{3}}}. \tag{3.63}$$

The + sign in equation (3.61) corresponds to $B < 0$, while the − sign corresponds to $B > 0$. In this case $C_f = \frac{6545}{768}$, which can be obtained from the appendix for the disturbing function in Murray and Dermott (1999). It can be shown that, for the range of parameter values of interest, the right-hand side of equation (3.61) is negligible compared with either term on the left-hand side. Approximately, therefore,

$$1 - \frac{4}{27}\frac{1}{J_{s0}}\frac{B^2}{C^2} = 0, \quad \text{and so} \quad B = \pm\sqrt{\frac{27}{4}J_{s0}C^2}.$$

This yields

$$X = \frac{(6+e_{10}^2)^3}{216}[4 - \frac{5}{16}\frac{m_3}{M}(1+\frac{e_{10}^2}{6})^3 \mp \sqrt{\frac{27}{4}J_{s0}C^2}], \tag{3.64}$$

where X has been approximated by 4 in the right-hand side.

3.6.4 Comparison with numerical data

Figures 3.16 demonstrate the results for stability obtained throughout this section, superimposed on the stability plots of section 3.3. Table 3.4 also presents results from equations (3.57) and (3.61) and results obtained from formulae by the authors from section 3.1.

The results for the 3 : 1 resonance, obtained by equations (3.57), show satisfactory agreement with the numerical integrations. They are represented by the two curves in the upper of figures 3.16, each one corresponding to a different sign of equation (3.57). The upper stability limit appears to give a good fit for moderate m_3, but it seems to fail for small and large m_3. However, it is likely

that the dynamical evolution of these systems is determined by resonances of other orders, e.g. $2:1$ resonance. Indeed it was suggested earlier that the $4:1$ resonance is important in systems with $m_3 = 0.16$ and $m_3 = 0.25$. It is possible that the fact that the triple systems are unstable as we move to the left of the left curve can be attributed to overlapping with other resonances.

The theoretical model for the $4:1$ resonance shows some discrepancy with the numerical results. As seen from the lower of figures 3.16, the theoretical curves are displaced to the right with respect to the numerical results. Although it is not very clear why this happens, it can be argued that the choice of the initial conditions can affect the position and the size of the area determined by the two curves. To be more specific, an averaged Hamiltonian has been used to describe the evolution of the system, but the initial conditions used in various phases of the calculation correspond to the untruncated problem. For instance, the inner semi-major axis was taken to be $a_1 = 1$ when L_{10} was computed. Just as with the eccentricity, the initial value of the semi-major axis that corresponds to the averaged problem would be different. Another improvement to the theory would be to include higher order secular and resonant terms in the Hamiltonian (3.28). However, it should be borne in mind that the numerical integrations were performed for a specific time span. Numerical simulations over larger time spans would be expected to give a higher initial period ratio for which the system disrupts. Nonetheless, the theoretical criterion given by equation (3.61) works much better than the other criteria described in section 3.1 (as will be discussed below). The only problem with it is that one must know in advance that the $4:1$ resonance affects the dynamics of the triple system in order to use the corresponding equation. (The same holds for the $3:1$ resonance criterion.) With that proviso, however, the technique we have developed is applicable in principle to any other resonance ($2:1$, $5:1$, etc.), as long as one component of

the inner binary is much less massive than the other two stars.

Finally, the values from the stability criteria by other authors disagree more seriously with the numerical results presented in Table 3.2. The values from the Szebehely-Zare c^2H criterion are always larger than the numerical ones and this is because of the sufficient nature of the criterion. Harrington's results are also larger than the numerical results and they also appear to be insufficiently sensitive to the variation of m_3. This probably has to do with Harrington's definition of stability and the time span of his numerical integations, as pointed out in section 3.1. The Graziani-Black criterion gives reasonable values for smaller m_3, but it fails as we move to systems with larger third bodies. This could be due to their ambiguous definition for stability or due to the choice of the triple systems they integrated. The Eggleton and Kiseleva formula seems to produce more consistent results compared to our numerical integrations. That was not unexpected, since their definition of stability is quite similar to ours and their criterion is empirical. However, the results are not very good for small and large m_3. Finally, the Mardling-Aarseth criterion predicts larger values for period ratios of stable configurations. Since the theoretical basis of this criterion is still unpublished, we do not have much information about it. It seems, however, that the theory involves the phenomenon of chaos, which has not been considered in our theory. (The criterion of Mardling and Aarseth is derived in analogy to chaotic energy exchange in the binary-tides problem.)

3.7 Conclusion

The aim of this chapter was to investigate the stability of hierarchical triple systems with small initial period ratio. We mainly focussed on systems in which one of the inner binary masses was small compared to the other two.

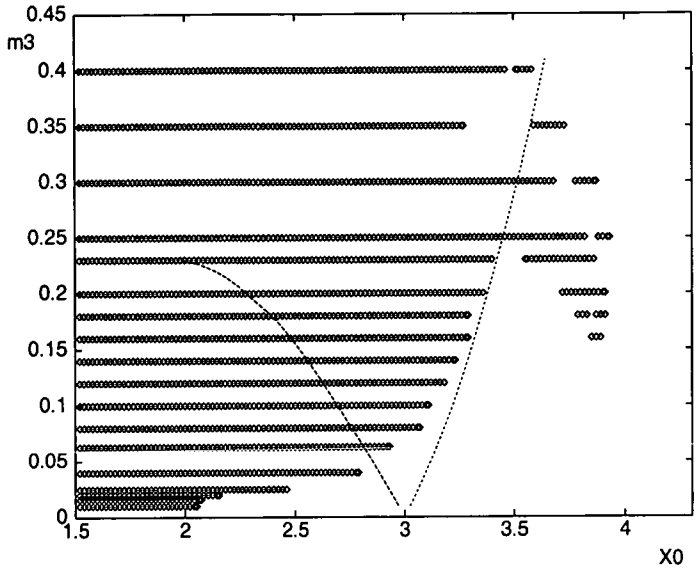

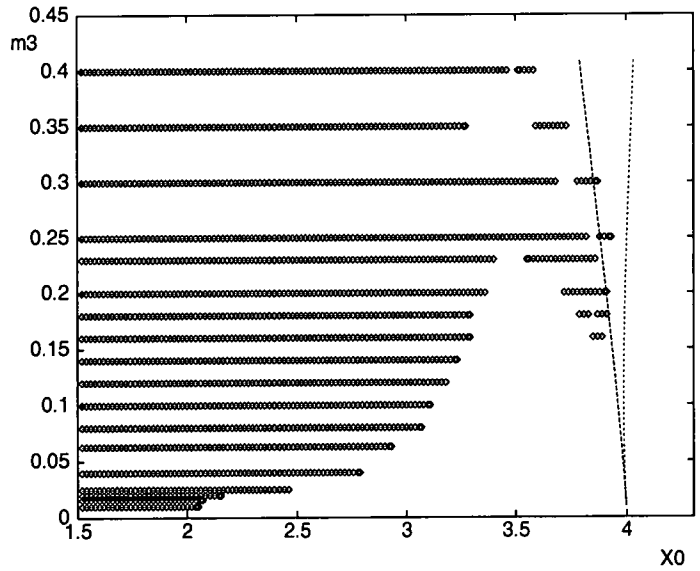

Figure 3.16: Outer mass m_3 against initial period ratio X_0, for which a system with $m_1 = 0.01$ and $m_2 = 0.99$ becomes unstable within 1000 outer orbital periods. The dots denote instability and are the results of numerical integrations of the full equations of motion. The superimposed curves are defined by equations (3.57) (upper graph) and (3.61) (lower graph).

Table 3.4: Comparison of the values of our criterion for $k = 2$ (denoted as NG2) and $k = 3$ (denoted as NG3) with the values of the Harrington (HR), Graziani and Black (GB), Eggleton and Kiseleva (EK), Mardling and Aarseth (MA), Szebehely and Zare (SZ) criteria for a system with $m_1 = 0.01$ and $m_2 = 0.99$. The Szebehely-Zare criterion values correspond to when exchange of m_1 between the other two bodies is possible.

m_3	NG2	NG3	HR	GB	EK	MA	SZ
0.08	2.75, 3.17	3.96, 3.98	5.38	2.98	2.82	4.72	4.11
0.10	2.69, 3.21	3.95, 3.98	5.38	3.16	2.96	4.73	4.20
0.12	2.62, 3.25	3.94, 3.98	5.38	3.32	3.08	4.73	4.28
0.14	2.55, 3.28	3.93, 3.98	5.38	3.46	3.19	4.74	4.36
0.16	2.48, 3.31	3.92, 3.98	5.38	3.60	3.28	4.75	4.44
0.18	2.39, 3.35	3.91, 3.99	5.38	3.72	3.37	4.76	4.51
0.20	2.28, 3.38	3.90, 3.99	5.37	3.84	3.46	4.77	4.58
0.23	1.98, 3.42	3.89, 3.99	5.37	4.00	3.57	4.78	4.68
0.25	3.45	3.88, 4.00	5.37	4.10	3.64	4.79	4.74
0.30	3.51	3.85, 4.00	5.37	4.33	3.79	4.80	4.88
0.35	3.57	3.82, 4.02	5.36	4.54	3.92	4.82	5.00
0.40	3.63	3.79, 4.03	5.36	4.73	4.04	4.84	5.11

The analytical criterion that was derived in section 3.6, seemed to be roughly consistent with the results from the numerical integrations. It should be pointed out that the study concerned systems in which the outer binary was initially 90° ahead of the inner one. It is not clear what would happen in the general case where the outer binary would start at an arbitrary angle ϕ with respect to the inner system.

The cases that have been investigated throughout this chapter constitute a very small part of the general problem. The stability of systems with more comparable masses, initially non-circular and non-coplanar orbits would be the logical next step in this investigation. It will also be interesting to study the effect of different initial phases on the stability of hierarchical triple systems. Although the present chapter has provided a rather brief insight into the dynamics of the stability of hierarchical triple systems, it sets a good base for any future work on the subject.

Appendix A

Equations of motion in the unequal masses, non-coplanar orbits, eccentric outer binary case

The complete secular equations of motion in the unequal masses, non-coplanar orbits, eccentric binary case, used in section 2.2.4, are:

$$\begin{aligned}
\frac{dx_S}{d\tau} &= \frac{5}{(1-e_T^2)^{\frac{3}{2}}}\sin^2 I\frac{1-x_S^2}{(1-x_S^2-y_S^2)^{\frac{1}{2}}}y_S+\frac{5}{16}\alpha\frac{e_T}{(1-e_T^2)^{\frac{5}{2}}}(1-x_S^2- \\
&-y_S^2)^{\frac{1}{2}}[\sin g_T\cos I(4+3(x_S^2+y_S^2)-5\sin^2 I(1-x_S^2+6y_S^2))- \\
&-10(1-x_S^2-y_S^2)\sin I^2\cos I\sin g_T+2(3+5\sin^2 I)(y_S^2\sin g_T\times \\
&\times\cos I+x_Sy_S\cos g_T)+20\sin^2 I\cos Iy_S^2\sin g_T-70\sin^2 I(y_S^2\times \\
&\times\sin g_T\cos I+x_Sy_S\cos g_T)]+\frac{5}{16}\alpha\beta\frac{e_T}{(1-e_T^2)^3}[y_S^2\sin g_T(4+ \\
&+3(x_S^2+y_S^2)-5\sin^2 I(1-x_S^2+6y_S^2))+10\cos I(y_S^2\sin g_T\times \\
&\times\cos I+x_Sy_S\cos g_T)(1-x_S^2+6y^2)+10(1-x_S^2-y_S^2)y_S^2\times \\
&\times\sin g_T(2\cos^2 I-\sin^2 I)]+\frac{5}{16}\alpha\frac{e_T}{(1-e_T^2)^{\frac{5}{2}}}\frac{1}{(1-x_S^2-y_S^2)^{\frac{1}{2}}}\times
\end{aligned}$$

$$\times[y_S^2 \sin g_T \cos I(4+3(x_S^2+y_S^2)-5\sin^2 I(1-x_S^2+6y_S^2))+$$

$$+10(y_S^2 \sin g_T \cos I + x_S y_S \cos g_T)\cos^2 I(1-x_S^2+6y_S^2)+$$

$$+10(1-x_S^2-y_S^2)y_S^2 \sin g_T(2\cos^2 I-\sin^2 I)\cos I]-$$

$$-\frac{\beta}{(1-e_T^2)^2}y_S \cos I(1-x_S^2+4y_S^2)-\frac{1}{(1-e_T^2)^{\frac{3}{2}}}y_S \times$$

$$\times\frac{2-2x_S^2+3y_S^2}{(1-x_S^2-y_S^2)^{\frac{1}{2}}}+\gamma\frac{3+2e_T^2}{(1-e_T^2)^3}(1-x_S^2-y_S^2)\cos I y_S(2\sin^2 I-$$

$$-\frac{25}{8})+\frac{1}{16}\beta\gamma\frac{3+2e_T^2}{(1-e_T^2)^{\frac{7}{2}}}(1-x_S^2-y_S^2)^{\frac{1}{2}}y_S[2-27x_S^2-57y_S^2-$$

$$-3\sin^2 I(1-x_S^2-16y_S^2)]+\frac{1}{8}\gamma\frac{3+2e_T^2}{(1-e_T^2)^3}\cos^3 I y_S(1-x_S^2-$$

$$-16y_S^2) \tag{A.1}$$

$$\frac{dy_S}{d\tau} = -\frac{5}{(1-e_T^2)^{\frac{3}{2}}}\sin^2 I\frac{x_S y_S^2}{(1-x_S^2-y_S^2)^{\frac{1}{2}}}y_S+\frac{5}{16}\alpha\frac{e_T}{(1-e_T^2)^{\frac{5}{2}}}(1-$$

$$-x_S^2-y_S^2)^{\frac{1}{2}}[-\cos g_T(4+3(x_S^2+y_S^2)-5\sin^2 I(1-x_S^2+$$

$$+6y_S^2))-2(3+5\sin^2 I)(x_S y_S \sin g_T \cos I + x_S^2 \cos g_T)-$$

$$-20\sin^2 I \cos I x_S y_S \sin g_T]+\frac{5}{16}\alpha\beta\frac{e_T}{(1-e_T^2)^3}[-x_S y_S \sin g_T \times$$

$$\times(4+3(x_S^2+y_S^2)-5\sin^2 I(1-x_S^2+6y_S^2))-10\cos I(x_S \times$$

$$\times y_S \sin g_T \cos I + x_S^2 \cos g_T)(1-x_S^2+6y_S^2)-10(1-x_S^2-$$

$$-y_S^2)x_S y_S \sin g_T(2\cos^2 I-\sin^2 I)]+\frac{5}{16}\alpha\frac{e_T}{(1-e_T^2)^{\frac{5}{2}}}\times$$

$$\times\frac{1}{(1-x_S^2-y_S^2)^{\frac{1}{2}}}[-x_S y_S \sin g_T \cos I(4+3(x_S^2+y_S^2)-5\sin^2 I\times$$

$$\times(1-x_S^2+6y_S^2))-10(x_S y_S \sin g_T \cos I + x_S^2 \cos g_T)\cos^2 I(1-$$

$$-x_S^2+6y_S^2)-10(1-x_S^2-y_S^2)x_S y_S \sin g_T(2\cos^2 I-\sin^2 I)\times$$

$$\times\cos I]+\frac{\beta}{(1-e_T^2)^2}x_S \cos I(1-x_S^2+4y_S^2)+\frac{1}{(1-e_T^2)^{\frac{3}{2}}}x_S \times$$

$$\times\frac{2-2x_S^2+3y_S^2}{(1-x_S^2-y_S^2)^{\frac{1}{2}}}+\gamma\frac{3+2e_T^2}{(1-e_T^2)^3}(1-x_S^2-y_S^2)\cos I x_S(\frac{25}{8}-$$

$$-\frac{1}{8}\sin^2 I)-\frac{1}{16}\beta\gamma\frac{3+2e_T^2}{(1-e_T^2)^{\frac{7}{2}}}(1-x_S^2-y_S^2)^{\frac{1}{2}}x_S[2-27x_S^2-$$

$$-57y_S^2-3\sin^2 I(1-x_S^2-16y_S^2)]-\frac{1}{8}\gamma\frac{3+2e_T^2}{(1-e_T^2)^3}\cos^3 I\times$$

$$\times x_S(1-x_S^2-16y_S^2) \tag{A.2}$$

$$\frac{dg_T}{d\tau} = \frac{1}{2}\frac{\beta}{(1-e_T^2)^2}[4+x_S^2+11y_S^2-5\sin^2 I(1-x_S^2+4y_S^2)]+$$
$$+\frac{1}{(1-x_S^2-y_S^2)^{\frac{1}{2}}(1-e_T^2)^{\frac{3}{2}}}\cos I(1-x_S^2+4y_S^2)-\frac{5}{16}\alpha\beta\times$$
$$\times\frac{1+4e_T^2}{(1-e_T^2)^3 e_T}[(y_S\sin g_T\cos I+x_S\cos g_T)(4+3(x_S^2+y_S^2)-$$
$$-5\sin^2 I(1-x_S^2+6y_S^2))-10(1-x_S^2-y_S^2)\sin^2 I\cos I\times$$
$$\times y_S\sin g_T]+(\frac{5}{16}\alpha\frac{e_T}{(1-e_T^2)^{\frac{5}{2}}}\frac{1}{(1-x_S^2-y_S^2)^{\frac{1}{2}}}+\frac{5}{16}\alpha\beta\times$$
$$\times\frac{e_T}{(1-e_T^2)^3}\cos I)[-y_S\sin g_T(4+3(x_S^2+y_S^2)-5\sin^2 I(1-$$
$$-x_S^2+6y_S^2))-10(y_S\sin g_T\cos I+x_S\cos g_T)\cos I(1-x_S^2+$$
$$+6y_S^2)-10(1-x_S^2-y_S^2)y_S\sin g_T(2\cos^2 I-\sin^2 I)]+\frac{1}{4}\beta\gamma\times$$
$$\times\frac{1}{(1-e_T^2)^{\frac{7}{2}}}(1-x_S^2-y_S^2)^{\frac{1}{2}}\cos I\{-\frac{3}{2}+\frac{631}{4}x_S^2+\frac{721}{4}y_S^2+$$
$$+\frac{31}{4}(1-x_S^2-16y_S^2)\sin^2 I+e_T^2[-1+\frac{127}{2}x_S^2+\frac{157}{2}y_S^2+$$
$$+\frac{7}{2}\sin^2 I(1-x_S^2-16y_S^2)]\}-\frac{1}{16}\gamma\frac{3+2e_T^2}{(1-e_T^2)^3}[2-27x_S^2-$$
$$-57y_S^2-3\sin^2 I(1-x_S^2-16y_S^2)] \qquad \text{(A.3)}$$

$$\frac{de_T}{d\tau} = \frac{5}{16}\frac{\alpha\beta}{(1-e_T^2)^2}[(y_S\cos g_T\cos I-x_S\sin g_T)(4+3(x_S^2+y_S^2)-$$
$$-5\sin^2 I(1-x_S^2+6y_S^2))-10(1-x_S^2-y_S^2)y_S\sin^2 I\times$$
$$\times\cos I\cos g_T] \qquad \text{(A.4)}$$

$$\frac{dI}{d\tau} = -\frac{x_S\dot{x_S}+y_S\dot{y_S}}{(1-x_S^2-y_S^2)^{\frac{1}{2}}}(\frac{1}{\tan I(1-x_S^2-y_S^2)^{\frac{1}{2}}}+\frac{\beta}{\sin I(1-e_T^2)^{\frac{1}{2}}})-$$
$$-\frac{e_T\dot{e_T}}{(1-e_T^2)^{\frac{1}{2}}}(\frac{1}{\beta\sin I(1-x_S^2-y_S^2)^{\frac{1}{2}}}+\frac{1}{\tan I(1-e_T^2)^{\frac{1}{2}}}) \qquad \text{(A.5)}$$

Appendix B

Second order expansion of the perturbing Hamiltonian

A second order expansion of the perturbing Hamiltonian used in sections 3.4.2 and 3.6.

For the P_2 term:

$$
\begin{aligned}
H_{P_2} \;=\; & \frac{1}{2}\frac{Gm_1m_2m_3}{m_1+m_2}\frac{a_1^2}{a_2^3}[-\frac{1}{2}-\frac{3}{2}\cos(2\lambda_1-2\lambda_2)+e_1\cos(\lambda_1-\varpi_1)+ \\
& +\frac{9}{2}e_1\cos(\lambda_1-2\lambda_2+\varpi_1)-\frac{3}{2}e_1\cos(3\lambda_1-2\lambda_2-\varpi_1)- \\
& -\frac{3}{2}e_2\cos(\lambda_2-\varpi_2)+\frac{3}{4}e_2\cos(2\lambda_1-\lambda_1-\varpi_2)- \\
& -\frac{21}{4}e_2\cos(2\lambda_1-3\lambda_2+\varpi_2)-\frac{3}{4}e_1^2+\frac{1}{4}e_1^2\cos(2\lambda_1-2\varpi_1)- \\
& -\frac{15}{4}e_1^2\cos(2\lambda_2-2\varpi_1)-\frac{3}{2}e_1^2\cos(4\lambda_1-2\lambda_2-2\varpi_1)+ \\
& +\frac{15}{4}e_1^2\cos(2\lambda_1-2\lambda_2)+\frac{3}{2}e_1e_2\cos(\lambda_1-\lambda_2-\varpi_1+\varpi_2)+ \\
& +\frac{3}{2}e_1e_2\cos(\lambda_1+\lambda_2-\varpi_1-\varpi_2)-\frac{9}{4}e_1e_2\cos(\lambda_1-\lambda_2+\varpi_1-\varpi_2)- \\
& -\frac{21}{4}e_1e_2\cos(3\lambda_1-3\lambda_2-\varpi_1+\varpi_2)+ \\
& +\frac{63}{4}e_1e_2\cos(\lambda_1-3\lambda_2+\varpi_1+\varpi_2)+ \\
& +\frac{3}{4}e_1e_2\cos(3\lambda_1-\lambda_2-\varpi_1-\varpi_2)-\frac{3}{4}e_2^2-\frac{9}{4}e_2^2\cos(2\lambda_2-2\varpi_2)- \\
& -\frac{51}{4}e_2^2\cos(2\lambda_1-4\lambda_2+2\varpi_2)+\frac{15}{4}e_2^2\cos(2\lambda_1-2\lambda_2)] \qquad \text{(B.1)}
\end{aligned}
$$

For the P_3 term:

$$
\begin{aligned}
H_{P_3} \;=\; & \frac{1}{2}\frac{Gm_1m_2m_3(m_1-m_2)}{(m_1+m_2)^2}\frac{a_1^3}{a_2^4}[-\frac{3}{4}\cos(\lambda_1-\lambda_2)- \\
& -\frac{5}{4}\cos(3\lambda_1-3\lambda_2)+\frac{3}{8}e_1\cos(2\lambda_1-\lambda_2-\varpi_1)+ \\
& +\frac{15}{8}e_1\cos(\lambda_2-\varpi_1)+\frac{45}{8}e_1\cos(2\lambda_1-3\lambda_2+\varpi_1)- \\
& -\frac{15}{8}e_1\cos(4\lambda_1-3\lambda_2-\varpi_1)-\frac{3}{4}e_2\cos(\lambda_1-\varpi_2)- \\
& -\frac{9}{4}e_2\cos(\lambda_1-2\lambda_2+\varpi_2)+\frac{5}{4}e_2\cos(3\lambda_1-2\lambda_2-\varpi_2)- \\
& -\frac{25}{4}e_2\cos(3\lambda_1-4\lambda_2+\varpi_2)-\frac{3}{2}e_1^2\cos(\lambda_1-\lambda_2)- \\
& -\frac{33}{32}e_1^2\cos(\lambda_1+\lambda_2-2\varpi_1)+\frac{9}{32}e_1^2\cos(3\lambda_1-\lambda_2-2\varpi_1)+ \\
& +\frac{15}{2}e_1^2\cos(3\lambda_1-3\lambda_2)-\frac{285}{32}e_1^2\cos(\lambda_1-3\lambda_2+2\varpi_1)- \\
& -\frac{75}{32}e_1^2\cos(5\lambda_1-3\lambda_2-2\varpi_1)+\frac{15}{8}e_1e_2\cos(\varpi_1-\varpi_2)+ \\
& +\frac{9}{8}e_1e_2\cos(2\lambda_1-2\lambda_2-\varpi_1+\varpi_2)+\frac{3}{8}e_1e_2\cos(2\lambda_1-\varpi_1-\varpi_2)+ \\
& +\frac{45}{8}e_1e_2\cos(2\lambda_2-\varpi_1-\varpi_2)-\frac{45}{8}e_1e_2\cos(2\lambda_1-2\lambda_2+\varpi_1-\varpi_2)- \\
& -\frac{75}{8}e_1e_2\cos(4\lambda_1-4\lambda_2-\varpi_1+\varpi_2)+ \\
& +\frac{15}{8}e_1e_2\cos(4\lambda_1-2\lambda_2-\varpi_1-\varpi_2)+ \\
& +\frac{225}{8}e_1e_2\cos(2\lambda_1-4\lambda_2+\varpi_1+\varpi_2)-\frac{3}{2}e_2^2\cos(\lambda_1-\lambda_2)- \\
& -\frac{33}{32}e_2^2\cos(\lambda_1+\lambda_2-2\varpi_2)-\frac{159}{32}e_2^2\cos(\lambda_1-3\lambda_2+2\varpi_2)+ \\
& +\frac{15}{2}e_2^2\cos(3\lambda_1-3\lambda_2)-\frac{5}{32}e_2^2\cos(3\lambda_1-\lambda_2-2\varpi_2)- \\
& -\frac{635}{32}e_2^2\cos(3\lambda_1-5\lambda_2+2\varpi_2) \qquad \text{(B.2)}
\end{aligned}
$$

Bibliography

[1] Aarseth, S. J., Zare, K. (1974). A regularization of the three-body problem. Celest. Mech. **10**, 185-205.

[2] Arnold, V. I. (1980). Mathematical methods of classical mechanics, 2nd ed. (Springer-Verlag, New York).

[3] Backer, D. C., Foster, R. S., Sallmen, S. (1993). A second companion of the millisecond pulsar 1620-26. Nature **365**, 817-819.

[4] Barrow-Green, J. (1997). Poincaré and the three-body problem (American Mathematical Society).

[5] Batten, A. H., Fletcher, J. M., MacCarthy, D. G. (1989). Eighth catalogue of the orbital elements of spectroscopic binary systems. Publ. Dom. Astrophys. Obs. **17**, 317p.

[6] Black, D. C. (1982). A simple criterion for determining the dynamical stability of three-body systems. Astron. J. **87**, 1333-1337.

[7] Bozis, G. (1981). Escape of the smallest mass of a triple system. Publ. Astron. Soc. Japan **33**, 67-75.

[8] Brouwer, D., Clemence, G.M. (1961). Methods of celestial mechanics (Academic Press, New York).

[9] Donnison, J. R. (1988). The effects of eccentricity on the hierarchical stability of low-mass binaries in three-body systems. Mon. Not. R. Astron. Soc. **231**, 85-95.

[10] Donnison, J. R., Mikulskis, D. F. (1992). Three-body orbital stability criteria for circular orbits. Mon. Not. R. Astron. Soc. **254**, 21-26.

[11] Donnison, J. R., Mikulskis, D. F. (1994). Three-body orbital stability criteria for circular retrograde orbits. Mon. Not. R. Astron. Soc. **266**, 25-30.

[12] Donnison, J. R., Mikulskis, D. F. (1995). The effect of eccentricity on three-body orbital stability criteria and its importance for triple star systems. Mon. Not. R. Astron. Soc. **272**, 1-10.

[13] Donnison, J. R., Williams, I. P. (1978). Orbital stability of massive protoplanets in the terrestrial planet region of the solar system. Moon and Planets **19**, 421-424.

[14] Donnison, J. R., Williams, I. P. (1983). The stability of coplanar three-body systems with application to the solar system. Celest. Mech. **31**, 123-128.

[15] Donnison, J. R., Williams, I. P. (1985). The hierarchical stability of satellite systems. Mon. Not. R. Astron. Soc. **215**, 567-573.

[16] Duquennoy, A., Mayor, M. (1991). Multiplicity among solar-type stars in the solar neighbourhood. II-Distribution of the orbital elements in an unbiased sample. Astron. Astrophys. **248**, 485-524.

[17] Dvorak, R. (1984). Numerical experiments on planetary orbits in double stars. Celest. Mech. **34**, 369-378.

[18] Dvorak, R. (1986). Critical orbits in the elliptic restricted three-body problem. Astron. Astrophys. **167**, 379-386.

[19] Dvorak, R., Froeschlé, Ch., Froeschlé, Cl. (1989). Stability of outer planetary orbits (P-types) in binaries. Astron. Astrophys. **226**, 335-342.

[20] Eggleton, P. P., Kiseleva, L. G. (1995). An empirical condition for stability of hierarchical triple systems. Astrophys. J. **455**, 640-645.

[21] Eggleton, P. P., Kiseleva, L. G. (1996). Stellar and dynamical evolution within triple stars. In R. A. M. J. Wijers et al. (eds), Evolutionary processes in binary stars, 345-364 (Kluwer Academic Publishers, The Netherlands).

[22] Fekel, F. C., Jr.; Tomkin, J. (1982). Secondaries of eclipsing binaries. IV - The triple system Lambda Tauri. Astrophys. J. **263**, 289-301.

[23] Ford, E. B., Joshi, K. J., Rasio, F. A., Zbarsky, B. (2000). Theoretical implications of the PSR B1620-26 Triple system and its planet. Astrophys. J. **528**, 336-350.

[24] Ford, E. B., Kozinsky, B., Rasio, F. A. (2000). Secular evolution of hierarchical triple star systems. Astrophys. J. **535**, 385-401.

[25] Funato, Y., Hut, P., McMillan, S., Makino, J. (1996). Time-symmetrized Kustaanheimo-Stiefel regularization. Astron. J. **112**, 1697-1708.

[26] Ghez, A. M., Neugebauer, G., Matthews, K. (1993). The multiplicity of T Tauri stars in the star forming regions Taurus-Auriga and Ophiuchus-Scorpius: A 2.2 micron speckle imaging survey. Astron. J. **106**, 2005-2023.

[27] Gladman, B., Duncan, M., Candy, J. (1991). Symplectic integrators for long-term integrations in celestial mechanics. Celest. Mech. Dyn. Astron. **52**, 221-240.

[28] Gliese, W., Jahreiss, H. (1988). The third catalogue of nearby stars with special emphasis on wide binaries. Astrophys. Space Sci. **142**, 49-56.

[29] Goldstein, H. (1980). Classical Mechanics, 2nd ed. (Addison-Wesley Publishing Company, USA).

[30] Graziani, F., Black, D. C. (1981). Orbital stability constraints on the nature of planetary systems. Astrophys. J. **251**, 337-341.

[31] Griffin, R. F., Gunn, J. E. (1981). Spectroscopic orbits for the Hyades dwarfs 23DEG635 VB162 and VB 182 and the nonmember J318. Astron. J. **86**, 588.

[32] Griffin, R. F., Griffin, R. E. M., Gunn, J. E., Zimmerman, B. A. (1985). Spectroscopic orbits for 16 more binaries in the Hyades field. Astron. J. **90**, 609-642.

[33] Harrington, R. S. (1968). Dynamical evolution of triple stars. Astron. J. **73**, 190-194.

[34] Harrington, R. S. (1972). Stability criteria for triple stars. Celest. Mech. **6**, 322-327.

[35] Harrington, R. S. (1975). Production of triple stars by the dynamical decay of small stellar systems. Astron. J. **80**, 1081-1086.

[36] Harrington, R. S. (1977). Planetary orbits in binary stars. Astron. J. **82**, 753-756.

[37] Henry, T. J., McCarthy, D. W., Jr. (1990). A systematic search for brown dwarfs orbiting nearby stars. Astrophys. J. **350**, 334-347.

[38] Hinkle, K. H., Fekel, F. C., Johnson, D. S., Scharlach, W. W. G. (1993). The triple symbiotic system CH Cygni. Astron. J. **105**, 1074-1086.

[39] Hoffleit, D., Jaschek, C. (1983). The Bright star catalogue, 4th ed. (Yale University Observatory, New Haven).

[40] Holman, M. J., Wiegert, P. A. (1999). Long-term stability of planets in binary systems. Astron. J. **117**, 621-628.

[41] Hut, P., Makino, J., McMillan, S. (1995). Building a better leapfrog. Astrophys. J. **443**, L93-L96.

[42] Jha, S., Torres, G., Stefanik, R. P., Latham, D. W., Mazeh, T. (2000). Studies of multiple stellar systems - III. Modulation of orbital elements in the triple-lined system HD 109648. Mon. Not. R. Astron. Soc. **317**, 375-84.

[43] Kinoshita, H., Yoshida, H., Nakai, H. (1991). Symplectic integrators and their application to dynamical astronomy. Celest. Mech. Dyn. Astron. **50**, 59-71.

[44] Kiseleva, L. G., Eggleton, P. P., Anosova, J. P. (1994). A note on the stability of hierarchical triple stars with initially circular orbits. Mon. Not. R. Astron. Soc. **267**, 161-166.

[45] Kiseleva, L. G., Eggleton, P. P., Mikkola, S. (1998). Tidal friction in triple stars. Mon. Not. R. Astron. Soc. **300**, 292-302.

[46] Kiseleva, L. G., Eggleton, P. P., Orlov, V. V. (1994). Instability of close triple systems with coplanar initial doubly circular motion. Mon. Not. R. Astron. Soc. **270**, 936-946.

[47] Kozai, Y. (1962). Secular perturbations of asteroids with high inclination and eccentricity. Astron. J. **67**, 591-598.

[48] Marchal, C. (1990). The three-body problem (Elsevier Science Publishers, the Netherlands).

[49] Mardling, R. A., Aarseth, S. J. (1999). Tidal circularization in star cluster simulations. Preprint.

[50] Mason, B. D., McAlister, H. A., Hartkopf, W. I., Bagnuolo, W. G., Jr. (1993). ICCD speckle observations of binary stars. VII - A duplicity survey of the Hyades cluster. Astron. J. **105**, 220-225.

[51] Mathieu, R. D., Latham, D. W., Griffin, R. F. (1990). Orbits of 22 spectroscopic binaries in the open cluster M67. Astron. J. **100**, 1859-1881.

[52] Mayer, P., Lorenz, R., Chochol, D., Irsmambetova, T. R. (1994). SZ Cam - early-type eclipsing binary with a third body. Astron. Astrophys. **288**, L13-L16.

[53] McMillan, S., Hut, P., Makino, J. (1991). Star cluster evolution with primordial binaries. II - Detailed analysis. Astrophys. J. **372**, 111-124.

[54] Mermilliod, J.-C., Duquennoy, A., Mayor, M. (1994). Investigation of the Praesepe cluster. 2: Three triple systems: KW 365, 367 and 495. Astron. Astrophys. **283**, 515-521.

[55] Mermilliod, J.-C., Rosvick, J. M., Duquennoy, A., Mayor, M. (1992). Investigation of the Pleiades cluster. II - Binary stars in the F5-K0 spectral region. Astron. Astrophys. **265**, 513-526.

[56] Mikkola, S. (1997). Practical symplectic methods with time transformation for the few-body problem. Celest. Mech. Dyn. Astr. **67**, 145-165.

[57] Murray, C. D., Dermott, S. F. (1999). Solar system dynamics (Cambridge University Press).

[58] Nacozy, P. E. (1976). On the stability of the solar system. Astron. J. **81**, 787-791.

[59] Pendleton Y. J., Black, D. C. (1983). Further studies on criteria for the onset of dynamical instability in general three-body systems. Astron. J. **88**, 1415-1419.

[60] Press, W. H., Teukolsky, S. A., Vetterling, W. T., Flannery, B. P. (1996). Numerical recipes in Fortran 77, 2nd ed. (Cambridge University Press).

[61] Rabl, G., Dvorak, R. (1988). Satellite-type planetary orbits in double stars: a numerical approach. Astron. Astrophys. **191**, 385-391.

[62] Rasio, F. A., McMillan, S., Hut, P. (1995). Binary-binary interactions and the formation of the PSR B1620-26 triple system in M4. Astrophys. J. **438**, L33-L36.

[63] Roy, A. E., Walker, I. W., Carusi, A., Valsecchi, G. B. (1984). The use of the energy and angular momentum integrals to obtain a stability criterion in the general hierarchical three-body problem. Astron. Astrophys. **141**, 25-29.

[64] Saha, P., Tremaine, S. (1992). Symplectic integrators for solar system dynamics. Astron. J. **104**, 1633-1640.

[65] Sanz-Serna, J. M. (1991). Sympectic integrators for Hamiltonian problems: an overview. Acta Num. **1**, 243-286.

[66] Szebehely, V. G. (1967). Theory of orbits (Academic Press, New York).

[67] Szebehely, V. G. (1980). Stability of planetary orbits in binary systems. Celest. Mech. **22**, 7-12.

[68] Szebehely, V. G., Mark, H. (1998). Adventures in celestial mechanics, 2nd ed. (John Wiley and Sons, New York).

[69] Szebehely, V. G., McKenzie, R. (1977). Stability of planetary systems with bifurcation theory. Astron. J. **82**, 79-83.

[70] Szebehely, V. G., McKenzie, R. (1977). Stability of the Sun-Earth-Moon system. Astron. J. **82**, 303-305.

[71] Szebehely, V. G., Zare, K. (1977). Stability of classical triplets and of their hierarchy. Astron. Astrophys. **58**, 145-152.

[72] Thorsett, S. E., Arzoumanian, Z., Camilo, F., Lyne, A. G. (1999). The Triple pulsar system PSR B1620-26 in M4. Astrophys. J. **523**, 763-770.

[73] Thorsett, S. E., Arzoumanian, Z., Taylor, J. H. (1993). PSR B1620-26 - A binary radio pulsar with a planetary companion? Astrophys. J. **412**, L33-L36.

[74] Tokovinin, A. A. (1997a). On the multiplicity of spectroscopic binary stars. Astron. Let. **23**, 727-730.

[75] Tokovinin, A. A. (1997b). MSC - a catalogue of physical multiple stars. Astron. Astrophys. Sup. series **124**, 75-84.

[76] Valtonen, M. J., Mikkola, S., Pietilä, H. (1995). Burrau's three-body problem in the post-Newtonian approximation. Mon. Not. R. Astron. Soc. **273**, 751-754.

[77] Van de Kamp, P. (1971). The nearby stars. Ann. Rev. Astron. Astrophys. **9**, 103-126.

[78] Wiegert, P. A., Holman, M. J. (1997). The stability of planets in the α Centauri system. Astron. J. **1997**, 1445-1450.

[79] Wisdom, J., Holman, M. (1991). Symplectic maps for the n-body problem. Astron. J. **102**, 1528-1538.

[80] Yoshida, H. (1990). Construction of higher order symplectic integrators. Phys. Lett. A. **150**, 262-268.

[81] Yoshida, H. (1993). Recent progress in the theory and application of symplectic integrators. Celest. Mech. **56**, 27-43.